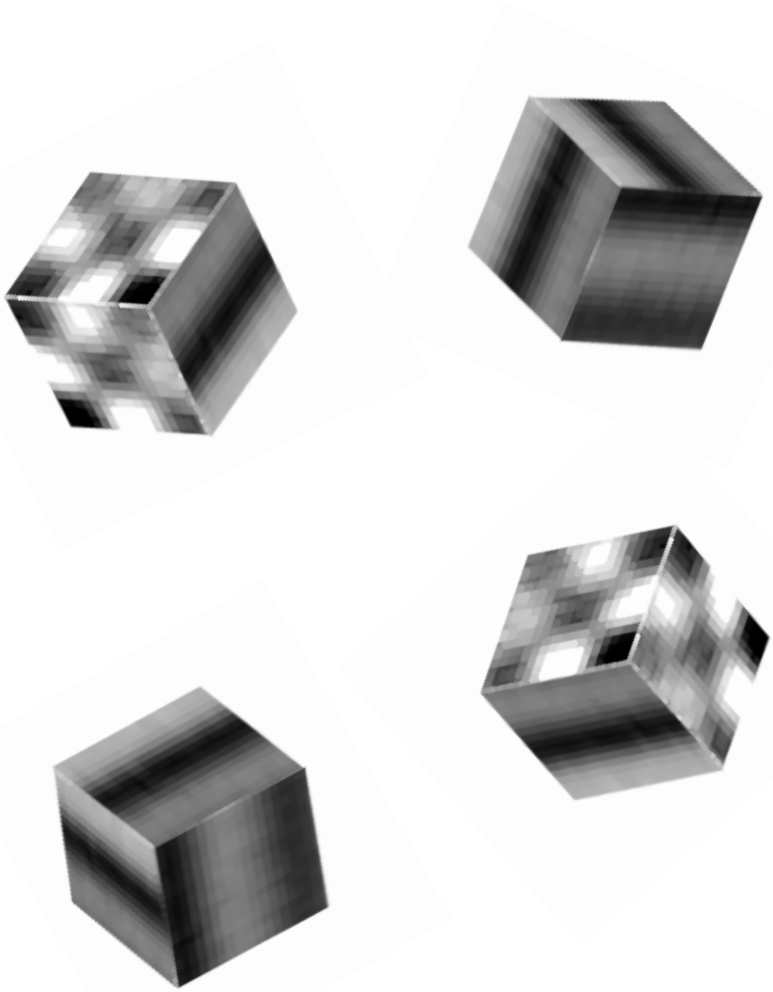
On the Quantum Measurement of Superconducting Flux Qubits



Thomas Picot

On the quantum measurement of superconducting flux qubits

On the quantum measurement of superconducting flux qubits

Proefschrift

ter verkrijging van de graad van doctor
aan de Technische Universiteit Delft,
op gezag van de Rector Magnificus Prof ir. K.C.A.M. Luyben,
voorzitter van het College voor Promoties,
in het openbaar te verdedigen
op woensdag 22 september 2010, om 12.30 uur

door

Thomas Stéphane Emmanuel PICOT

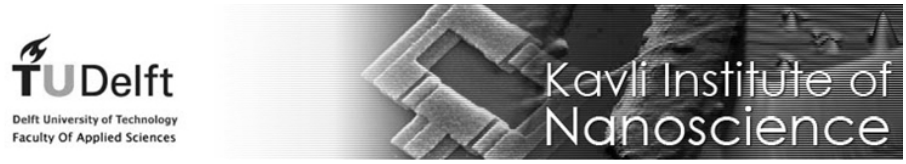
General engineering diploma of ESPCI, Paris (FRANCE)
geboren te Clichy (FRANCE)

Dit proefschrift is goedgekeurd door de promotor:
Prof. dr. ir. J.E. Mooij

Copromotor:
Dr. C.J.P.M. Harmans

Samenstelling van de promotiecommissie

Rector Magnificus	Voorzitter
Prof. dr. ir. J.E. Mooij	Technische Universiteit Delft, promotor
Dr. C.J.P.M. Harmans	Technische Universiteit Delft, copromotor
Prof. dr. D. Esteve	CEA Saclay
Prof. dr. C. Van Haesendonck	Katholieke Universiteit Leuven
Prof. dr. G. Johansson	Chalmers University of Technology
Prof. dr. Y.V. Nazarov	Technische Universiteit Delft
Prof. dr. ir. C.H. van der Wal	Rijksuniverisiteit Groningen
Prof. dr. H.W.M. Salemink	Technische Universiteit Delft





Published by: Thomas Picot
Printed by: Gildeprint Drukkerijen B.V., Enschede
ISBN: 978-90-8593-924-5

Contents

Preface **ix**

1 Quantum mechanics with superconducting circuits **1**
1.1 Quantum mechanics and quantum computing 1
1.2 Superconducting circuits: general aspects 2
1.2.1 Charge and flux as quantum conjugated variables 2
1.2.2 The Josephson junction, the "transistor" of superconducting circuits 3
1.3 The superconducting flux qubit 4
1.4 The DC-SQUID 6

2 Theory of quantum measurement **11**
2.1 General framework to describe a detector 12
2.1.1 Linear continuous measurement 12
2.1.2 Switching detector versus continuous detector 14
2.2 Quantum measurement of a qubit with a switching detector . . . 16
2.2.1 Quantum limited measurement 17
2.2.2 Quantum nondemolition measurement 19
2.2.3 Correlations between two successive measurements 19
2.3 Summary 22

3 The different modes of operation of the DC-SQUID for qubit readout **25**
3.1 Relation between the sensitivity and the back-action of a flux-sensitive interferometer 26
3.2 AC-continuous readout 27
3.2.1 General principle 27
3.2.2 Sensitivity 29
3.2.3 Back-action 30
3.3 DC-switching readout 32
3.3.1 Principle 32
3.3.2 Sensitivity 34
3.3.3 Back-action 35
3.4 AC-switching readout 37

3.4.1 General principle . . . 37
3.4.2 Sensitivity . . . 38
3.4.3 Back-action . . . 39
3.5 Summary . . . 40

4 QND measurement with the AC-switching readout 43
4.1 Introduction . . . 44
4.2 Sample design and experimental setup . . . 44
4.2.1 Readout circuit and measurement setup . . . 44
4.2.2 Effective temperature of the oscillator . . . 46
4.2.3 Qubit properties . . . 48
4.3 QND measurement with the AC-switching readout . . . 49
4.3.1 Qubit relaxation between two successive readouts . . . 49
4.3.2 Qubit rotation between two successive readouts . . . 49
4.3.3 QND Fidelity . . . 50
4.4 Analysis of the relaxation during the measurement . . . 52
4.4.1 Qubit relaxation during the holding plateau . . . 52
4.4.2 Qubit relaxation during the switching plateau . . . 53
4.5 Summary . . . 57

5 QND measurement with the DC-switching readout 61
5.1 Why and How to reduce the back-action of the DC-switch readout 62
5.2 Characterization of the readout circuit . . . 63
5.2.1 I-V characteristics of the SQUIDs . . . 64
5.2.2 Operation of the SQUID for qubit readout . . . 66
5.2.3 Response time of the detector . . . 66
5.2.4 Qubit relaxation induced by the resistor . . . 67
5.2.5 Qubit properties . . . 68
5.2.6 Effective temperature of the SQUID . . . 70
5.3 QND measurement with the DC-switching readout . . . 71
5.3.1 Qubit relaxation between two successive readouts . . . 71
5.3.2 Qubit rotation between two successive readouts . . . 72
5.3.3 QND Fidelity . . . 74
5.4 Back-action for larger qubit-SQUID interaction strengths . . . 75
5.5 Discussion and perspectives for high QND fidelity with large readout contrast . . . 77
5.6 Summary . . . 79

6 Perspectives for the quantum measurement of flux qubits 83

Summary 89

Samenvatting 91

Curriculum Vitae 93

List of publications 95

Preface

A book is generally more interesting to read starting from the end. Looking back at the intensive and demanding years of my PhD in Delft, I must say that I'm quite happy not only about my results but also from all that I learned about myself and the others. A group like QT demands each PhD gives the best of himself while leaving him with an amazing degree of freedom. This necessarily implies that all PhDs are confronted one day, in one way or another, with their own limits and that they have to find a way to overcome them. I would like to thank my supervisors Hans Mooij and Kees Harmans for the opportunity they gave me to do my PhD in such a great group and for the sincere care they always had to let each student find his own path.

If I had to describe myself with only one word, I would say that I'm a dreamer. Unfortunately, reality is generally quite far from a dream. However, sometimes in some magic circumstances dreams and reality do meet each other. To me, looking for a such magic place and try to reach it constitutes one of the most essential driving force of life.

During my first year in QT, I had the chance to be initiated to the field of superconducting qubits by Adrian Lupaşcu who had developed the AC-dispersive readout for the flux qubit in Delft. Together with Shiro Saito, we investigated for the first time the quantum nondemolition (QND) character of an AC-dispersive detector. Adrian and Shiro, I'm very grateful for all what I learned from you and for all the support you gave me.

Finding my own path during the next years was a real challenge for me. In particular, the confrontation of my strong idealism with the very pragmatic and focused research approach necessary to start a project was a real source of difficulties. One day, however, a magic crossing point suddenly appeared very clearly in my mind: what if we could do a QND measurement of a flux qubit with one of the most basic detector for the superconducting flux qubit, the DC-switching readout? Since that particular moment, all the obstacles which were lying in front of me suddenly appeared considerably easier to overcome as before.

During the last months of my PhD, at a crazy time where five different flux qubits experiments were to be realized with a high priority on three cryogenic fridges, Pol and I had to build and share a measurement setup to run in parallel and at full speed two different experiments in one fridge. Without your constant efforts to collaborate with a positive and constructive attitude, we would never

have overcome this difficult period in the way we did. Thank you Pol for all the efforts you did.

Pieter, you are to me a model in many aspects. You are not only smart, pragmatic and efficient; you are also truly concerned about all the people around you. I'm sure Margreet did the right choice when she said 'yes'.

I would like to thank all the present and past members of the flux qubit team in Delft for all the nice and stimulating discussions we had. Raymond and Ruud, your electronic modules, your cryogenic amplifier and your knowledge are worth an infinite amount of gold. Rein thank you very much for your help in FPGA programming. I learned a lot from you. Bram, Remco and Peter, thank you for your constant efforts to fix all the machines that we need in order to fabricate and measure our samples, despite our great ability to damage them. Emile van der Drift and your team, it is impressive to see how you manage to let so many people work in the cleanroom with a full freedom and responsibility to use this wonderful machine called EBPG. Thank you Yuki and Angele for all the administrative details you solved so efficiently for us. Angele, you were investing yourself fully in the group. Bram will certainly not be the only one missing your beautiful smile in the coming months. Lucky are the other ones who will be close to you then. Yuli, your active presence at the werkbespreking always makes it a great time. I also appreciate very much all the discussions we had together and with Hongduo.

Many people in the group have a real talent to make nice and spicy presentations after each PhD defense. Floris Zwanenburg, Maarten van Kouwen, Juriaan, Katja, Lan and Pol, to cite only a few of them. I hope the next generation of PhD will be as brilliant as you in this respect. This is a great tradition. More generally, I would like to thank all the people of QT who are actively participating in creating such dynamical and stimulating atmosphere to work. I hope that the positive QT spirit will stay as it is for many more generations.

Vincent de Lange, mijn soulmate. Wij begrijpen elkaar zonder woorden. Ik heb je ontmoet enkele maanden na mijn aankomst in dit land en het klikte onmiddellijk. Jij hebt mij jaren langen gesteund tot het einde van mijn doctoraat. Jouw vriendschap is van grote waarde voor mij. Ik ben heel blij en trots dat je mijn paranimf zal zijn tijdens mijn promotie.

Enfin pour finir, je voudrais remercier ma famille qui m'a toujours soutenu dans mes projets. Lucille, je suis très fier d'être ton parrain, je pense beaucoup à toi et j'espère te revoir bientôt. Tania, ma princesse et mon étoile, nos voyages en train représentent une distance plus grande que trois fois la circonférence de la Terre. Quelqu'un nous a dit un jour que l'amour entre deux personnes se mesure avec la distance qui les sépare. Moi je crois qu'il a raison. La force de notre amour est capable de faire des miracles. Notre rêve de vivre ensemble va enfin se réaliser. Merci pour la patience et l'amour infini que tu as eus pendant toutes ces années.

Many thanks to all of you,

Thomas Picot
Delft , August 2010

Chapter 1

Quantum mechanics with superconducting circuits

1.1 Quantum mechanics and quantum computing

The theory of quantum mechanics was initially developed in the beginning of the twentieth century in order to explain the properties of elementary particles at a microscopic scale. At this length scale, the behavior of matter differs fundamentally from our "daily-life" macroscopic scale. For example, a single electron can be moving to the left and to the right at the same time. This property, known as quantum superposition, is a striking aspect of quantum mechanics which does not have a classical equivalent. The revolutionary implications of this discovery were intensively discussed by the founding fathers of quantum mechanics during the 20-30's in their famous 'thought' experiments [1, 2]. In those discussions the issue of quantum measurement and the apparent non-locality of quantum mechanics were of particular importance. At that time, however, the technology necessary to investigate such fundamental aspects of quantum mechanics was not available. Between 1940 and 1980, most of the experiments related to quantum mechanics were investigating the properties of large ensemble of identical quantum systems where the issues of quantum measurement and non-locality of quantum mechanics were not of direct relevance. The first experiments tackling those questions seriously were performed in the 1980's and they confirmed the predictions of quantum mechanics [3].

At that time some theoreticians such as Richard Feynman and David Deutsch started to realize the remarkable power of a computer based on a quantum system compared to a traditional computer [4, 5]. In such a quantum computer the basic unit of information is a quantum bit (or qubit), whose state can be 0 or 1 as in a classical computer, but more importantly, it can also be a quantum superposition of the two states (that is 0 and 1 at the same time). Similarly, in a

quantum computer, a "number" can be in a quantum superposition of different numbers, i.e., it may have multiple values at the same time. As the number of possible superpositions grow exponentially with the number of qubits, a quantum computer provides unprecedentedly large parallel calculation power and could thereby quickly outperform any classical computer. This is illustrated for example with the quantum algorithm for the factorization of a number into its prime numbers invented by Peter Shor in 1994 [6], which can be performed in a time exponentially faster than any other classical algorithms.

In practice, however, the realization of a quantum computer is a very challenging task requiring a high degree of control of the state of the quantum system and a very good isolation from external perturbations which can easily deteriorate the qubit properties. So far, elementary quantum computers have been implemented using different systems such as optical photons [7], molecular Nuclear Magnetic Resonance [8], ions traps [9], and more recently using nanofabricated superconducting circuits [10].

In this thesis, we present a detailed analysis of the quantum measurement of a superconducting flux qubit using two types of detectors. The motivation for this study is two-fold. First, quantum measurement plays a central role in quantum mechanics. A low back-action quantum state detector is very interesting to investigate experimentally different aspects of the theory of quantum measurement, such as partial collapse [13], uncollapse (or measurement reversal) [12, 13], quantum feedback [14], measurement of weak values [15, 16], simultaneous measurement of non-commutating variables [17], and other types of experiments where quantum mechanics has not been extensively investigated so far. Secondly, the development of a highly efficient detector for the readout of a qubit is an essential requirement for quantum computing.

1.2 Superconducting circuits: general aspects

In the last couples of decades, it has become possible to fabricate artificial nanoscale electronic circuits showing clear signature of quantum behavior [18]. In such circuits, currents and voltages are no longer described with well defined numbers, but with operators obeying the general rules of quantum mechanics. In the following, we will briefly review the basic properties of such circuits and introduce the superconducting flux qubit and its detector (a more detailed introduction to the quantum properties of electrical circuits can be found in [19]).

1.2.1 Charge and flux as quantum conjugated variables

The simplest example of a non-dissipative electrical circuit is an harmonic oscillator, constituted of an inductor L and a capacitor C in a loop (shown in figure 1.1a). The dynamics of the oscillator is described by the Hamiltonian

$$H = \frac{\Phi^2}{2L} + \frac{Q^2}{2C}, \tag{1.1}$$

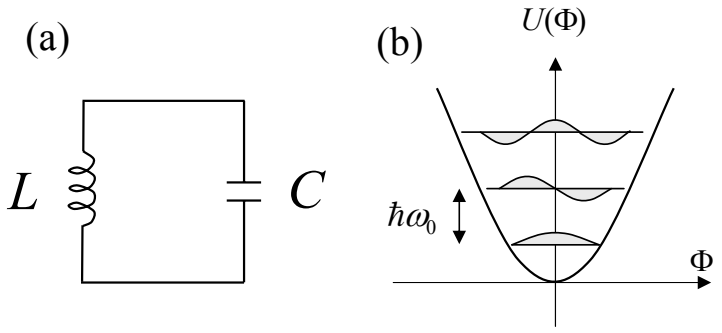


Figure 1.1: (a) LC oscillator electrical circuit and (b) its corresponding potential energy $U(\Phi)$. The flux Φ stored in the inductance and the charge Q stored in the capacitor are equivalent to the position X and momentum P of a mechanical oscillator. In the quantum regime, the energy is quantized in units of $\hbar\omega_0$. For each energy level, we show a qualitative representation of the circuit wavefunction $\Psi(\Phi)$.

where Φ if the flux stored in the inductance and Q is the charge stored in the capacitor. Here, Φ and Q are playing a role analogue to the position X and the momentum P of a particle. If the energy of the thermal fluctuations kT is smaller than the elementary energy quantum $\hbar\omega_0$ of the oscillator (where $\omega_0 = 1/\sqrt{LC}$ is the oscillator resonance frequency), the dynamics of the oscillator enters the quantum regime, and Φ and Q are replaced by quantum conjugated variables obeying the Heisenberg uncertainty principle

$$[\hat{\Phi}, \hat{Q}] = i\hbar. \tag{1.2}$$

Although an LC oscillator can be operated in the quantum regime, if it is driven by a classical source, its response is identical to a classical oscillator. In order to observe quantum effects in an electrical circuit nonlinear elements are essential.

1.2.2 The Josephson junction, the "transistor" of superconducting circuits

The key element of all superconducting quantum circuits is the Josephson junction, consisting of two superconductors separated by a very thin insulating barrier. A Josephson junction can sustain a supercurrent I by tunneling of Cooper pairs through the barrier up to a maximum value I_c denoted as the critical current of the junction. The constitutive relation of a Josephson junction can be expressed as

$$I(\gamma) = I_c \sin(\gamma), \tag{1.3}$$

where

$$\gamma = \frac{2\pi}{\Phi_0}\int_{-\infty}^{t} V(t')dt', \tag{1.4}$$

is the gauge invariant superconducting phase difference between the two sides of the barrier, which is directly related to the voltage difference V across the barrier and the flux quantum $\Phi_0 = \frac{h}{2e}$.

For a current I much smaller than the junction critical current $I/I_c << 1$, relation (1.3) reduces to the linear phase-current relation of an inductance with a value $L_J = \Phi_0/(2\pi I_c)$. For larger currents, the Josephson inductance is nonlinear and depends on the value of the current $L_J = \Phi_0/(2\pi\sqrt{I_c^2 - I^2})$.

In addition to its inductive component, a Josephson junction also has a capacitive component due to the insulating barrier, which is modeled by a capacitance C in parallel with the inductive channel.

For a current close to the junction critical current, the relation (1.3) is highly nonlinear. Consider for example the case where $\gamma(t)$ increases linearly in time $\gamma(t) = 2\pi Ft$. From (1.4) and (1.3), it follows

$$\begin{cases} I(t) &= I_c \sin(2\pi Ft) \\ V(t) &= \Phi_0 F. \end{cases} \tag{1.5}$$

A Josephson junction can thus sustain an AC current while the voltage across it is constant. This is a highly nonlinear phenomenon which relates a voltage with a frequency via fundamental constants only. This effect has important applications in metrology and high precision voltage standards.

1.3 The superconducting flux qubit

The superconducting flux qubit studied in this thesis, originally called the Josephson Persistent-Current qubit [20], consists of a superconducting loop interrupted by 3 Josephson junctions and biased with a flux Φ_{ext} close to half a flux quantum $\Phi_0/2$. One of the junctions has a smaller critical current than the other two by a factor $\alpha \simeq 0.75$, such that the potential energy of the circuit $U(\gamma)$, where γ is the phase difference across the smallest junction, has a double well shape as illustrated in figure 1.2b. The two minima of the potential corresponds to two opposite values of the circulating current $\pm I_p$. Due to the confining potential, the energy spectrum of the circuit is discrete. The two important energy scales determining the properties of the energy spectrum are the Josephson energy $E_J = \frac{I_c\Phi_0}{2\pi}$ and the charging energy $E_C = \frac{1}{2}\frac{e^2}{C}$ of the two largest junctions. The ratio E_J/E_C and the value of α are chosen is such a way that the first two energy levels are well isolated from the higher energy levels, forming a well defined quantum two-level system, or qubit. In the following, we denote the first two energy levels as ground $|g>$ and excited $|e>$ respectively.

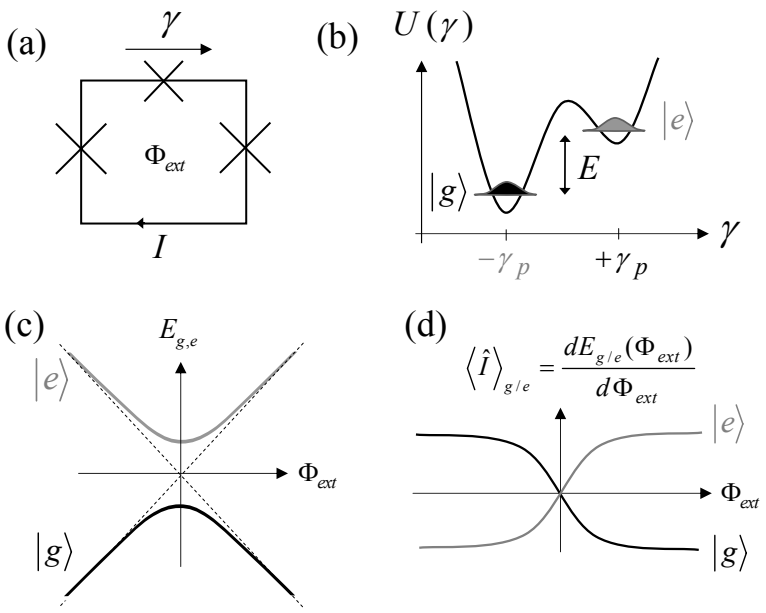


Figure 1.2: (a) The Josephson Persistent-Current flux qubit and (b) its potential energy as a function of the phase γ across the small junction, with a schematic representation of the wavefunction of the two qubit energy levels. (c) Energy spectrum of the flux qubit as a function of the external flux bias Φ_{ext}. (d) Expectation value of the persistent circulating current $< \hat{I} >$ in the qubit loop for the two energy eigenstates of the qubit.

The two energy eigenstates $|g>$ and $|e>$ can be expressed as a linear superposition of two states corresponding to oppositely circulating persistent currents of magnitude I_p and denoted as $|+>$ and $|->$. In the basis of these current states the Hamiltonian of the flux qubit can be written as:

$$\hat{H} = -\frac{1}{2}(\epsilon\hat{\sigma_z} + \Delta\hat{\sigma_x}), \tag{1.6}$$

where $\hat{\sigma_x}$, $\hat{\sigma_z}$ are Pauli spin matrices, $\epsilon = 2I_p(\Phi_{ext} - \Phi_0/2)$ is the flux bias energy and Δ is the quantum tunneling energy between the two current states.

In general, the state of the qubit can be expressed as

$$|\Psi>= \cos\frac{\theta}{2}|g> + e^{i\varphi}\sin\frac{\theta}{2}|g>, \tag{1.7}$$

where φ is the quantum phase of the qubit. The time during which φ is well defined, so called the coherence time T_2, is generally limited. Two types of

processes can affect the qubit coherence:
- transitions between the two qubit energy states ($|e>\rightarrow|g>$ or $|g>\rightarrow|e>$) referred to as relaxation and excitation characterized by two transition rates $\Gamma_\downarrow$ and $\Gamma_\uparrow$, resulting in a qubit energy decay rate $\Gamma_1 = \Gamma_\downarrow + \Gamma_\uparrow$.
- low frequency fluctuations of the qubit energy splitting, which cause a gradual randomization of the value of φ. This process is generally referred to as "pure" dephasing and is characterized by a dephasing rate Γ_φ.
Both relaxation and dephasing result in qubit decoherence which is described by a decoherence rate:

$$\Gamma_2 = \frac{\Gamma_1}{2} + \Gamma_\varphi, \tag{1.8}$$

or equivalently with a coherence time $T_2 = 1/\Gamma_2$.

Figure 1.2a shows the two energy eigenvalues E_g and E_e of the qubit as a function of the flux through the qubit loop. At $\Phi_{ext} = \Phi_0/2$, so called the degeneracy point, the qubit energy splitting is independent of the external flux bias ($dE/d\Phi_{ext} = 0$). At this particular point, the qubit energy splitting is less sensitive to fluctuations of the magnetic flux leading to longer dephasing times [21].

Commonly, the state of the flux qubit is read out by measuring the flux generated by the current circulating in its loop. The expectation value of the circulating current in the two states $|g>$ and $|e>$ is given by the first derivative of the qubit energy with respect to flux $<\hat{I}>_{g/e}= \frac{dE_{g,e}(\Phi_{ext})}{d\Phi_{ext}}$. In the all the experiments presented in this thesis the measurements are performed at a bias $|\epsilon| >> \Delta$, such that the energy eigenstates $|g>$ and $|e>$ approximately coincide with the current states $|+>$ and $|->$. At such bias, $<\hat{I}>$ corresponds either to $+I_p$ or $-I_p$.

Alternatively, the qubit state can be detected by measuring the quantum inductance of the qubit [22] related to the second derivative of the energy with respect to flux $1/L_{g,e} = \frac{d^2E_{g,e}(\Phi_{ext})}{d\Phi^2_{ext}}$. The advantage of this detection scheme is that it allows to perform a measurement at the degeneracy point, where the qubit coherence is maximum. However, in the case of the flux qubit the sensitivity of this detection scheme is generally smaller than a direct measurement of the flux generated by the qubit far from the degeneracy point.

1.4 The DC-SQUID

The magnetic field generated by the current circulating in the qubit loop is measured using a DC-SQUID, one of the most sensitive magnetometer [23]. A DC-SQUID consists of two Josephson junctions in a loop, as shown in figure 1.3. The currents in the two branches of the SQUID given by $I_1 = I_{c0}\sin\gamma_1$ and $I_2 = I_{c0}\sin\gamma_2$ can be re-expressed as a function of the transport current I through the SQUID and the current circulating J in the SQUID loop as $I_1 = I/2 + J$, $I_2 = I/2 - J$, with

$$\begin{cases} I = 2I_{c0}\sin(\gamma)\cos(\pi\phi) & (1.9) \\ \\ J = I_{c0}\cos(\gamma)\sin(\pi\phi) & (1.10) \end{cases}$$

where $\phi = \Phi/\Phi_0 = (\gamma_1 - \gamma_2 + n2\pi)/(2\pi)$ is the external magnetic frustration applied to the SQUID loop and $\gamma = \frac{\gamma_1+\gamma_2}{2}$ is the internal phase of the SQUID.

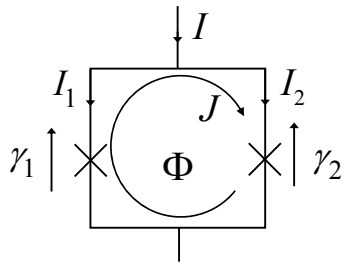


Figure 1.3: The DC-SQUID.

As can be seen from equation (1.9), a symmetric SQUID is equivalent to a single Josephson junction with a variable critical current depending on the magnetic frustration of the SQUID

$$I_c(\Phi) = 2I_{c0}\cos(\pi\phi) \quad (1.11)$$

.

Several modes of operation of the DC-SQUID are possible to readout the state of the flux qubit. In the simplest mode, called the DC-switching readout, the SQUID is biased with a current close to its critical current $I_c(\Phi)$, where it may switch from its superconducting state S to a dissipative state D with a probability P. As the critical current depends on the flux Φ through the SQUID loop, P is highly sensitive to Φ and so to the state of the qubit. Although this readout scheme is very simple to use, its back-action on the qubit is commonly very strong (see chapter 3).

Alternatively, the SQUID can also be operated using a small AC driving current and detecting the Josephson inductance of the SQUID given by $L_J(\Phi) = \frac{\Phi_0}{2\pi I_c(\Phi)}$ instead of its critical current. This is the principle of the AC-continuous readout and the AC-switching readout presented in chapter 3.

Bibliography

[1] E. Schrödinger, *Die gegenwärtige Situation in der Quantenmechanik (The Present Situation in Quantum Mechanics)*, Die Naturwissenschaften **48**, 52 (1935)

[2] A. Einstein, B. Podolsky, and N. Rosen, *Can quantum-mechanical description of physical reality be considered complete?*, Physical Review **47**, 777 (1935).

[3] A. Aspect, P. Grangier, G. Roger *Experimental Tests of Realistic Local Theories via Bell's Theorem*, Physical Review Letters **47**, 460 (1981)

[4] R. Feynman, *Simulating Physics with Computers*, International Journal of Theoretical Physics **21**, 467 (1982)

[5] D. Deutsch, *Quantum theory, the Church-Turing principle and the universal quantum computer*, Proceedings of the Royal Society of London, Series A **400**, 97 (1985)

[6] P. Shor, *Algorithms for quantum computation: discrete logarithms and factoring*, Proceeding of the 35th Annual Symposium on the Foundations of Computer Science, edited by S. Goldwasser, 124, IEEE Computer Society (1994)

[7] A. Politi, J.C.F. Matthews, J.L. O'Brien, *Shors Quantum Factoring Algorithm on a Photonic Chip*, Science **325**, 1221 (2009)

[8] L.M.K. Vandersypen,M. Steffen, G. Breyta1, C.S. Yannoni, M.H. Sherwood, I.L. Chuang, *Experimental realization of Shor's quantum factoring algorithm using nuclear magnetic resonance*, Nature **414**, 883 (2001)

[9] D. Leibfried, E. Knill, S. Seidelin, J. Britton, R.B. Blakestad, J. Chiaverini, D.B. Hume, W.M. Itano, J.D. Jost, C. Langer, R. Ozeri, R. Reichle and D.J. Wineland, *Creation of a six-atom 'Schrodinger Cat' state*, Nature **438** 639 (2005)

[10] L. DiCarlo, J.M. Chow, J.M. Gambetta, L.S. Bishop, B.R. Johnson, D.I. Schuster, J. Majer, A. Blais, L. Frunzio, S.M. Girvin, R.J. Schoelkopf, *Demonstration of two-qubit algorithms with a superconducting quantum processor*, Nature **460**, 240 (2009)

[11] N. Katz, M. Ansmann, R. C. Bialczak, E. Lucero, R. McDermott, M. Neeley, M. Steffen, E. M. Weig, A. N. Cleland, J.M. Martinis and A. Korotkov, *Coherent State Evolution in a Superconducting Qubit from Partial-Collapse Measurement*, Science **312**, 1498 (2006)

[12] A.N. Korotkov and A.N. Jordan, *Undoing a Weak Quantum Measurement of a Solid-State Qubit*, Physical Review Letters **97**, 166805 (2006)

[13] N. Katz, M. Neeley, M. Ansmann, R.C. Bialczak, M. Hofheinz, E. Lucero, A. O'Connell, H. Wang, A.N. Cleland, J.M. Martinis and A.N. Korotkov *Reversal of the Weak Measurement of a Quantum State in a Superconducting Phase Qubit*, Physical Review Letters **101**, 200401 (2008)

[14] R. Ruskov and A.N. Korotkov *Quantum feedback control of a solid-state qubit*, Physical Review B **66**, 041401(R), (2002)

[15] Y. Aharonov, D.Z. Albert, and L. Vaidman, *How the result of a measurement of a component of the spin of a spin-1/2 particle can turn out to be 100*, Physical Review Letters **60**, 1351 (1988)

[16] N.S. Williams and A.N. Jordan, *Weak Values and the Leggett-Garg Inequality in Solid-State Qubits*, Physical Review Letters **100**, 026804 (2008)

[17] H. Wei, Y. Nazarov *Statistics of measurement of noncommuting quantum variables: Monitoring and purification of a qubit*, Physical Review B **78**, 045308 (2008)

[18] M.H. Devoret, J.M. Martinis, J. Clarke, *Measurement of Macroscopic Quantum Tunneling out of the Zero-Voltage State of a Current-Biased Josephson Junction*, Physical Review Letters **55**, 1908 (1985)

[19] M.H. Devoret *Quantum fluctuations in electrical circuits*, Les Houches Session LXIII, Quantum Fluctuations p. 351-386 (1995).

[20] J.E. Mooij, T.P. Orlando, L. Levitov, Lin Tian, C.H. van der Wal, S. Lloyd, *Josephson Persistent-Current Qubit*, Science **285**, 1036 (1999)

[21] P. Bertet, I. Chiorescu, G. Burkard, K. Semba, C.J.P.M. Harmans, D.P. DiVincenzo, and J.E. Mooij, *Dephasing of a Superconducting Qubit Induced by Photon Noise*, Physical Review Letters **95**, 257002 (2005)

[22] Y.S. Greenberg, A. Izmalkov, M. Grajcar, E. Ilichev, W. Krech, H.G. Meyer, M.H.S. Amin, A.M. van den Brink, *Low-frequency characterization of quantum tunneling in flux qubits*, Physical Review B **66** 214525 (2002)

[23] J. Clarke and A.I. Braginski *The SQUID handbook* **1**, Wiley (2004)

Chapter 2

Theory of quantum measurement

In contrast to classical mechanics, where physical quantities have a well-defined value which, in principle, can be measured with arbitrary precision without perturbing the measured object, in quantum mechanics the process of measurement necessarily introduces a fundamental back-action on the state of the measured object. This back-action is directly related to the Heisenberg uncertainty principle which forbids a physical variable and its quantum conjugate to be determined simultaneously. In this chapter, we first present a general framework to describe a measurement with a linear continuous detector. Secondly, by analogy with a linear continuous detector, we introduce a definition for the effective sensitivity of a switching detector allowing a quantitative comparison of the sensitivity of continuous detectors with switching detectors. Finally, we discuss the central concepts of quantum nondemolition measurement and quantum limited measurement of a two level quantum system.

2.1 General framework to describe a detector

2.1.1 Linear continuous measurement

In this section we present a general framework for the measurement of a physical quantity $\hat{\Phi}$ of a system using a linear continuous detector [1, 2, 3]. We consider three systems, shown in figure 2.1, formed by the object to measure, the linear detector, and an observer monitoring the output of the detector. The detector is described by an Hamiltonian $\hat{H}_{det}$, which is time-independent in the absence of coupling with the source of the signal to measure. The interaction Hamiltonian between the detector and the object measured has the form $\hat{H}_\Phi = \hat{\Phi}\hat{J}$, where $\hat{\Phi}$ is the physical quantity to be measured and $\hat{J}$ is an internal variable of the detector. Similarly, the interaction between the detector and the observer has the form $\hat{H}_Q = \hat{V}\hat{Q}$, where $\hat{V}$ is the output variable of the detector and $\hat{Q}$ is an internal variable of the observer. This description is very general and applies to any linear continuous detector. Here, we choose the notation to illustrate the case of a flux detector based on a DC-SQUID, where the quantity measured is the flux $\hat{\Phi}$ through the SQUID loop and the output variable of the detector is the voltage $\hat{V}$ across the SQUID. The observer consists of a voltage meter such as a voltage amplifier or an oscilloscope. The internal variable of the observer which couples to the SQUID is then the charge of a capacitor $\hat{Q}$ used to monitor the voltage. In this section, all the operators are in the Heisenberg representation. $\hat{V}_0$ corresponds to the operator $\hat{V}$ in the absence of coupling to the object to measure and the observer. The statistical average of the operator $\hat{V}$ is denoted as $< \hat{V} >$.

The interaction between the detector and the measured object is supposed to be small, such that the response of the detector is linear. For a given input signal $< \hat{\Phi}(t') >$ the output of the detector is given by

$$< \hat{V}(t) >=< \hat{V}_0(t) > + \int_{-\infty}^{t} \chi(t-t') < \hat{\Phi}(t') > dt', \tag{2.1}$$

where $\chi(t'-t)$ is the response function of the detector (note that causality necessarily implies that $\chi(t-t') = 0$ for $t - t' < 0$). Using time-dependent

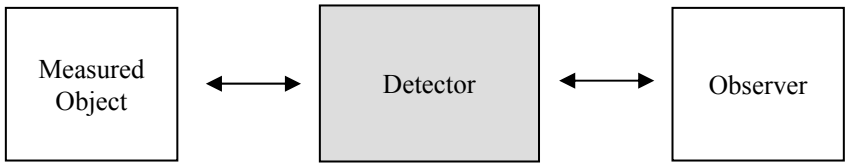


Figure 2.1: The three systems formed by the object to measure, the linear detector and an observer, and their interaction.

perturbation theory $< \hat{V}(t) >$ can be developed to first order in the interaction H_Φ, yielding

$$< \hat{V}(t) >=< \hat{V}_0(t) > + \frac{i}{\hbar} \int_{-\infty}^{t} < [\hat{H}_\Phi(t'), \hat{V}_0(t)] > dt'. \tag{2.2}$$

Given the form of the interaction $\hat{H}_\Phi = \hat{\Phi}\hat{J}$, equations (2.1) and (2.2) lead to

$$\chi(t-t') = \frac{i}{\hbar} < [\hat{J}_0(t'), \hat{V}_0(t)] > . \tag{2.3}$$

Formula (2.3) relates the linear response function of the detector to the commutator of $\hat{J}$ and $\hat{V}$ and the Planck constant. It is related to the Heisenberg uncertainty principle for two conjugate variables. Unless the sensitivity of the detector is nul, $\hat{V}$ and $\hat{J}$ can not be determined simultaneously to arbitrary precision. Therefore, fluctuations of $\hat{J}$ will always cause a minimum back-action on the measured object.

More generally the global response of a linear detector to a change of the external variables $\hat{\Phi}(t)$ and $\hat{Q}(t)$ can be described by four response functions $\chi_{12}(t)$, $\chi_{21}(t)$, $\chi_{11}(t)$ and $\chi_{22}(t)$, corresponding to the direct response function, the reverse response function, the input and the output conductances of the detector, defined as

$$\begin{array}{l} < \hat{V}(t) >=< \hat{V}_0(t) > + \int_{-\infty}^{t} \{\chi_{12}(t-t') < \hat{\Phi}(t') > + \chi_{22}(t-t') < \hat{Q}(t') >\} dt' \\ < \hat{J}(t) >=< \hat{J}_0(t) > + \int_{-\infty}^{t} \{\chi_{21}(t-t') < \hat{Q}(t') > + \chi_{11}(t-t') < \hat{\Phi}(t') >\} dt', \end{array} \tag{2.4}$$

each of them being related to one of the commutators of $\hat{J}$ and $\hat{V}$ via a Kubo-like formula

$$\begin{array}{rcl} < [\hat{V}_0(t), \hat{J}_0(0)] > & = & i\hbar\chi_{12}(t) \\ < [\hat{J}_0(t), \hat{V}_0(0)] > & = & i\hbar\chi_{21}(t) \\ < [\hat{J}_0(t), \hat{J}_0(0)] > & = & i\hbar\chi_{11}(t) \\ < [\hat{V}_0(t), \hat{V}_0(0)] > & = & i\hbar\chi_{22}(t). \end{array} \tag{2.5}$$

where $t > 0$.

Each detector response functions χ_{pq} can be re-expressed as a function of its Fourier transform $\tilde{\chi}_{pq}(\omega) = \int_{-\infty}^{+\infty} \chi_{pq}(t) e^{i\omega t} dt$. In general, detectors are strongly directional: while the output variable V depends on the variable to measure Φ, the reverse response function χ_{21} (or reverse gain) is negligibly small. In the following, we consider the ideal case $\tilde{\chi}_{21} = 0$. We denote the DC response coefficient of the detector as $\tilde{\chi}_{12}(0) = \lambda$.

The amplitude of the fluctuations of the detector input and output variables are characterized by their noise spectral densities

$$\left\{ \begin{array}{rcl} S_V(\omega) & = & \int_{-\infty}^{\infty} e^{i\omega t} < \tilde{V}(0)\tilde{V}(t) > dt \\ S_J(\omega) & = & \int_{-\infty}^{\infty} e^{i\omega t} < \tilde{J}(0)\tilde{J}(t) > dt \\ S_{VJ}(\omega) & = & \int_{-\infty}^{\infty} e^{i\omega t} < \tilde{V}(t)\tilde{J}(0) > dt, \end{array} \right. \tag{2.6}$$

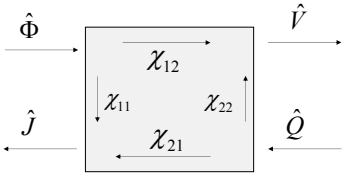


Figure 2.2: Input and output ports of a linear continuous detector

where $\tilde{V} = \hat{V}_0 - < \hat{V}_0 >$ and $\tilde{J} = \hat{J}_0 - < \hat{J}_0 >$. The noise level of the output of the detector, described by $S_V(\omega)$, is related to the sensitivity of the detector, while the fluctuations of J, described by $S_J(\omega)$, are related to the back-action of the detector. Based on equations (2.5) and (2.6), a general inequality can be derived for the fluctuations of the input and output variables of the detector [1]. In the case of a DC measurement, this inequality reads

$$S_J(0)S_V(0) \geq \frac{\hbar^2}{4}\lambda^2. \tag{2.7}$$

Introducing the *equivalent* flux spectral noise density $S_\Phi(0) \equiv S_V(0)/\lambda^2$, inequality (2.7) can be rewritten as

$$S_J(0)S_\Phi(0) \geq \frac{\hbar^2}{4}. \tag{2.8}$$

$S_\Phi(0)$ corresponds to the *fictitious* fluctuation of Φ that would result in an output noise level $S_V(0)$ given in (2.6). Inequality (2.8) is the equivalent of the Heisenberg uncertainty principle for a detector.

2.1.2 Switching detector versus continuous detector

The output signal of a switching detector can only take two values associated with the two possible states of the detector: switched or not switched. This is in marked contrast with a continuous detector whose output signal is continuous. (In that sense the comparison of a switching detector with a continuous detector is not straightforward). In this section, we will show that we can define the effective sensitivity of a switching readout in a form similar to the case of a continuous readout. From that perspective a quantitative comparison between the sensitivity of a switching readout and a continuous readout becomes possible.

The key variable describing a switching detector is its switching probability P, obtained after averaging the outcome of N identical readout sequences ($N >> 1$). For simplicity, we assume that the N readouts are independent,

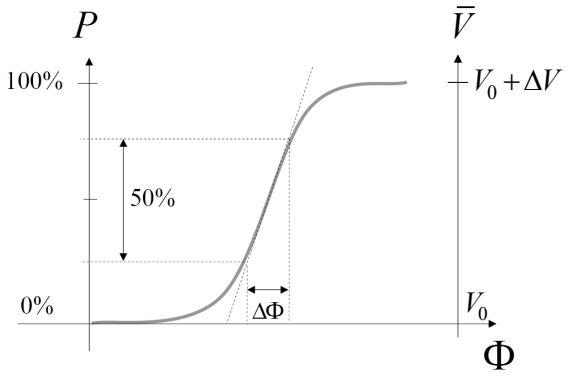


Figure 2.3: Switching probability as a function of the flux

and that the two states of the detector (switched or not switched) can be well discriminated. Note that the switching probability is a continuous variable which can be determined to an arbitrary precision provided N is large enough (see figure 2.3). The sensitivity of the detector comes from the dependence of the switching probability on the flux $P(\Phi)$ or equivalently its first derivative $dP(\Phi)/d\Phi$. The resolution of a flux measurement for a single readout can be defined as the difference of flux resulting in a difference of switching probability of 50 %, i.e. $\Delta\Phi = 1/(2dP(\Phi)/d\Phi)$. This corresponds to the minimum flux which can be resolved with about one standard deviation in a single readout. The resolution of the flux measurement can be improved by averaging the results of N successive readouts. In this case, as the readouts are independent, the minimum flux that can be resolved is $\Delta\Phi/\sqrt{N}$. This can be directly compared with a measurement using a continuous detector whose output signal, averaged over a duration t_m, allows to resolve a difference of flux: $\Delta\Phi = \sqrt{S_\Phi(0)/t_m}$, where $S_\Phi(0)$ is the equivalent flux noise spectral density of the continuous detector at zero frequency. Given the time interval between two successive switching readouts t_{rep}, and the first derivative of the switching probability with respect to flux $dP(\Phi)/d\Phi$, the sensitivity of a switching detector can be described by an *equivalent* flux noise spectral density

$$S_\Phi(0) = \frac{t_{rep}}{4}\left(\frac{dP(\Phi)}{d\Phi}\right)^{-2}. \tag{2.9}$$

Note that $S_\Phi(0)$ does not depend on the voltage difference between the two states of the detector. This is logical since we assumed that the two states of the detector can be fully discriminated. The only parameters relevant to define the

sensitivity of a switching detector are its $P(\Phi)$, and the measurement repetition period t_{rep}.

The equivalent noise spectral density $S_\Phi(0)$ can also be derived from the flux-to-voltage transfer function $\lambda = dV/d\Phi$ and the noise spectral density of the output voltage $S_V(0)$. Given the voltage difference ΔV between the two states of the detector (switched or not switched), the average value of the output voltage is (figure 2.3)

$$\overline{V} = V_0 + \Delta V P(\Phi), \tag{2.10}$$

where V_0 is the output voltage of the detector when there is no switching event. The flux-to-voltage transfer function of the detector is thus

$$\lambda = \frac{d\bar{V}}{d\Phi} = \Delta V \frac{dP(\Phi)}{d\Phi}. \tag{2.11}$$

In a single readout, the RMS fluctuations of the output voltage are $V_{RMS}^2 = \overline{(V-\overline{V})^2} = \Delta V^2 P(1-P)$. The maximum sensitivity corresponds to a switching probability of $P \sim 50\%$ where the average output voltage is $\bar{V} = \Delta V/2$ and the voltage RMS fluctuations are $V_{RMS} = \Delta V/2$. In this case the output voltage noise spectral density is

$$S_V(0) = t_{rep}\frac{\Delta V^2}{4} \tag{2.12}$$

Similarly to section 2.1.1, the equivalent flux noise spectral density $S_\Phi(0)$ can be obtained by dividing the output voltage noise spectral density (2.12) by the flux-to-voltage transfer function (2.11) leading to the same result as (2.9).

2.2 Quantum measurement of a qubit with a switching detector

In this section, we consider the measurement of a quantum two-level system (or qubit) with a switching detector. In general the state of the qubit $|\Psi>$ can be written in the energy basis ($|g>$,$|e>$) as

$$|\Psi> = \cos\left(\frac{\theta}{2}\right)|g> + e^{i\varphi}\sin\left(\frac{\theta}{2}\right)|e> . \tag{2.13}$$

The detector can only give two types of outcome depending on the state of the detector: switched (denoted as state H) or not switched (denoted as state L). As seen in section 2.1.2, the switching process is a stochastic phenomenon described by a switching probability P. The principle of the measurement is based on the dependence of the detector switching probability P on the state of the qubit. In the following we consider a measurement of the qubit in its energy basis. The detector switching probabilities when the qubit is in state $|g>$ or $|e>$ are denoted as P_g and P_e respectively. The discrimination efficiency between the two states of the qubit (or readout contrast), is then given by

$$C_m = P_g - P_e. \tag{2.14}$$

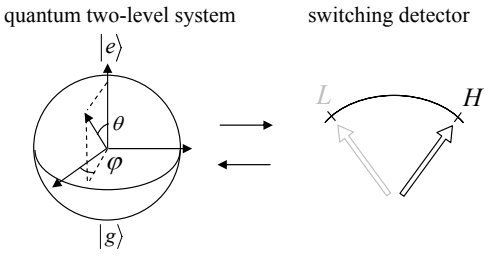


Figure 2.4: Relation between the state of the qubit and the state of the detector.

In the ideal case $C_m = 1$ the state of the qubit can be inferred directly from the state of the detector in a single shot (if the detector is in state L, the qubit state is $|e>$ whereas if the detector is in the state H, the qubit state is $|g>$). In the case that $|C_m| < 1$, a single measurement reveals only partially the qubit state which can thus not be inferred with certainty. However, the qubit state can be determined with a high precision from the average outcome of an ensemble of measurements.

2.2.1 Quantum limited measurement

In quantum mechanics a measurement with two possible outcomes $i = H$ or $i = L$ is described by two measurement operators $\hat{M}_i$ associated with each measurement outcome [1]. Given the initial density matrix of the qubit, the measurement operators allows to calculate the probability P_i to get the measurement outcome i, and the qubit density matrix $\hat{\rho}_i$ after a measurement with outcome i:

$$\begin{cases} P_i &= tr(\hat{M}_i \hat{\rho}_0 M_i^\dagger) \\ \hat{\rho}_i &= \frac{1}{P_i} \hat{M}_i \hat{\rho}_0 M_i^\dagger \end{cases} \tag{2.15}$$

To ensure that the sum of the probabilities of all the measurement outcomes is unity, the measurement operators must satisfy $\sum_i \hat{M}_i \hat{M}_i^\dagger = \hat{I}$. In the case of a measurement with a switching detector, the measurement operators can be simply expressed as a function of the detector switching probabilities

$$\begin{cases} \hat{M}_H &= \sqrt{P_g}|g><g| + \sqrt{P_e}|e><e| \\ \hat{M}_L &= \sqrt{(1-P_g)}|g><g| + \sqrt{(1-P_e)}|e><e| \end{cases} \tag{2.16}$$

A measurement which extracts information from the qubit necessarily causes decoherence of the qubit. This can be illustrated by considering the initial state $|\Psi>= \frac{1}{\sqrt{2}}(|e>+|g>)$. After the measurement, the density matrix of the qubit

(disregarding the measurement outcome) is:

$$\hat{\rho}_{final} = \frac{1}{2}\begin{pmatrix} 1 & A_\varphi \\ A_\varphi & 1 \end{pmatrix}, \tag{2.17}$$

where the diagonal terms represent the classical occupation probabilities of the two qubit energy states and the off-diagonal coefficients A_φ of the density matrix represent the remaining quantum coherence of the qubit after the measurement. Based on equations (2.15) and (2.16), it is possible to derive a direct relation between A_φ, which is a measure of the back-action of the measurement in terms of decoherence, and the contrast of the readout $C_m = P_g - P_e$ (assuming that $(P_g + P_e)/2 = 1/2$),

$$A_\varphi^2 + C_m^2 = 1. \tag{2.18}$$

As can be seen from equations (2.15) and (2.16), in the case of a high readout contrast ($C_m \to 1$, $P_g \to 1$ and $P_e \to 0$), the measurement operators are given by $\hat{M}_H \simeq |g><g|$ and $\hat{M}_L \simeq |e><e|$ respectively. The qubit is thus strongly projected either into $|e>$ or $|g>$ after the measurement and the coherence of the qubit is completely lost. In the case of a low readout contrast ($C_m \to 0$, $P_g \to 1/2$ and $P_e \to 1/2$), $\hat{M}_L \simeq \hat{M}_H \simeq \sqrt{2}/2\hat{I}$. The qubit is then only weakly projected and the coherence remains nearly unaffected.

Relation (2.18) corresponds to the ideal quantum limit for the measurement of a qubit with a switching detector. In this case, the amount of decoherence of the qubit corresponds to the minimum allowed by quantum mechanics for the given amount of information extracted from the qubit. In practice, any source of noise can reduce the coherence of the qubit leading to

$$A_\varphi^2 \leq 1 - C_m^2. \tag{2.19}$$

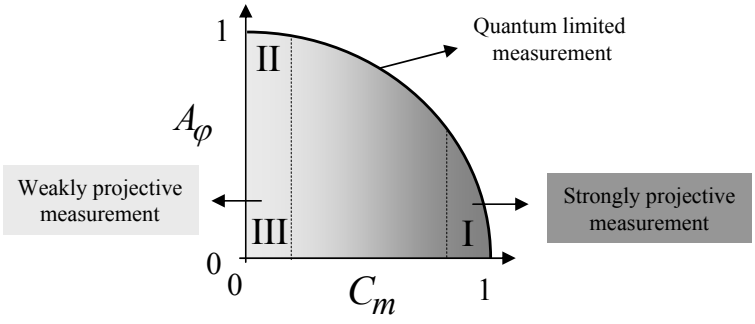


Figure 2.5: Coherence A_φ versus readout contrast C_m and the different regimes of a quantum measurement.

2.2.2 Quantum nondemolition measurement

According to the Heisenberg uncertainty principle the measurement of a physical variable necessarily perturbs its quantum conjugate variable. In the previous section we described a measurement of a qubit in its energy basis. In this case, the measured variable is the probability for the qubit to be in the state $|e>$, given by $p(e) = \sin^2(\theta/2)$, while φ is the perturbed conjugate variable. If the dynamics of the perturbed variable is coupled to the measured variable, this can lead to a fundamental limit on the precision of the measurement. For example, the measurement of the position $\hat{X}$ of an harmonic oscillator causes a perturbation of its momentum $\hat{P}$ which in turn leads to an uncertainty of the position. However, it is in principle possible to design the measurement interaction in such a way that the dynamics of the variable which is measured is decoupled from the perturbed conjugate variable. This is the central idea in the concept of quantum nondemolition (QND) measurement, which was initially developed to perform high precision measurements beyond the standard quantum limit [1]. QND measurement became an important paradigm of quantum mechanics of particular interest for fundamental studies of quantum systems. A simple criterion ensuring that a measurement is QND is that the Hamiltonians of the bare quantum system and of the interaction between the quantum system and the detector do commute. So far, QND measurements have been demonstrated experimentally in quantum optics [4], in cavity QED with Rydberg atoms [5] and with trapped single electrons [6]. In the chapters 4 and 5 of this thesis, we will show that QND measurements can also be realized with superconducting qubits.

In the measurement presented in the previous section, the measurement basis coincides with the energy basis of the quantum system. Therefore, the simple criterion for a QND measurement is satisfied. In this case, the main requirement for the measurement to be QND is that no transitions occur between $|e>$ and $|g>$ during the measurement. In this thesis, we define the QND fidelity of the measurement as the average probability that the states $|g>$ and $|e>$ are preserved during the measurement irrespective of the measurement outcome. Denoting the probabilities that the qubit state is preserved during the measurement when it is initially in $|g>$ or $|e>$ as $p(g|g)$ and $p(e|e)$ respectively, the QND fidelity is

$$F_{QND} = \frac{p(g|g) + p(e|e)}{2}. \tag{2.20}$$

2.2.3 Correlations between two successive measurements

In order to show the quantum nondemolition character of a measurement, it is necessary to use a sequence of two successive measurements. In the case of an ideal QND measurement, the average outcome of the two measurements should be equal (for any initial state of the qubit). However, this could also be the case if the second readout would systematically give the same result as the first readout due to some crosstalk between the measurements. To prove unambiguously that

the results of the two measurements are equal because the qubit state is well preserved during the measurement and not because of measurement crosstalk, one possibility is to reverse the qubit state between the two measurements. If the qubit state is really preserved after the first measurement, the result of the second measurement should be reversed compared to the result of the first measurement.

Manipulating the qubit coherently between the two measurements is also essential to quantify the amount of decoherence induced by the measurement as well as to characterize the efficiency of the readout compared with the quantum limit [7, 8].

In this section, we present a sequence including two Rabi rotation pulses and two readout pulses (shown in figure 2.6) to analyze various aspects of a quantum measurement.

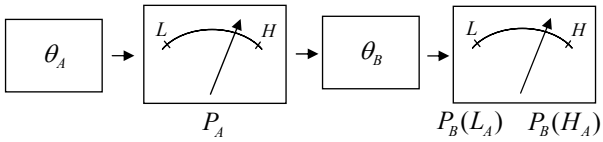


Figure 2.6: Sequence to analyze the correlation between two consecutive measurements.

We discuss three different regimes (see also figure 2.5):

I	Strongly projective measurement
II	Weakly projective quantum limited measurement
III	Weakly projective measurement far from the quantum limit

In general two consecutive readouts A and B lead to four possible outcomes each associated with a certain probability. As the sum of the four probabilities is unity, only three probabilities are independent. We consider the switching probability in the readout A denoted as P_A, and the two conditional switching probabilities in readout B given the result of readout A, denoted as $P_B(L_A)$ and $P_B(H_A)$.

The qubit is initially in the ground state $|g>$. The first Rabi rotation brings the qubit state to a quantum superposition $|\psi_A>$ with an excited state occupation probability: $p(e_A) = \sin^2\left(\frac{\theta_A}{2}\right)$.

In the case $C_m = 1$ (regime I), the qubit state is fully projected either to the state $|g>$ if the outcome of the measurement is H or to the state $|e>$ if the measurement outcome is L. The second Rabi pulse rotates the qubit state by an angle θ_B, starting either from $|e>$ or $|g>$. The excited state occupation probability before the second measurement is thus either

$$p(e_B)_{\text{I}} = \sin^2\left(\frac{\theta_B}{2}\right) \quad \text{or} \quad p(e_B)_{\text{I}} = \cos^2\left(\frac{\theta_B}{2}\right) \tag{2.21}$$

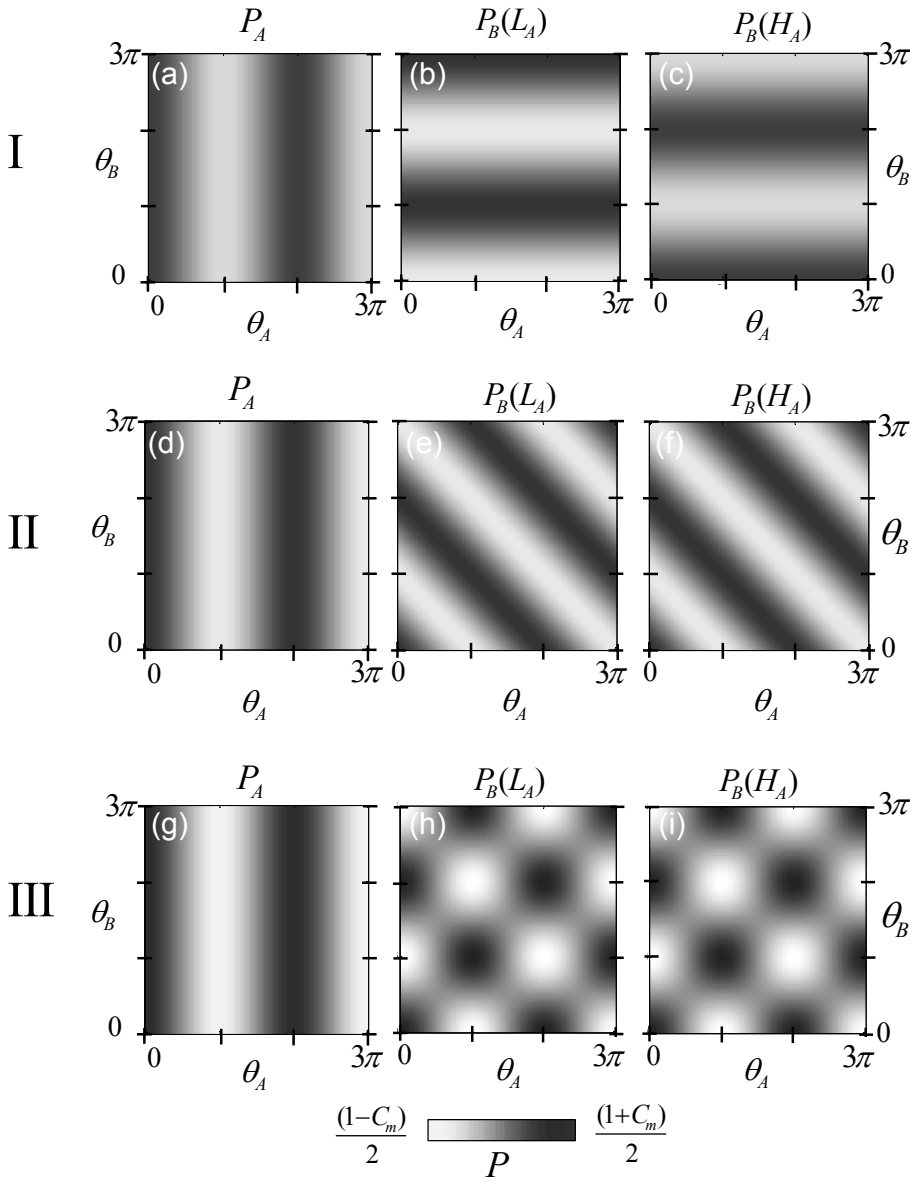


Figure 2.7: Results of the two consecutive readouts A and B as a function of the two angles θ_A and θ_B of the Rabi rotations preceding each readout pulse. P_A is the switching probability in readout A while $P_B(L_A)$ and $P_B(H_A)$ are the conditional switching probabilities in readout B given the result of readout A. Three different regimes are illustrated: (I) strongly projective measurement, (II) weakly projective and quantum limited measurement and (III) weakly projective measurement far from the quantum limit.

if the outcome of the readout A was H or L respectively. As the qubit state is fully projected after readout A, $P_B(H_A)$ and $P_B(L_A)$ are independent of θ_A as shown in figures 2.7b,c.

In the case $|C_m| << 1$ (regime II and III), the state of the detector is very weakly correlated with the state of the qubit. Consequently, the measurement is only very weakly projective. If the measurement is quantum limited (regime II), the back-action is so small that the qubit coherence is nearly not affected. The rotation of the second Rabi pulse is thus coherent with the first one, leading to a total rotation angle of $\theta_A + \theta_B$. The qubit excited state occupation probability before the readout B is then

$$p(e_B)_{\text{II}} = \sin^2\left(\frac{\theta_A + \theta_B}{2}\right). \tag{2.22}$$

If the measurement is far from the quantum limit, the qubit coherence after readout A is lost. The state of the qubit before the second Rabi rotation is therefore equivalent to a purely classical mixture of $|e>$ and $|g>$ and the two Rabi pulses are incoherent. The qubit state after the second Rabi pulse is then

$$p(e_B)_{\text{III}} = \sin^2\left(\frac{\theta_A}{2}\right)\sin^2\left(\frac{\theta_B}{2}\right). \tag{2.23}$$

In regimes II and III, the qubit state is very weakly projected after readout A, therefore $P_B(H_A)$ is nearly identical to $P_B(L_A)$ as shown in figures 2.7e,f,h,i.

2.3 Summary

In this chapter, we have presented a general framework to describe a detector and discussed different aspects of the theory of quantum measurement. In the next chapter, we will present and compare three different types of detection scheme for the superconducting flux qubit based on the general framework of this chapter. In chapters 4 and 5 we will present experiments to quantify the QND character of the AC-switching readout and the DC-switching using a sequence of two consecutive readouts. Finally, in chapter 6 we will discuss how quantum limited measurements of superconducting qubits could be realized in the near future.

Bibliography

[1] V.B. Braginsky, F.Y. Khalili *Quantum Measurement*, edited by K.S. Thorne, Cambridge University Press 1995

[2] A.A. Clerk, M.H. Devoret, S.M. Girvin, F. Marquardt, R.J. Schoelkopf, *Introduction to quantum noise, measurement, and amplification*, Review of Modern Physics **82** (2010)

[3] A.A. Clerk, S.M. Girvin, and A.D. Stone, *Quantum-limited measurement and information in mesoscopic detectors*, Physical Review B (2003) **67**,165324.

[4] P. Grangier, J.A. Levenson, J.-P. Poizat, *Quantum non-demolition measurements in optics*, Nature **396**, 537 (1998).

[5] C. Guerlin, J. Bernu, S. Deléglise, C. Sayrin, S. Gleyzes, S. Kuhr, M. Brune, J.M. Raimond, S. Haroche, *Progressive field-state collapse and quantum non-demolition photon counting*, Nature **448**, 889 (2007)

[6] S. Peil, G. Gabrielse, *Observing the Quantum Limit of an Electron Cyclotron: QND Measurements of Quantum Jumps between Fock States*, Physical Review Letters **83**, 1287 (1999)

[7] N. Katz, M. Ansmann, R. C. Bialczak, E. Lucero, R. McDermott, M. Neeley, M. Steffen, E. M. Weig, A. N. Cleland, J.M. Martinis and A. Korotkov, *Coherent State Evolution in a Superconducting Qubit from Partial-Collapse Measurement* Science **312**, 1498 (2006)

[8] K. Kakuyanagi, H. Nakano, S. Kagei, R. Koibuchi, S. Saito, A. Lupaşcu, K. Semba, *Readout strength dependence of state projection in superconducting qubit*, arxiv 1004.0182v2)

Chapter 3

The different modes of operation of the DC-SQUID for qubit readout

In this chapter we study the sensitivity and the back-action of the DC-SQUID as a flux detector, based on the general framework presented in chapter 2. In section 3.1, we derive a relation between the sensitivity and the back-action of a flux-sensitive interferometer based on general thermodynamical arguments. Secondly, in section 3.2, 3.3 and 3.4, we estimate the intrinsic sensitivity of different readout schemes based on a DC-SQUID operated in three different modes: AC-continuous, DC-switching and AC-switching. We find that the intrinsic sensitivity of the SQUID is of the same order of magnitude irrespective of the mode in which the SQUID is operated. However, in practice, due to several effects specific of each readout, the effective sensitivity of the SQUID is lower than its intrinsic sensitivity. In particular, for typical parameters of the readout circuits, the sensitivity of the SQUID in the AC-continuous readout and the DC-switching readout is more than one order of magnitude lower. This is in contrast with the AC-switching readout whose effective sensitivity is only about a factor two smaller than its intrinsic sensitivity. We discuss how the sensitivity of each readout could be improved.

3.1 Relation between the sensitivity and the back-action of a flux-sensitive interferometer

In this section we consider a superconducting interferometer constituted solely of inductive elements (such as Josephson junctions and linear inductors), comprising an interferometric loop threaded by an external magnetic flux Φ and carrying a circulating current J. We denote the transport current through the device as I, the voltage between the two external points of the device as V and the gauge invariant phase difference across the device as $\gamma(t) = \frac{2\pi}{\Phi_0}\int_{-\infty}^{t} V dt'$.

The superconducting interferometer is characterized by two relations:

$$\begin{cases} I = I(\gamma, \Phi) & (3.1) \\ J = J(\gamma, \Phi) & (3.2) \end{cases}$$

As an example, the two relations characterizing the DC-SQUID presented in chapter 1 are given by equations (1.9) and (1.10).

The sensitivity of the interferometer is based on the dependence of the current-phase relation (3.1) on the external flux Φ. On the other hand, J is the internal variable of the interferometer responsible of its back-action on the source of the magnetic flux Φ. In the following we will show that there is a general relation between (3.1) and (3.2).

We denote $U(\Phi, \gamma)$ as the internal energy of the interferometer as a function of the two external parameters Φ and γ. The work done by the external source of Φ on the interferometer when Φ changes by $d\Phi$ (and γ is fixed) is

$$\delta W = J(\gamma, \Phi) d\Phi. \tag{3.3}$$

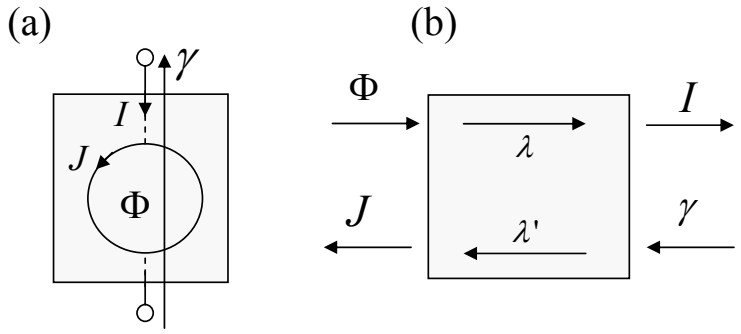


Figure 3.1: (a) Superconducting interferometer (such as a DC-SQUID), comprising a loop threaded by an external flux Φ and carrying a circulating current J. (b) Interferometer seen as a two-port dissipationless linear device.

The energy conservation $\delta W = dU$ leads to:

$$\frac{\partial U(\gamma,\Phi)}{\partial \Phi} = J(\gamma,\Phi). \tag{3.4}$$

Similarly, the work done by the external source of γ to change γ by $d\gamma$, keeping Φ fixed, is

$$\delta W = VIdt = \frac{\Phi_0}{2\pi} I(\gamma,\Phi) d\gamma, \tag{3.5}$$

which following the same argument as previously leads to

$$\frac{\partial U(\gamma,\Phi)}{\partial \gamma} = \frac{\Phi_0}{2\pi} I(\gamma,\Phi). \tag{3.6}$$

Using equations (3.6) and (3.4), and the permutation of derivatives $\frac{\partial}{\partial \gamma}\left(\frac{\partial U}{\partial \Phi}\right) = \frac{\partial}{\partial \Phi}\left(\frac{\partial U}{\partial \gamma}\right)$, it follows that:

$$\frac{\partial I}{\partial \Phi} = \frac{2\pi}{\Phi_0}\frac{\partial J}{\partial \gamma}. \tag{3.7}$$

Relation (3.7) shows that the sensitivity of the interferometer to flux $\frac{\partial I}{\partial \Phi}$ is directly related to its back-action $\frac{\partial J}{\partial \gamma}$. In particular, a vanishing back-action $\frac{\partial J}{\partial \gamma}$=0 necessarily implies a vanishing sensitivity of the interferometer to flux. This indicates a fundamental relation between the sensitivity and the back-action of the interferometer.

3.2 AC-continuous readout

3.2.1 General principle

In the AC-continuous readout, a SQUID is driven by a small AC current $I_{ac}(t) = |I_{ac}|\cos(\omega t)$. As the driving amplitude $|I_{ac}|$ is much smaller than the critical current I_c, the SQUID acts as a linear inductance L_J which depends on the flux through the SQUID loop (see equation (1.7)). Placed in parallel with a capacitor C, it forms a harmonic oscillator whose resonance frequency $f_0 = \frac{1}{2\pi\sqrt{L_J(\Phi)C}}$ depends on the flux and so on the state of the qubit. The principle of such dispersive detector is rather generic and can be applied for the readout of different types of superconducting qubits [1, 2]. The oscillator is operated via a coaxial line of impedance $Z_0 = 50\,\Omega$ which determines the quality factor of the oscillator $Q = Z_0\sqrt{\frac{C}{L_J}}$. We assume that $Q >> 1$. The oscillator is equivalent to a parallel RLC circuit including the SQUID inductance $L_J(\Phi)$, the capacitor C and a resistor $R = Z_0$, driven with a current source I_{ac}.

For the readout, a microwave signal $V_{in} = |V_{in}|\cos(2\pi f_d t)$ with frequency f_d close to f_0 is send to the oscillator, and the phase α of the reflected signal

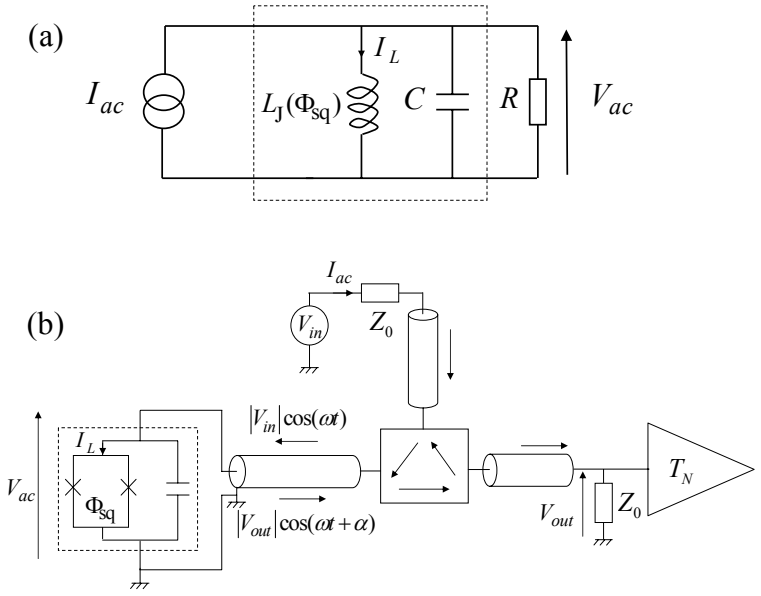


Figure 3.2: Dispersive AC-continuous readout with a DC-SQUID. (a) Equivalent RLC circuit. (b) Schematic of the measurement setup.

$V_{out} = |V_{out}| \cos(2\pi f_d t + \alpha)$ is measured. The amplitude and the phase of the reflected signal are given by the complex reflection coefficient:

$$\Gamma = \frac{Z - Z_0}{Z + Z_0}, \tag{3.8}$$

where Z is the impedance of the SQUID and the capacitor

$$\frac{1}{Z} = \frac{1}{jL_J\omega} + jC\omega, \tag{3.9}$$

and $\omega = 2\pi f_d$. As Z is purely imaginary, the power of the reflected signal is equal to the power of the incoming signal, i.e. $|\Gamma| = 1$ and $|V_{out}| = |V_{in}|$. All the information extracted by the detector is thus contained in the phase of the reflected microwave. As the resonance frequency depends on the flux Φ through the SQUID loop, a small change of Φ will slightly shift the resonance frequency and the phase α of the reflected signal. In the case of a small detuning between the driving frequency and the oscillator resonance frequency $\Delta f = f_0 - f_d << f_0$, the reflection coefficient is given to first order in Δf by

$$\Gamma \simeq 1 + 4jQ\frac{\Delta f}{f_0}. \tag{3.10}$$

Therefore, a change of the resonance frequency by Δf_0 results in a change of the phase of the reflected signal of

$$\Delta\alpha = 4Q\frac{\Delta f_0}{f_0}. \tag{3.11}$$

The amplitude of the reflected microwave signal is constant $|V_{out}| = \frac{|V_{ac}|}{2} = \frac{R|I_{ac}|}{2}$ and the current through the SQUID is $|I_L| = Q|I_{ac}|$.

3.2.2 Sensitivity

The sensitivity of the linear dispersive readout is limited by the noise generated in the resistor R. The minimum noise corresponds to the quantum limit

$$S_{\tilde{V}_{ac}}(f) = 2hfR\theta(f), \tag{3.12}$$

where $\theta(f) = 1$ if $f > 0$ and $\theta(f) = 0$ if $f < 0$. As the input impedance of the amplifier and the output impedance of the voltage source V_{in} are both matched to the impedance of the transmission line ($Z_0 = R$), the resulting voltage noise at the input of the amplifier is given by $S_{\tilde{V}_{out}} = S_{\tilde{V}_{ac}}/2$. In order to compare quantitatively the amplitude of the signal (3.11) with the amplitude of the noise (3.12), we include in our analysis an ideal mixer converting the AC output voltage V_{out} to a DC output voltage V_α, as shown in figure 3.3. The DC voltage is obtained by multiplying the AC output voltage $V_{out} = |V_{out}|\cos(\omega t + \alpha)$ with a reference AC voltage $V_{ref} = |V_{ref}|\sin(\omega t)$ using a mixer (we use the notation $\omega = 2\pi f_d$). The output voltage of the mixer is given by $V_{mix}(t) = kV_{ref}(t)V_{out}(t)$. The phase α is obtained from the DC average value of the mixer output voltage V_α using a low pass filter

$$V_\alpha = k|V_{ref}|\frac{|V_{out}|}{2}\sin\alpha \simeq \frac{|V_{out}|}{2}\alpha, \tag{3.13}$$

if $\alpha << 1$ and assuming that $k|V_{ref}| = 1$.

Note that this method does not extract optimally all the information about the phase of reflected signal. In fact the AC component of the output voltage of the mixer contains as much information as the DC component. Therefore, with

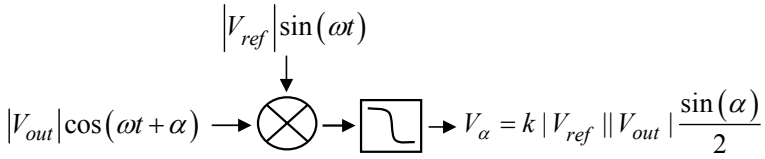


Figure 3.3: Extraction of the phase α of the AC output voltage using a mixer and a low pass filter.

this simple quadrature measurement, half of the information about the phase is lost.

A shift of the resonance frequency Δf_0 results in a difference of voltage

$$\Delta V_\alpha = \frac{|V_{out}|}{2}\Delta\alpha = RI_c\frac{I_L}{I_c}\frac{\Delta f_0}{f_0}. \tag{3.14}$$

The inductance of the SQUID is given by $L_J(\Phi) = \frac{\Phi_0}{2\pi}\left[2I_{c0}\cos(\pi\phi)\right]^{-1}$ with $\phi = \Phi/\Phi_0$. Therefore, a change of flux $\Delta\Phi$ causes a shift of the resonance frequency

$$\frac{\Delta f_0}{f_0} = \frac{1}{2}\frac{\Delta I_c}{I_c} = \frac{\pi\tan(\pi\phi)}{2}\frac{\Delta\Phi}{\Phi_0}, \tag{3.15}$$

The flux-to-voltage transfer function is thus

$$\lambda = \frac{\Delta V_\alpha}{\Delta\Phi} = \frac{RI_c}{2}\frac{\pi\tan(\pi\phi)}{\Phi_0}\frac{I_L}{I_c}. \tag{3.16}$$

The spectral density of the output of the mixer is given by the convolution of the noise spectral density of the AC output voltage with the spectral density of the AC reference voltage: $S_{mix}(f) = k^2\int_{-\infty}^{+\infty} S_{\tilde{V}_{out}}(f')S_{V_{ref}}(f-f')df'$. The spectral density of an ideal AC reference voltage: $V_{ref} = |V_{ref}|\sin(\omega t)$, is $S_{V_{ref}}(f) = \frac{|V_{ref}|^2}{2}\frac{\delta(f_0-f)+\delta(f_0+f)}{2}$, from which it follows that

$$S_{V_\alpha}(0) = \frac{Rhf_0}{4}. \tag{3.17}$$

Combining (3.16) and (3.17), the equivalent flux noise spectral density is

$$S_\Phi(0) \equiv \frac{S_{V_\alpha}(0)}{\lambda^2} = \frac{\hbar}{E_J}\frac{\Phi_0^2}{\pi^2\tan^2(\pi\phi)}\left(\frac{I_c}{I_L}\right)^2\frac{1}{Q}. \tag{3.18}$$

As mentioned in chapter 2, $S_\Phi(0)$ corresponds to the *fictitious* flux fluctuations that would lead to a noise level in the output voltage equal to (3.12). For typical parameters of the readout circuit, $I_c = 250$ nA, $I_L/I_c = 0.5$, $Q = 20$, $\phi = \Phi/\Phi_0 = 0.375$ we find $\sqrt{S_\Phi} = 7\ 10^{-8}\ \Phi_0/\sqrt{\text{Hz}}$.

In practice, however, the noise level of the microwave cryogenic amplifier used to record the SQUID voltage, characterized by its noise temperature T_N (defined as $S_V = 4k_BT_NZ_0$ with $Z_0 = 50\ \Omega$), is much higher than the quantum limit (commonly for $f_0 \simeq 2GHz$, $T_N \simeq 4$ K, two orders of magnitude higher than the quantum limit $\frac{hf_0}{2k_B}$). Therefore, the effective sensitivity of the readout is much lower, (in the case of detector with the parameters given previously, $\sqrt{S_\Phi} = 7\ 10^{-7}\ \Phi_0/\sqrt{\text{Hz}}$).

3.2.3 Back-action

The interaction Hamiltonian between the SQUID and the magnetic field source has the form $H_\Phi = \Phi J$, where J is the current circulating in the SQUID

loop and Φ is the magnetic flux generated by the source in the SQUID loop. The back-action of the detector is caused by fluctuations of the circulating current J, characterized by the noise spectral density

$$S_J(f) = \int_{-\infty}^{+\infty} < J(t)J(0) > e^{i2\pi ft} dt. \tag{3.19}$$

The fluctuations of J are directly related to the fluctuations of the SQUID transport current I_L. Using relations (1.9) and (1.10), J can be expressed as a function of I_L

$$J = \frac{I_c}{2} \tan(\pi\phi) \sqrt{1 - \left(\frac{I_L}{I_c}\right)^2}. \tag{3.20}$$

Noise generated by the resistor R causes fluctuations of I_L which in turn cause fluctuations of J. During the AC readout, the DC bias current through the SQUID is zero and $\frac{\partial J}{\partial I_L} = 0$. Thus J depends quadratically on I_L:

$$\Delta J = -\frac{\tan(\pi\phi)}{4I_c} I_L^2. \tag{3.21}$$

In general I_L is given by $I_L(t) = I_d(t) + I_n(t)$, where $I_d(t) = Q|I_{ac}| \cos\omega_0 t$ is the oscillating current induced by the driving of the oscillator and $I_n(t)$ is the fluctuation of I_L due to the resistor. The main contributions to the variations of J are given by

$$\Delta J(t) = -\frac{\tan(\pi\phi)}{4I_c} (I_d(t)^2 + 2I_d(t)I_n(t)) \tag{3.22}$$

where the first term $I_d(t)^2$ corresponds to deterministic oscillations of J due to the driving and the second term $I_d(t)I_n(t)$ represents the first order noise contribution, which is proportional to the driving amplitude. The noise spectral density S_J is thus given by the convolution of the spectral densities of I_d and I_n

$$S_J(0) = \frac{\tan^2(\pi\phi)}{4I_c^2} \int_{-\infty}^{+\infty} S_{I_d}(f') S_{I_n}(-f') df'. \tag{3.23}$$

For a driving amplitude I_{ac} at the oscillator resonance frequency $S_{I_d}(f) = Q^2|I_{ac}|^2 \left[\delta(f - f_0) + \delta(f + f_0)\right]/4$. Given the voltage noise spectral density (3.12), it follows that $S_{I_n}(f_0) = 2Q^2 h f_0 / R$ and

$$S_J(0) = \hbar E_J \frac{\pi^2 \tan^2(\pi\phi)}{\Phi_0^2} \left(\frac{I_L}{I_c}\right)^2 \frac{Q}{2}. \tag{3.24}$$

The fluctuation of J causes a variation of the qubit energy splitting which in turn induces dephasing of the qubit (see chapter 1). When the qubit is biased far from the degeneracy point, the qubit dephasing rate due to the fluctuation of J is given by:

$$\Gamma_\varphi = 2 \left(\frac{M I_p}{\hbar}\right)^2 S_J(0). \tag{3.25}$$

The driving of the oscillator also causes an oscillation of the qubit flux bias (due to the term in I_d^2 in equation (3.22)). For a given driving sequence, it results in an additional phase of the qubit. Note however, that this effect is deterministic and can be corrected. It does not leads to qubit dephasing.

Fluctuations of J at the qubit frequency might induce relaxation of the qubit during the measurement. However, provided the high frequency noise of the current through the SQUID is properly filtered in the range of the qubit frequency, qubit relaxation induced by the driving of the oscillator should be negligible.

Combining (3.18) and (3.24), we find that

$$S_\Phi(0)S_J(0) = \frac{\hbar^2}{2}. \tag{3.26}$$

This result shows that a DC-SQUID operated in the AC-continuous mode is nearly a quantum limited detector (the factor 2 missing compared to the quantum limit (2.8) is due to the fact that the simple quadrature measurement shown in figure 3.3 loses half of the information about the phase). In practice, however, the noise of the cryogenic amplifier used to measure the SQUID output voltage is a few orders of magnitude higher than the quantum limit for the noise (3.12).

The recent development of quantum limited parametric amplifiers based on superconducting circuits is very interesting and might allow in the near future to use AC-continuous detectors to perform quantum limited measurement of superconducting qubits [3, 4].

3.3 DC-switching readout

3.3.1 Principle

In the DC-switching readout, a SQUID is biased close to its critical current (corresponding to the maximum superconducting current it can hold), and might switch from a zero-voltage superconducting state (S) to a finite-voltage dissipative state (D). As the critical current of the SQUID depends on the flux through its loop, the switching probability of the SQUID depends on the flux.

The dynamics of the SQUID can be simply illustrated based on the analogy between a Josephson junction and a particle in a potential (figure 3.4). The phase γ across the junction corresponds to the position of the particle, while the voltage $V = \frac{\Phi_0}{2\pi}\frac{d\gamma}{dt}$ corresponds to its velocity. In the superconducting state, the particle resides in one of the potential well minima and $V \sim \frac{d\gamma}{dt} = 0$. When the SQUID is biased with a current close to its critical current, the height of the energy barrier separating two minima is very small and the particle might overcome the energy barrier either via thermal fluctuations or by quantum tunneling through the barrier. In this case, the particle starts to fall down in the potential and the velocity (or the SQUID voltage) increases until a equilibrium involving a dissipation mechanism is reached. In the case of a SQUID with

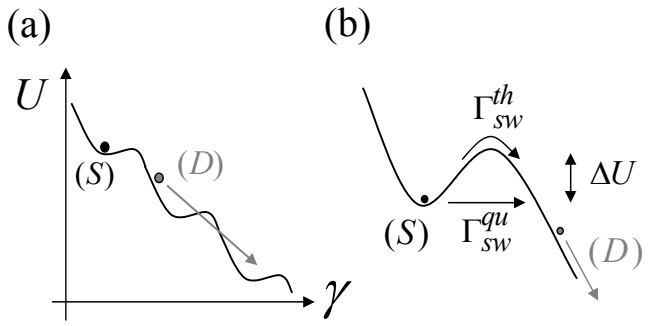


Figure 3.4: (a) Potential energy U of the SQUID as a function of the superconducting phase γ. Biased close to its critical current, the SQUID can switch from a zero-voltage state (S) where $d\gamma/dt = 0$ to a finite voltage dissipative state (D) where $d\gamma/dt \neq 0$. (b) Two switching mechanisms are possible either by overcoming the barrier energy via thermal fluctuations or by direct quantum tunneling through the barrier.

critical current I_c shunted with an external resistor R, the voltage in the dissipative state in on the order of $V_D \simeq RI_c$. In the case of an unshunted or weakly shunted SQUID, the value of the voltage in the dissipative state (D) is on the order of the superconducting gap, which in the case of aluminium is about 400 μV. The large difference of voltage between the two states (S) and (D) allows to discriminate efficiently the state of the detector.

The switching of the detector to state D either via quantum tunneling or thermal activation is a stochastic process described with a switching probability P. As the critical current of the SQUID depends on the flux through the SQUID loop, the switching probability depends on the flux. For the readout, a current pulse of amplitude $I_b \simeq I_c$ and duration t_{sw} is applied to the SQUID. The detector switching probability is given by

$$P(\Phi) = 1 - \exp\{-\Gamma_{sw}(\Phi)t_{sw}\}. \tag{3.27}$$

The switching rate Γ_{sw} can be evaluated in two different regimes [5]. In the thermal regime,

$$\Gamma_{sw}^{th} = f_0 \exp\left\{-\frac{U_0}{kT}\left[1 - \frac{I_b}{I_c}\right]^{3/2}\right\}, \tag{3.28}$$

where f_0 is the plasma frequency of the SQUID and $U_0 = \frac{4\sqrt{2}}{3}E_J$. In the quantum regime,

$$\Gamma_{sw}^{qu} = a_{qu} f_0 \exp\left\{-\frac{5}{36}\frac{U_0}{hf_0}\left[1 - \frac{I_b}{I_c}\right]^{3/2}\right\}, \tag{3.29}$$

where $a_{qu} = \sqrt{120\pi\frac{36}{5}\frac{U_0}{hf_0}}$. For simplicity, we neglect the dependence of the

plasma frequency on the bias current as it results only in a minor change of the SQUID sensitivity.

Note that equations (3.28) and (3.29) are valid if $\Gamma_{sw} << f_0/Q$. For the qubit readout however, the duration of the readout pulse is generally chosen as short as possible (commonly on the order of the SQUID response time $t_r = Q/f_0$) in order to avoid qubit relaxation and optimize the readout contrast. In this case, $\Gamma_{sw} \sim f_0/Q$. Equations (3.28) and (3.29) can be used to estimate the readout contrast, however, one should be cautious when using them in a quantitative manner for very short readout pulses.

3.3.2 Sensitivity

The flux sensitivity of the DC-switching readout can be compared to the sensitivity of the AC-continuous readout using formula (2.9) given the derivative of the switching probability to flux $dP(\Phi)/d\Phi$ (taking a bias point such that $P(\Phi) = 50$ %) and the measurement repetition period t_{rep}.

From equations (3.27) and (3.28), it follows

$$\frac{dP(\Phi)}{d\Phi} = \frac{3\ln 2}{4}\frac{36}{5}\frac{U_0}{hf_0}\sqrt{1-\frac{I_b}{I_c}}\frac{I_b}{I_c}\frac{1}{I_c}\frac{dI_c(\Phi)}{d\Phi} \tag{3.30}$$

and

$$\left[1-\frac{I_b}{I_c}\right] = \left(\frac{U_0}{kT}\right)^{-2/3}\left[\frac{36}{5}\ln\frac{t_{sw}f_0a_{qu}}{\ln 2}\right]^{-2/3}. \tag{3.31}$$

From the dependence of the SQUID critical current on the flux, $I_c(\Phi) = 2I_{c0}\cos(\pi\phi)$ with $\phi = \Phi/\Phi_0$ we have

$$\frac{1}{I_c}\frac{dI_c(\Phi)}{d\Phi} = \frac{\pi\tan(\pi\phi)}{\Phi_0}. \tag{3.32}$$

Combining the previous results and using the notation $t = \frac{t_{sw}\omega_0}{Q}$, we find

$$\frac{dP(\Phi)}{d\Phi} = \left(\frac{E_J}{hf_0}\right)^{2/3}\frac{\pi\tan(\pi\phi)}{\Phi_0}x_{qu}, \tag{3.33}$$

where $x_{qu} = \frac{3\ln 2}{4}\left[\frac{36}{5}\frac{4\sqrt{2}}{3}\right]^{2/3}\left[\ln\frac{a_qQt}{2\pi\ln 2}\right]^{1/3}$.

Based on formula (2.9), and for a measurement repetition period $t_{rep} = 2t_{sw}$ the effective sensitivity of the DC-switching readout in the quantum regime is

$$S_\Phi^{qu} = \frac{\hbar}{E_J}\frac{\Phi_0^2}{\pi^2\tan^2(\pi\phi)}\left(\frac{hf_0}{E_J}\right)^{1/3}\frac{Qt}{2x_{qu}^2}. \tag{3.34}$$

For typical parameters of the readout circuit, $I_c = 250$ nA, $f_0 = 1.5$ GHz, $Q = 20$, $t = 5$ (corresponding to $t_{sw} = 70$ ns and $t_{rep} = 140$ ns), and $\phi = \Phi/\Phi_0 = 0.375$ we find $\sqrt{S_\Phi^{qu}} = 10^{-7}\ \Phi_0\sqrt{\text{Hz}}$

In practice, the quantum regime is very difficult to reach as it requires an effective temperature $kT < \frac{5}{36} hf_0$, much lower than the plasma frequency. In the thermal regime, the sensitivity of the DC-switching readout is

$$S_\Phi^{th} = \frac{\hbar}{E_J} \frac{\Phi_0^2}{\pi^2 \tan^2(\pi\phi)} \frac{kT}{hf_0} \left(\frac{kT}{E_J}\right)^{1/3} \frac{Qt}{2x_{th}^2}, \tag{3.35}$$

where $x_{th} = \frac{3\ln 2}{4} \left[\frac{4\sqrt{2}}{3}\right]^{2/3} \left[\ln \frac{Qt}{2\pi \ln 2}\right]^{1/3}$. For a noise temperature $T_{eff} \simeq 150$ mK, the effective sensitivity of the readout circuit with the previous parameters is $\sqrt{S_\Phi^{th}} = 7\ 10^{-7}\ \Phi_0\sqrt{\text{Hz}}$.

The readout contrast is directly related to the derivative of the switching probability to flux: $C = \frac{dP(\Phi)}{d\Phi}\Delta\Phi$. Given the previous parameters of the circuit and for a difference of flux of $\Delta\Phi = 5\ \text{m}\Phi_0$, the readout contrast in the thermal regime should be 50%. Note that C can be enhanced by increasing I_c.

The effective sensitivity of the DC-switching readout could be considerably improved and reach the quantum regime using a higher plasma frequency such that $hf_0 > \frac{35}{6} kT$. In the case that $T_{eff} \simeq 150$ mK, it would require a plasma frequency $f_0 \simeq 20$ GHz. Note that the contrast of a single readout would not be significantly improved. The effective sensitivity of the detector would be higher because a single readout could be completed much faster: ideally a total measurement time on the order of 1 ns should be possible. Note that, as the difference of voltage between the two states of the SQUID in the DC-switching readout can be very large, the state of the SQUID can be determined extremely fast using a cryogenic amplifier.

3.3.3 Back-action

In the previous section, we estimated the intrinsic sensitivity of the DC-switching readout in the ideal case where successive measurements do not influence each other, allowing for very high measurement repetition rates. In practice, however, the back-action of the DC-switching readout is very strong.

In general, three main effects can be distinguished. First, heating due to the dissipation in the SQUID and local resistive elements leads to additional noise. The dissipated energy also leads to an increased temperature of substrate and qubit. Secondly, when the SQUID is at a nonzero voltage, the AC Josephson effect gives rise to currents at frequencies of tens to hundreds of GHz, which couple into the qubit and may cause non-adiabatic transitions and quantum leakage to higher levels. Finally, the generation of quasiparticles in the SQUID junctions if the voltage is larger than the superconducting gap deteriorates the superconducting properties. Quasiparticle generation in the qubit by transferred RF fields, and by direct diffusion when the qubit is galvanically attached, is detrimental to qubit performance. As quasiparticle recombination and heat relaxation are slow at low temperatures, the recuperation times for SQUID and qubit between successive readouts is very long, commonly limiting the measurement repetition rate to a few tens of kHz. As $\sqrt{S_\Phi}$ scale as

$\sqrt{t_{rep}}$ (see equation (2.9)), this effect reduces considerably the effective sensitivity of the SQUID. In the example discussed previously, it would be about $\sqrt{S_\Phi} \simeq 10^{-4}..10^{-3}\ \Phi_0/\sqrt{\text{Hz}}$.

In chapter 5, we will show that the back-action of the DC-switching readout can be considerably reduced by lowering the switching voltage and using a fast cryogenic amplifier, allowing for much higher measurement repetition rates. One effect, however, can hardly be avoided: the non-adiabatic shift of the qubit bias due to the high frequency Josephson oscillations of the current in the SQUID when a DC voltage is present across the SQUID. Commonly, in the case of a DC-switching readout with a large contrast, the amplitude of the qubit frequency shift is on the order of $g \simeq MI_pI_c/h \simeq 10$ GHz [6, 7]. As the frequency of the Josephson oscillations is much larger than the separation of the qubit avoided crossing at the degeneracy point ($\Phi_{ext} = \Phi/2$), it can induces Landau-Zener transitions between the two energy levels of the qubit if the amplitude of the qubit shift is large enough to cross the degeneracy point (see3.5b)). The qubit can also be excited resonantly to higher energy levels (as shown in figure 3.5a). Finally, one can expect that the large oscillation of the qubit bias can enhance the qubit relaxation similarly to the case of the AC-switching readout (see chapter 4).

As can be seen from the relation (3.7), the amplitude of the qubit bias shift due to the AC-Josephson effect (which is proportional to the amplitude of the oscillation of the SQUID circulating current J) is directly related to the sensitivity of the detector. The oscillation of the qubit shift due to the AC-Josephson effect can not vanish unless the sensitivity of the detector is nul. However, it can be reduced using a smaller value of the qubit-SQUID interaction. In this case the readout contrast would also be smaller. For a readout circuit

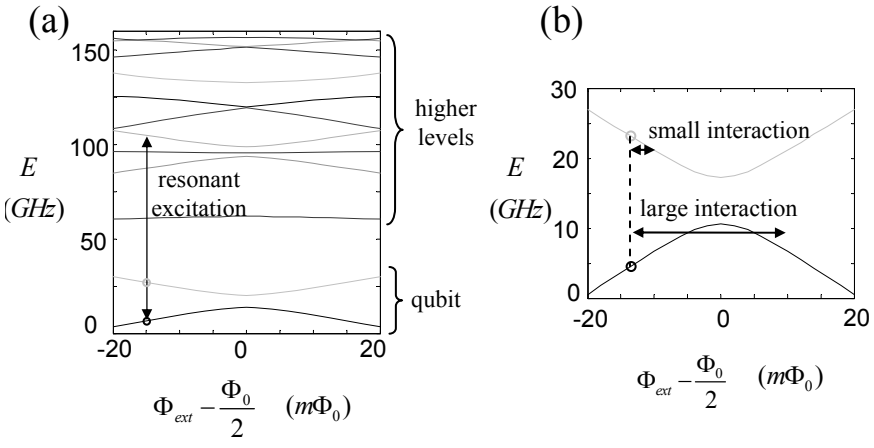


Figure 3.5: (a) Energy spectrum of the flux qubit. (b) Amplitude of the oscillation of the qubit flux bias (due to the AC-Josephson effect) during the measurement in the case of a large or small qubit-SQUID interaction.

with the same parameters as in the previous section ($I_c = 250$ nA, $T_{eff} = 150$ mK, $f_0 = 1.5$ GHz), and a difference of flux $2MI_p \simeq 3$ mΦ_0 between the two states of the qubit, the qubit-SQUID interaction is $2MI_pI_c/h \simeq 1$ GHz and the readout contrast should be about 30 %.

3.4 AC-switching readout

3.4.1 General principle

The AC-switching readout is based on a circuit very similar to the AC-continuous readout, with a driven oscillator including a SQUID, whose resonance frequency depends on the flux through the SQUID loop. However, in this readout scheme, the oscillator is driven more strongly, such that $I_L \simeq I_c$, resulting in a nonlinear response of the Josephson inductor [8, 9]. Taking into account the first nonlinear term in the SQUID inductance, the equation of motion for the superconducting phase γ of the SQUID is

$$\frac{d^2\gamma}{dt^2} = \omega_0^2\gamma - \frac{\omega_0}{Q}\frac{d\gamma}{dt} - \frac{\omega_0^2}{6}\gamma^3 + \frac{I_{ac}}{I_c}\cos\omega t. \tag{3.36}$$

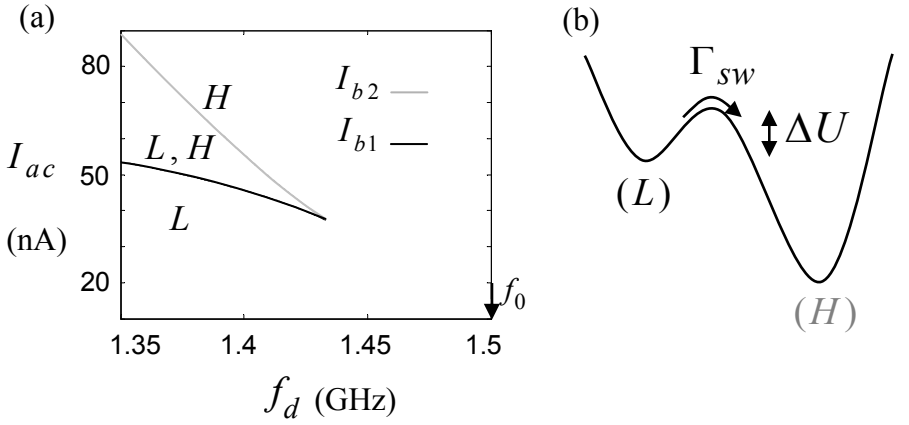


Figure 3.6: (a) Bistability diagram of the driven nonlinear oscillator, in the case $f_0 = 1.5$ GHz, $Q = 20$ and $I_c = 1$ μA. For a driving amplitude $I_{ac} < I_{b1}$ the oscillator is in the state L. For a driving amplitude $I_{ac} > I_{b2}$ the oscillator is in the state H. For a driving amplitude $I_{b1} < I_{ac} < I_{b2}$ the oscillator is either in state L or in state H. (b) Effective potential of the oscillator in the bistable regime.

Below a critical driving frequency $\omega < (1 - \frac{\sqrt{3}}{2Q})\omega_0$, and in a certain range of driving amplitude $I_{b1}(\omega) < I_{ac} < I_{b2}(\omega)$, two oscillatory solutions for (3.36)

exist with either a low oscillation amplitude, denoted as state L, or a high oscillation amplitude, denoted as state H. I_{b1} and I_{b2}, shown in figure 3.6, are given by [10]:

$$\frac{I_{b1/2}}{I_c} = \frac{16}{3\sqrt{3}}\alpha^{3/2}\frac{1}{\sqrt{2}}\sqrt{1+\frac{9}{4\alpha^2Q^2} \pm \left(1-\frac{3}{4\alpha^2Q^2}\right)^{3/2}} \tag{3.37}$$

where

$$\alpha = \frac{\omega_0 - \omega}{\omega_0} > \frac{\sqrt{3}}{2Q} \tag{3.38}$$

is the detuning between the driving frequency and the oscillator resonance frequency. For values of the detuning much larger than the critical detuning $\alpha_c = \frac{\sqrt{3}}{2Q}$, the threshold amplitude I_{b2} reduces to

$$I_{b2} = \frac{16}{3\sqrt{3}} I_c \alpha^{3/2}. \tag{3.39}$$

For the readout, the SQUID is driven with a driving amplitude I_{ac} close to the threshold of disappearance of the L state I_{b2}. The oscillator can switch from the state L to the state H with a probability $P(H)$. Similarly to equation (3.27), the detector switching probability for a pulse of duration t_{sw} is

$$P(\Phi) = 1 - \exp\{-\Gamma_{sw}(\Phi)t_{sw}\}, \tag{3.40}$$

where the switching rate Γ_{sw} in the thermal regime is given by [10]

$$\Gamma_{sw} = \Gamma_0 \exp\left\{-\frac{U_0}{kT}\left[1-\left(\frac{I_{ac}}{I_{b2}}\right)^2\right]^{3/2}\right\}, \tag{3.41}$$

with $U_0 = \frac{128}{18\sqrt{3}}E_J\alpha$ and $\Gamma_0 = \frac{1}{\sqrt{3}}\frac{\omega_0}{Q}\left(\frac{\alpha}{\alpha_c}\right)^2\sqrt{1-\left(\frac{I_{ac}}{I_{b2}}\right)^2}$.

Similarly to the DC-switching readout, equation (3.41) is valid if $\Gamma_{sw} << f_0/Q$. As the duration of the readout pulse is commonly on the order of the SQUID response time this implies that $\Gamma_{sw} \sim f_0/Q$. Equation (3.41) can be used to estimate the readout contrast, however as before, one should be cautious when using it in a quantitative manner for very short readout pulses.

3.4.2 Sensitivity

In order to determine the sensitivity of the AC-switching readout, we follow the same approach as in section 3.3.2 and calculate the first derivative of the switching probability with respect to the flux (taking a bias such that $P(\Phi) = 0.5$). From equations (3.40) it follows that

$$\frac{dP(\Phi)}{d\Phi} = \frac{3\ln 2}{2}\frac{U_0}{hf_0}\sqrt{1-\left(\frac{I_{ac}}{I_{b2}}\right)^2}\left(\frac{I_{ac}}{I_{b2}}\right)^2\frac{1}{I_{b2}}\frac{dI_{b2}(\Phi)}{d\Phi} \tag{3.42}$$

and

$$\left[1-\left(\frac{I_{ac}}{I_{b2}}\right)^2\right]=\left(\frac{U_0}{kT}\right)^{-2/3}\left[\ln\frac{\Gamma_0 t_{sw}}{\ln 2}\right]^{-2/3}. \tag{3.43}$$

Equation (3.39) leads to

$$\frac{1}{I_{b2}}\frac{dI_{b2}(\Phi)}{d\Phi}=\frac{1}{I_c}\frac{dI_c(\Phi)}{d\Phi}\frac{3}{4\alpha}=\frac{\pi\tan(\pi\phi)}{\Phi_0}\frac{3}{4\alpha}. \tag{3.44}$$

Combining the previous results and using the notation $t = t_{sw}\omega_0/Q$ and $d = \alpha/\alpha_c$, we find

$$\frac{dP(\Phi)}{d\Phi}=x\left(\frac{E_J}{kT}\right)^{2/3}\frac{\pi\tan(\pi\phi)}{\Phi_0}\left(\frac{Q}{d}\right)^{1/3}, \tag{3.45}$$

where $x=\frac{3\ln 2}{2}\frac{3}{4}\left[\frac{128}{18\sqrt{3}}\right]^{2/3}\left[\frac{2}{\sqrt{3}}\ln\left(\frac{td^2}{\sqrt{3}\ln 2}\right)\right]^{1/3}$.

Based on equation (2.9), for a measurement repetition period $t_{rep} = 2t_{sw}$, the effective sensitivity of the AC-switching readout in the thermal regime is

$$S_\Phi^{th}=\frac{\hbar}{E_J}\frac{\Phi_0^2}{\pi^2\tan^2(\pi\phi)}\frac{kT}{\hbar\omega_0}\left(\frac{kT}{E_J}\right)^{1/3}\frac{Q^{1/3}d^{2/3}t}{2x^2}. \tag{3.46}$$

For a noise temperature of $T_{eff} \simeq 150$ mK, the effective sensitivity of the readout circuit with the previous parameters would be $\sqrt{S_\Phi} = 1.3\ 10^{-7}\ \Phi_0\sqrt{\text{Hz}}$.

The readout contrast is directly related to the derivative of the switching probability to flux: $C = \frac{dP(\Phi)}{d\Phi}\Delta\Phi$, and therefore can be estimated using equation (3.45). Given the previous parameters of the circuit and for a difference of flux of $\Delta\Phi = 1\ \text{m}\Phi_0$, the readout contrast in the thermal regime should be 50%.

In the quantum regime, switching occurs via quantum activation [11]. The term kT is then replaced by $\frac{\hbar\omega_0}{2}$

$$S_\Phi^{qu}=\frac{\hbar}{E_J}\frac{\Phi_0^2}{\pi^2\tan^2(\pi\phi)}\left(\frac{\hbar\omega_0}{E_J}\right)^{1/3}\frac{Q^{1/3}d^{2/3}t}{2x^2 2^{4/3}}. \tag{3.47}$$

For typical parameters of the readout circuit, $I_c = 250$ nA, $f_0 = 1.5$ GHz $Q = 20$, $t = 5$, $d = 2$ and $\phi = \Phi/\Phi_0 = 0.375$ we find $\sqrt{S_\Phi^{qu}} = 6\ 10^{-8}\ \Phi_0\sqrt{\text{Hz}}$.

3.4.3 Back-action

A clear advantage of the AC-switching readout compared to the DC-switching readout is that there is no dissipation in the superconducting circuit itself (all the dissipation is localized in the input resistance of the cryogenic amplifier). Therefore the back-action of the AC-switching readout is much lower than the DC-switching readout. Due to the highly nonlinear dynamics of the SQUID in the AC-switching readout, a quantitative calculation of the back-action is difficult.

As we will see in chapter 4, the qubit relaxation is strongly enhanced by the operation of the detector. When the oscillator is in state H, the qubit relaxation can be one order of magnitude faster than when the oscillator is in state L [12]. Furthermore, the qubit relaxation when the oscillator is in state L increases rapidly close to the bifurcation threshold. This observation is in good qualitative agreement with some theoretical calculations of the qubit relaxation when the oscillator is driven in the bistability regime [13].

Experiments with two AC-switching detectors relatively close to each other have shown that the crosstalk between the two detectors can be very low [14].

3.5 Summary

In this chapter, we have analyzed the sensitivity and the back-action of the DC-SQUID operated in different modes: AC-continuous, DC-switching and AC-switching. We found that the intrinsic sensitivity of the SQUID is on the same order of magnitude in all modes of operation. However, in practice, in each readout method, the effective sensitivity of the SQUID is generally lower than the intrinsic sensitivity of the SQUID.

In the case of the AC-continuous readout, the output voltage of the SQUID is small compared to the noise level of the following cryogenic amplifier, reducing the effective sensitivity of the SQUID by about one order of magnitude. However, one important advantage of the AC-continuous readout is that its back-action is minimal. Recent development of nearly quantum limited amplifiers at microwave frequencies might allow, in the near future, to perform quantum limited measurements of superconducting qubits.

In the AC-switching and DC-switching readout, the difference of voltage between the two states of the detector is very large. Therefore the constraints on the noise of the following amplifier are smaller. Instead, the sensitivity of switching detectors is mostly limited by the effective temperature of the SQUID determining the switching probability of the detector. In the case of a SQUID with low plasma frequency ($\simeq$ 1 GHz) and an effective temperature of about 150 mK, we found that the contrast of the AC-switching readout can be much larger than the DC-switching readout for similar parameters of the readout circuit. However, provided the SQUID plasma frequency is higher (about 20 GHz), the sensitivity of the DC-switching readout should be comparable to the AC-switching readout.

One important issue of the DC-switching readout is its back-action when the SQUID is in the dissipative state D. This commonly limits the measurement repetition frequency to few tens of kHz and therefore reduces the effective sensitivity of the SQUID by few orders of magnitude. In chapter 5, however, we will see that the back-action of the DC-switching readout in its dissipative state can be considerably reduced by reducing the switching voltage and using a fast cryogenic amplifier.

Bibliography

[1] A. Wallraff, D.I. Schuster, A. Blais, L. Frunzio, J. Majer, M.H. Devoret, S.M. Girvin, R.J. Schoelkopf, *Approaching Unit Visibility for Control of a Superconducting Qubit with Dispersive Readout* Physical Review Letters, **95**, 060501 (2005)

[2] A. Lupaşcu, C.J.M. Verwijs, R.N. Schouten, C.J.P.M. Harmans, J.E. Mooij, *Nondestructive Readout for a Superconducting Flux Qubit*, Physical Review Letters, **93**,177006 (2004)

[3] M.A. Castellanos-Beltran, K.D. Irwin, G.C. Hilton, L.R. Vale, K.W. Lehnert, *Amplification and squeezing of quantum noise with a tunable Josephson metamaterial*, Nature Physics **4**, 929 (2008)

[4] N. Bergeal, F. Schackert, M. Metcalfe, R. Vijay, V.E. Manucharyan, L. Frunzio, D.E. Prober, R.J. Schoelkopf, S.M. Girvin, M.H. Devoret *Phase-preserving amplification near the quantum limit with a Josephson ring modulator*, Nature **465** 64 (2010)

[5] J.M. Martinis, M.H. Devoret, J. Clarke, *Experimental tests for the quantum behavior of a macroscopic degree of freedom: The phase difference across a Josephson junction*, Physical review B **35**, 10 (1987)

[6] F. Yoshihara, K. Harrabi, A.O. Niskanen, Y. Nakamura, J.S. Tsai, *Decoherence of Flux Qubits due to 1/f Flux Noise*, Physical Review Letters **97**, 167001 (2006)

[7] I. Chiorescu, Y. Nakamura, C.J.P.M. Harmans, J.E. Mooij, *Coherent Quantum Dynamics of a Superconducting Flux Qubit* Science **299**, 1869 (2003)

[8] I. Siddiqi, R. Vijay, F. Pierre, C.M. Wilson, M. Metcalfe, C. Rigetti, L. Frunzio, M.H. Devoret, *RF-Driven Josephson Bifurcation Amplifier for Quantum Measurement*, Physical Review Letters **93**, 207002 (2004)

[9] A. Lupaşcu, E.F.C. Driessen, L. Roschier, C.J.P.M. Harmans, J.E. Mooij, *High-Contrast Dispersive Readout of a Superconducting Flux Qubit Using a Nonlinear Resonator*, Physical Review Letters, **96**, 127003 (2006)

[10] M.I. Dykman and M.A. Krivoglaz, *Fluctuations in nonlinear systems near bifucartions corresponding to the appearance of new stable states*, Physica **104A**, 480 (1980)

[11] M.I. Dykman, *Critical exponents in metastable decay via quantum activation*, Physical Review E **75**, 011101 (2007)

[12] T. Picot, A. Lupaşcu, S. Saito, C.J.P.M. Harmans, J.E. Mooij, *Role of relaxation in the quantum measurement of a superconducting qubit using a nonlinear oscillator* Physical Review B **78**, 132508 (2008)

[13] I. Serban, M.I. Dykman, F.K. Wilhelm, *Relaxation of a qubit measured by a driven Duffing oscillator*, Physical Review A, **81**, 022305 (2010)

[14] P.C. de Groot, A.F. van Loo, J. Lisenfeld, R. N. Schouten, A. Lupaşcu, C.J.P.M Harmans, J.E. Mooij, *Low-crosstalk bifurcation detectors for coupled flux qubits*, Applied Physics Letters **96**, 123508 (2010)

Chapter 4

QND measurement with the AC-switching readout

T. Picot, A. Lupaşcu, S. Saito, C.J.P.M. Harmans, J.E. Mooij

We investigate the readout of a superconducting qubit using a nonlinear oscillator comprising a DC-SQUID driven in the bifurcation regime, acting as an AC-switching dispersive detector. By carrying out two consecutive readouts, we show that a quantum nondemolition measurement of a superconducting qubit can be performed with a QND fidelity of 88 %. The strong correlation between the measurement outcomes reveals the highly projective character of measurement. Secondly, we introduce a simple model to analyze the evolution of the qubit and the detector during the measurement, including the qubit relaxation and the oscillator switching process. We find that qubit relaxation increases significantly due to the operation of the detector. Corrected for qubit relaxation and initial qubit preparation errors, the readout fidelity is at least 95 %.

The main results of this chapter were published in Nature Physics **3**, 119 (2007) and Physical Review B **78**, 132508 (2008)

4.1 Introduction

During the last decade, low back-action detectors have been developed for the readout of superconducting qubits based on dispersive coupling with an oscillator [1, 2]. In chapter 3, we presented two types of dispersive detectors for the readout of the flux qubit: the AC-continuous readout and the AC-switching readout. In the AC-continuous readout, the SQUID is driven with a small AC current such that it behaves as an harmonic oscillator. As we saw in section 3.2.3, the back-action of this detector is so small that it can reach the minimum imposed by the Heisenberg uncertainty principle. However, in practice, the sensitivity is limited by the noise of the cryogenic microwave amplifier used to monitor the SQUID voltage. Driving the oscillator more strongly into its nonlinear regime results in higher sensitivities and faster measurements [3]. In the AC-switching readout, the SQUID is driven across its bifurcation threshold acting as a switching detector which can lead to very high measurement contrast [4].

In this chapter, we study the quantum nondemolition (QND) character of the AC-switching readout and analyze the role of qubit relaxation during the measurement. In section 4.2, we present the experimental setup and the basic properties of the qubit and the detector. In section 4.3, we describe the experiment to analyze the QND character and projectiveness of the measurement based on a sequence of two consecutive readouts. Finally, in section 4.4, we introduce a simple model to analyze the evolution of the qubit and the detector during the measurement and quantify the errors due to qubit relaxation during the measurement.

4.2 Sample design and experimental setup

4.2.1 Readout circuit and measurement setup

The detector is an oscillator formed by a SQUID with Josephson inductance $L_J = \phi_0/(2\pi I_c)$ in series with a small stray inductance $L_s = 80$ pH and shunted with a large capacitor $C = 37$ pF (see figures 4.1a-b). Each junction of the SQUID has a critical current I_{c0}=2 μA. The principle of the AC-switching readout, discussed in detail in chapter 3, is based on the dependence of the SQUID Josephson inductance on the flux through the SQUID loop (associated with the modulation of the critical current) which in turn causes a shift of the oscillator resonance frequency $f_0 = 1/\{2\pi\sqrt{(L_J + L_s)C}\}$. In contrast with the AC-continuous readout, the oscillator is driven with a strong amplitude into a highly nonlinear regime where the oscillator can be bistable and acts as a switching detector. For the readout of the qubit, the SQUID is biased at a flux such that $f_0 = 1.5$ GHz.

The measurement consists of sending a microwave pulse to the oscillator with a frequency f_d slightly lower than f_0 and detecting the microwave signal reflected. As there is no dissipation in the SQUID, the amplitudes of the incom-

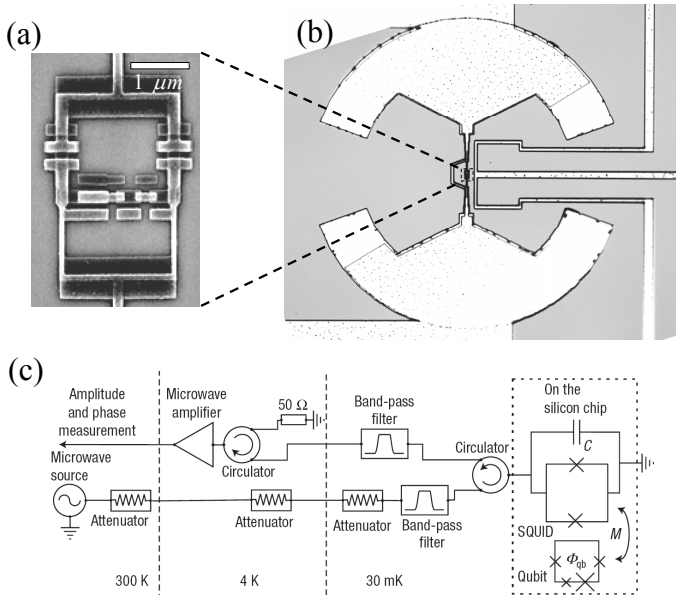


Figure 4.1: (a) Scanning electron microscopy picture of the SQUID and qubit. (b) Optical picture of the readout circuit. (c) Schematic of the measurement setup

ing and reflected microwaves are equal. All the information extracted by the detector is thus contained in the phase α of the reflected microwave. The setup of the readout circuit is shown in figure 4.1c. The microwave pulse, generated by modulating the amplitude of a microwave source, is attenuated at the different temperature stages inside the dilution refrigerator in order to reduce the thermal noise. A circulator placed at the lowest temperature of the cryostat (30 mK) allows to separate the injected and reflected microwaves. This circulator is an important element of the readout circuit which allows to transmit the signal reflected by the oscillator to the microwave amplifier with very low loss, while strongly attenuating the noise arriving from the readout line to the sample. A second circulator, placed at the 4 K temperature stage, reduces the reflection at the amplifier input and further suppresses noise. The overall detection noise is determined by the noise of the cryogenic amplifier characterized by a noise temperature of about $T_n \simeq 3$ K. The reflected microwave from the resonator is further amplified at room temperature and the phase α is obtained by mixing with a reference signal.

In the AC-switching readout, the oscillator is driven with an amplitude I_{ac} into a regime where it becomes bistable. The two possible states of the oscillator,

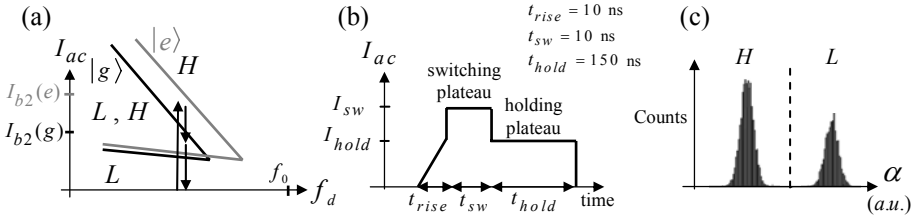


Figure 4.2: (a) Bifurcation diagram of the nonlinear oscillator for the two cases where the qubit is in state $|g>$ or $|e>$. (b) Oscillator driving amplitude for qubit readout. (c) Typical histogram of the phase α of the reflected microwave for a holding plateau of duration $t_{hold} = 150$ ns.

denoted as L and H, have a low or a high oscillation amplitude. Figure 4.2a shows the oscillator bistability diagram with the two bifurcation thresholds I_{b1} and I_{b2}. Three situations are possible depending on the value of I_{ac} compared with I_{b1} and I_{b2}. For weak driving $I_{ac} < I_{b1}$ the oscillator is in state L. For strong driving $I_{ac} > I_{b2}$ the oscillator is in state H. For intermediate driving, $I_{b1} < I_{ac} < I_{b2}$ the oscillator is bistable and can be in either of the L/H states. Due to the dependence of the Josephson inductance on the flux through the SQUID, I_{b2} strongly depends on the flux and so on the state of the qubit. We denote $I_{b2}(e)$ and $I_{b2}(g)$ as the values of I_{b2} when the qubit is in state $|e>$ or $|g>$. For the qubit readout, the oscillator is driven with an amplitude I_{sw} such that $I_{b2}(g) < I_{sw} < I_{b2}(e)$, where it might switch to the state H with a probability P which depends on the state of the qubit. Denoting the oscillator switching probabilities when the qubit is in state $|g>$ or $|e>$ as $P(g)$ and $P(e)$ and defining the readout contrast as $C_m = P(e) - P(g)$, the switching probability P for a general qubit state $|\Psi>$ with an excited state occupation probability $p(e)$ is given by

$$P = P(g) + C_m p(e) \tag{4.1}$$

To optimally discriminate between the two states of the oscillator, noise from the detection electronics needs to be averaged out. This is performed during the holding plateau (figure 4.2b) for a duration t_{hold} where the driving amplitude is decreased to a level such that both oscillator states can be maintained without switching or retrapping. Figure 4.2c shows a typical histogram of the phase α of the reflected microwave obtained with $t_{hold} = 150$ ns and $N = 10^4$ identical readout sequences, allowing to discriminate the two states of the oscillator with a fidelity of 99.99 %.

4.2.2 Effective temperature of the oscillator

As explained in chapter 3, the sensitivity of the AC-switching readout depends on the effective temperature of the detector T_{eff}. To characterize it we measure the switching probability as a function of the driving amplitude I_{sw} for

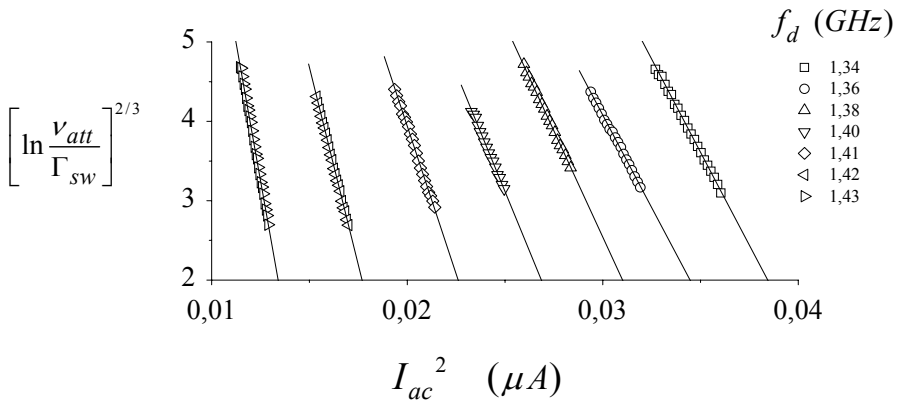


Figure 4.3: $\left[\ln\left(\frac{\nu_{att}}{\Gamma_{sw}}\right)\right]^{2/3}$ as a function of the square of the amplitude of the driving current for different values of the driving frequency f_d. Solid lines are linear fitting curves allowing to extract the effective temperature T_{eff} as defined in equation (4.2). In these measurements the resonance frequency of the oscillator is $f_0 = 1.59$ GHz

different values of the detuning α. The readout pulse has a switching plateau of duration $t_{sw} = 200$ ns much longer than in a typical qubit readout pulse (where $t_{sw} \simeq 10$ ns), such that t_{sw} is much longer than the oscillator response time $t_r = Q/f_0 = 13$ ns. In this case, the switching probability is given by $P_{sw} = 1 - \exp(-\Gamma_{sw} t_{sw})$, where the switching rate in the thermal regime is given by [5]

$$\Gamma_{sw} = \nu_{att} \exp\left(-\frac{\Delta U}{kT_{eff}}\right). \tag{4.2}$$

$\Delta U = U_0[1-(I_{ac}/I_{b2})^2]^{3/2}$ is the effective potential barrier (with $U_0 = 7.1\alpha E_J$) and $\nu_{att} = 0.77 f_0 Q\alpha^2\sqrt{1-(I_{ac}/I_b)^2}$ the attempt frequency; $\alpha = (f_d - f_0)/f_0$ is the detuning between the driving frequency f_d and the resonance frequency f_0.

The switching rate Γ_{sw} is obtained from the switching probability for a fix switching plateau duration. In figure 4.3, we plot $[\ln \nu_{att}/\Gamma_{sw}]^{2/3}$ as a function of I_{sw}^2. From equation (4.2) and the dependence of ΔU on I_b, one finds that $[\ln \nu_{att}/\Gamma_{sw}]^{2/3}$ depends linearly on I_{sw}^2. From a linear fit, we obtain the ratio U_0/kT_{eff} and deduce an effective temperature of $T_{eff} = 100 \pm 20$ mK similar for all values of the detuning α.

4.2.3 Qubit properties

The qubit is characterized by a persistent current $I_p = 340$ nA and a quantum tunneling energy $\Delta = h \times 5$ GHz, obtained from spectroscopy measurements (shown in figure 4.4b). In the following, the qubit is operated at a frequency $F_{qb} = 14.2$ GHz. Figure 4.4c shows the switching probability as a function of the amplitude of the driving current during the switching plateau I_{sw} when the qubit is prepared in state $|g>$ or $|e>$. The two bifurcation currents $I_{b2}(g)$ and $I_{b2}(e)$ can be resolved remarkably well. The optimal driving amplitude for the readout of the qubit is $I_{sw}^{opt} = 115$ nA, where $P(g) = 99.7$ % and $P(e) = 14.6$ %, resulting in a readout contrast of 85 %. Based on the period $T = 3.2$ ns and the decay time $\tau = 15$ ns of the Rabi oscillations, shown in figure 4.4d, we estimate the loss of contrast due to qubit state preparation errors to be 5 %. The fact that the main loss of readout contrast occurs when the qubit is in the excited

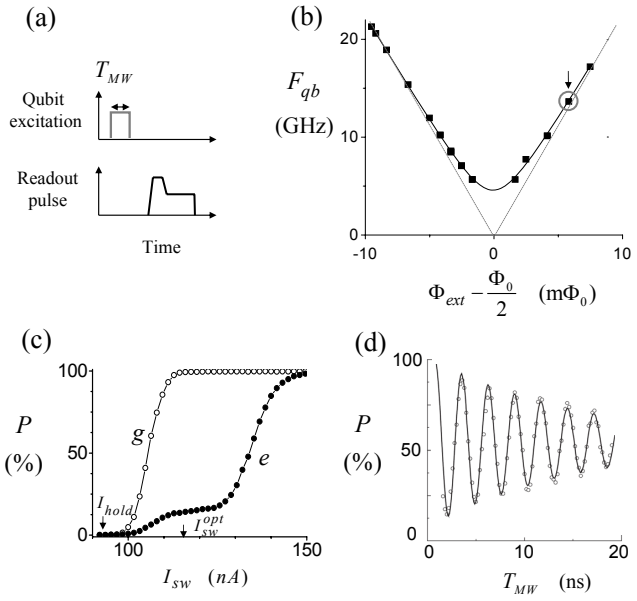


Figure 4.4: (a) Qubit excitation and readout sequence. (b) Qubit frequency F_{qb} as a function of the flux bias $\Phi_{ext} - \Phi_0/2$. The arrow indicates the external flux bias used in the experiments presented in this chapter. (c) Switching probability as a function of the amplitude of the driving current during the switching plateau. The optimal readout contrast $C_m = 85$ % occurs at a driving current $I_{sw}^{opt} = 115$ nA. (d) Switching probability as a function of the length of the excitation pulse T_{MW} showing Rabi oscillations.

state suggests that the readout fidelity is limited by qubit relaxation before or during the measurement. The role of relaxation during the measurement will be analyzed in detail in section 4.4.

4.3 QND measurement with the AC-switching readout

In this section, we analyze the QND character and the projectiveness of the AC-switching readout using a sequence of two consecutive readouts A and B. The measurement settings are chosen such that the qubit states $|e>$ and $|g>$ are associated with the states L and H of the oscillator respectively.

4.3.1 Qubit relaxation between two successive readouts

We first carry out a sequence of two consecutive measurements when the qubit state is initially prepared with a $\frac{\pi}{2}$ Rabi pulse, as illustrated in figure 4.5a. To limit qubit relaxation during the measurement, the holding plateau of readout A has a duration of only 30 ns. With this duration, the two states L and H of the oscillator are discriminated with an efficiency of 99.7%. Figure 4.5b shows the results of readouts A and B as a function of the delay between the two measurements. The switching probability in readout A is constant with a value of $P_A \simeq 50$ %. The switching probability in readout B strongly depends on the outcome of readout A. We denote the conditional switching probabilities in readout B given the result L or H of readout A as $P_B(L_A)$ and $P_B(H_A)$. The fact that the correlation $P_B(H_A) - P_B(L_A)$ between the two readouts is very high if the readouts follow each other immediately indicates that the measurement is strongly projective, as expected from the high readout contrast. This regime was discussed in detail in section 2.2. $P_B(L_A)$ increases with the delay time between measurements. The observed decay is exponential with a characteristic time equal to the qubit relaxation time, measured independently. These results are consistent with the following picture. If readout A yields the result L, the qubit is projected to the state $|e>$, and subsequently decays to the $|g>$ state. This decay results in an increased switching probability in readout B. $P_B(H_A)$ is constant because after readout A the qubit is projected to the state $|g>$ which is well preserved between the two measurements.

4.3.2 Qubit rotation between two successive readouts

To clarify whether the correlation between the two readouts is really due to the projection of the qubit state after the measurement and not to an artefact of our measurement procedure, it is necessary to measure $P_B(L_A)$ and $P_B(H_A)$ for any arbitrary initial qubit state and verify that the correlation between the measurements can be reversed by rotating the qubit state between the two measurements. For this we use the control and readout sequence shown in figure 4.6a including two Rabi pulses with duration T_{RA} and T_{RB}. The results

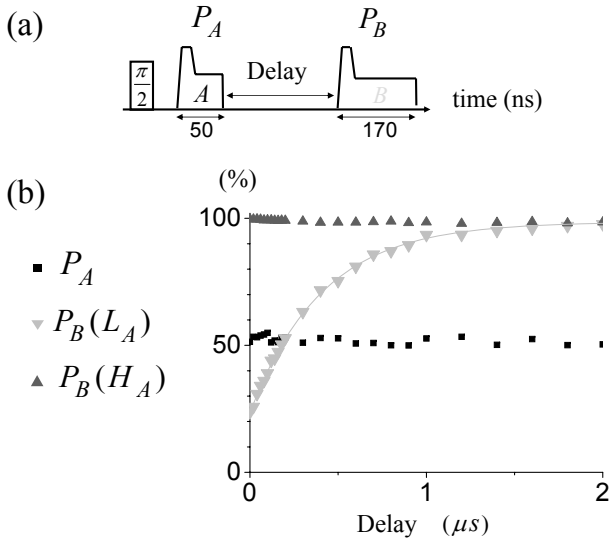


Figure 4.5: (a) Qubit excitation and readout sequence. (b) Results of the two measurements as a function of the delay between the two readout pulses. P_A is the switching probability in readout A, while $P_B(L_A)$ and $P_B(H_A)$ are the conditional switching probabilities in readout B in the cases that the outcome of readout A is L or H. The solid curve is an exponential decay fitting curve $P_B(L_A)$ whose decay time corresponds to the free qubit relaxation time.

of the two measurements are shown in figures 4.6b-c as a function of T_{RA} for two different values of T_{RB} corresponding to two rotation angles of $\theta_B = 0$ and $\theta_B = \pi$ respectively. The switching probability P_A in readout A varies sinusoidally with T_{RA} as a result of induced qubit Rabi oscillations. As expected for a strongly projective measurement, the conditional switching probabilities $P_B(L_A)$ and $P_B(H_A)$ in readout B are constant (i.e. independent of T_{RA}) even though the qubit may have many initial states. The fact that the correlation between the two measurements can be reversed by a applying a Rabi pulse $\theta_B = \pi$ between the measurement (figure 4.6c) proves that the correlation is indeed due to the qubit projection and not to crosstalk between the measurements.

4.3.3 QND Fidelity

We define the QND fidelity as the probability that the qubit initial state is preserved after the measurement, irrespective of the measurement outcome, when it is initially in $|g>$ or in $|e>$ with an equal probability. Denoting as $p(g|g)$ and $p(e|e)$ the probabilities that the qubit state is preserved after the

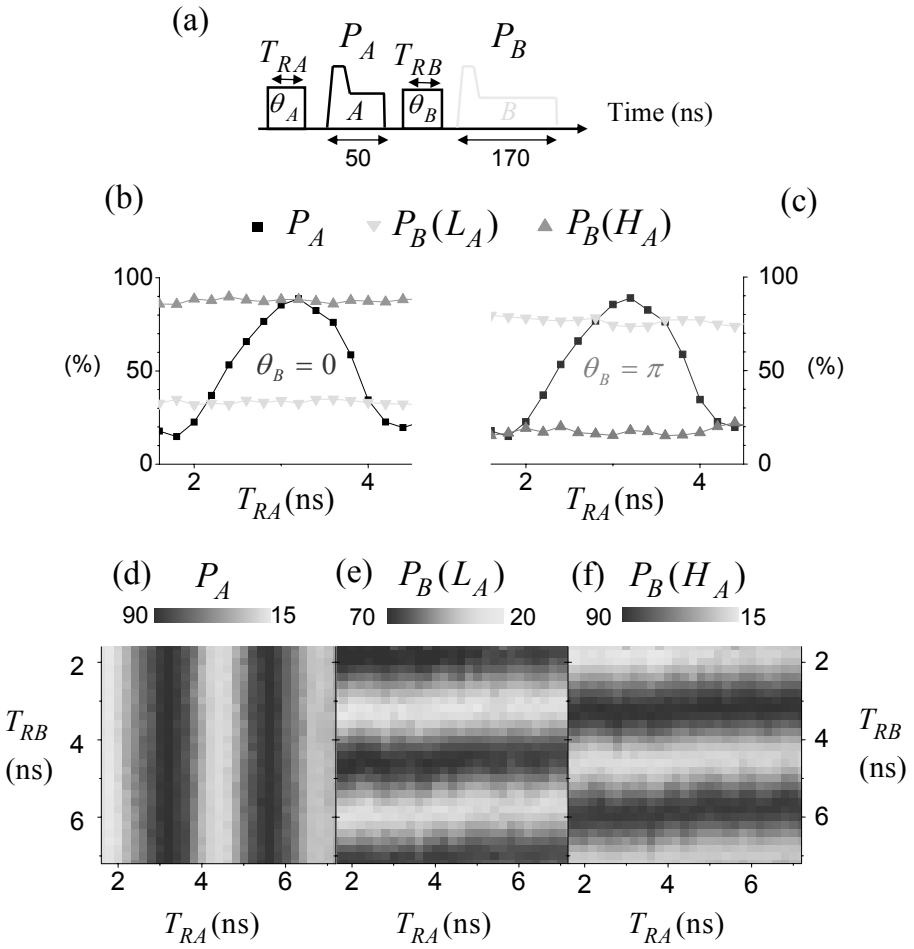


Figure 4.6: (a) Qubit excitation and readout sequence including two Rabi pulses of duration T_{RA} and T_{RB} (corresponding to two rotations of angle θ_A and θ_B respectively) and two readouts A and B. (b),(c) Results of the two readouts as a function of T_{RA} in the cases $\theta_B = 0$ (b) and $\theta_B = \pi$ (c). P_A is the switching probability in readout A, while $P_B(L_A)$ and $P_B(H_A)$ are the conditional switching probabilities in readout B in the cases that the outcome of readout A is L or H respectively. (d,e,f) P_A, $P_B(L_A)$ and $P_B(H_A)$ as a function of T_{RA} and T_{RB}.

measurement when it is initially in $|g>$ or in $|e>$, the QND fidelity is

$$F_{QND} = \frac{p(g|g) + p(e|e)}{2}. \tag{4.3}$$

In the experiment presented above, the qubit state after a measurement given the measurement outcome is independent of the initial state of the qubit. In this case, F_{QND} can be directly re-expressed as a function of the correlation $C = P_B(H_A) - P_B(L_A)$ between the two measurements

$$F_{QND} = \frac{1}{2}\left[1 + C\right]. \tag{4.4}$$

From the measurements shown in figure 4.5b, for the shortest delay between the two readouts, we find $C = 75$ % and $F_{QND} = 88$ %.

4.4 Analysis of the relaxation during the measurement

4.4.1 Qubit relaxation during the holding plateau

The fact that the main loss of readout contrast occurs when the qubit is in the excited state (as can be seen in figure 4.4c) suggests that the fidelity of the measurement is limited by qubit relaxation before or during the measurement. This can be understood qualitatively. In practical flux qubits one finds a very irregular dependence of the relaxation on flux bias due to electromagnetic modes and 'natural' two-level systems. The qubit is operated at a flux bias where the relaxation rate is locally minimal. During the measurement, the operation of the SQUID causes an oscillation of the transport current and the circulating current of the SQUID which in turn shifts the qubit bias. In the H state, the flux is modulated over a range as large as $2MJ \simeq MI_c \simeq 5$ mΦ_0 corresponding to a sweep of the qubit frequency on the order of 10 GHz. The qubit can thus be swept through regions where the relaxation rate is much higher. Moreover, the driving of the oscillator increases the spectral density $S_J(f)$ of the fluctuations of the SQUID circulating current, not only at zero frequency $f = 0$ (as was calculated in the case of the AC-continuous readout in section 3.2.3), but possibly also at the qubit frequency $f = F_{qb}$ resulting in additional qubit relaxation [6, 7].

We first measure the qubit relaxation under conditions where the oscillator is fixed in either the low L or the high H oscillation amplitude state. The qubit is initially prepared in $|e>$. Next the oscillator is set either in the H state or in the L state. To prepare H a short high driving pulse $I_{ac} > I^e_{b2}$ is applied (dashed line in figure 4.7a). Subsequently the oscillator is driven for a variable time t_{drive} at an amplitude I_{drive}. Afterwards the qubit state is read out with a regular measurement pulse. Figure 4.7b shows the decay in time of the switching probability when the oscillator is driven with an amplitude corresponding to the holding plateau $I_{drive} = I_{hold}$. This decay is exponential

and is due to qubit relaxation. The two qubit relaxation rates $\Gamma_{\downarrow}^{L}$ and $\Gamma_{\downarrow}^{H}$ when the oscillator is in state L or H are significantly different. The dependence of the qubit relaxation rates on the oscillator driving amplitude is shown in figure 4.7c for $I_{drive} < I_{hold}$ and $I_{drive} > I_{hold}$ when the oscillator is in the L or H state, respectively. Whereas $\Gamma_{\downarrow}^{H}$ is almost constant, $\Gamma_{\downarrow}^{L}$ increases significantly with the driving amplitude.

4.4.2 Qubit relaxation during the switching plateau

The approach used in the previous section is well suited to analyze the qubit relaxation for a driving amplitude where the oscillator is in a stable state. However for higher driving amplitude $I_{drive} > I_{hold}$ and especially at the driving amplitude during the switching plateau, state L is metastable and the detector can switch to state H. Therefore to analyze the qubit relaxation, the oscillator switching process needs to be included. In the following we analyze the oscillator switching and the qubit relaxation during the switching plateau. The solid line in figure 4.8b shows the oscillator switching probability when the qubit is in $|g>$ as a function of the duration of the switching plateau t_{sw}. We distinguish two regimes, indicated as I and II. The boundary of the two regimes is after a

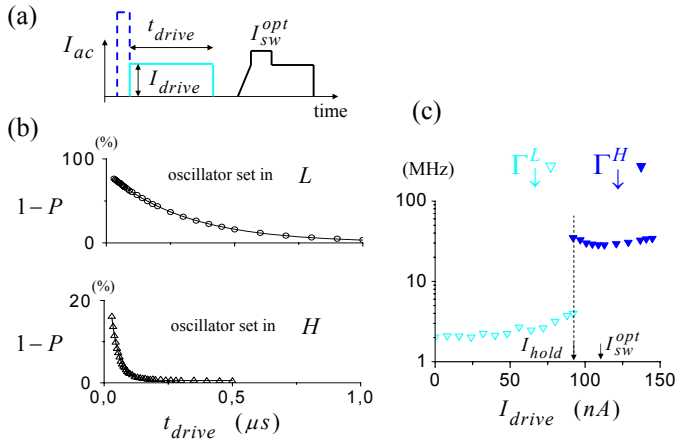


Figure 4.7: (a) Oscillator driving sequence used to analyze the qubit relaxation. In the first driving pulse the oscillator is set either in L or H. (b) Decay of the switching probability as a function of the length of the driving pulse t_{drive} (due to the qubit relaxation). (c) Qubit relaxation rates versus oscillator driving amplitude I_{drive} when the oscillator in the state L or H.

time of about 10 ns, indicated as $t_{I/II}$. In regime I the switching probability increases very fast. At the origin of the switching plateau, the oscillator driving amplitude is increased in about 1 ns, probably leading to non-adiabatic effects. In regime II the switching probability increases with a constant rate Γ_{sw}. The switching rate Γ_{sw} from state L to state H depends on the height of the effective potential barrier $\Delta U = U_0[1-(I_{ac}/I_{b2})^2]^{3/2}$ between L and H [5]. For a driving current I_{ac} close to the upper bifurcation current I_{b2}, the oscillator switching rate Γ_{sw} increases strongly by a few orders of magnitude. As I_{b2} is different for the two qubit states, Γ_{sw} strongly depends on the qubit state, which is the principle of the measurement. As $I_{b2}(g) < I_{b2}(e)$, it follows that $\Gamma^g_{sw} >> \Gamma^e_{sw}$ (figure 4.8c).

We describe the qubit and the oscillator as a 4-state system (g, L), (g, H), (e, L) and (e, H), with 4 corresponding occupation probabilities. Due to normalization, only 3 probabilities are independent. We use $P(H) = P(e, H)+P(g, H)$, $P(e, H)$ and $P(e, L)$. In regime II, oscillator switching ($L \rightarrow H$) and qubit relaxation ($e \rightarrow g$) are described with the set of four rates $\Gamma^g_{sw}, \Gamma^e_{sw}$ and $\Gamma^L_{\downarrow}, \Gamma^H_{\downarrow}$ (figure 4.8d). Oscillator retrapping ($H \rightarrow L$) and qubit excitation ($g \rightarrow e$) are negligible. The evolution of the occupation probabilities is given by:

$$\begin{cases} \frac{dP(e,L)}{dt} &= -P(e,L)(\Gamma^e_{sw} + \Gamma^L_{\downarrow}) \\ \frac{dP(e,H)}{dt} &= P(e,L)\Gamma^e_{sw} - P(e,H)\Gamma^H_{\downarrow} \\ \frac{dP(g,L)}{dt} &= P(e,L)\Gamma^L_{\downarrow} - P(g,L)\Gamma^g_{sw} \\ \frac{dP(g,H)}{dt} &= P(g,L)\Gamma^g_{sw} + P(e,H)\Gamma^H_{\downarrow} \end{cases} \tag{4.5}$$

For a given initial qubit state i (g or e) at the origin of the switching plateau $t = 0$, we denote as P^I_i, $P^I_i(e, H)$, and $P^I_i(e, L)$ the initial conditions for the set of equations (4.5). They quantify the evolution of the qubit and the oscillator evolution during regime I. We choose to define the initial conditions at $t = 0$, and not at $t = t_{I/II}$. They are obtained by extrapolating $P(H)$, $P(e, H)$ and $P(g, L)$ in regime II to $t = 0$. In the more general case of an initial qubit state with an occupation probability of $|e>$: $P(e) = x$, the initial conditions are: $P_0(H) = xP^e_0(H) + (1 - x)P^g_0(H)$ (and similarly for $P_0(e, H)$ and $P_0(e, L)$).

The 6 independent parameters describing the evolution of the qubit and the oscillator during regime I can be expressed as a function of the two switching probabilities $P^I_i = P^I_i(H)$ depending on the initial qubit state (i=g or i=e), two qubit relaxation probabilities $R^I_L = P^I_e(g, L)/P^I_e(L)$ and $R^I_H = P^I_e(g, H)/P^I_e(H)$ depending on the state of the oscillator (L or H)and similarly two qubit excitation probabilities E^I_H and E^I_L (which we assume to be negligible).

If the qubit is initially in $|g>$, the only relevant rate is Γ^g_{sw} and the set of equations (4.5) reduces to: $dP(H)/dt = [1 - P(H)]\Gamma^g_{sw}$. For a given switching plateau driving amplitude I_{sw}, P^I_g and Γ^g_{sw} are extracted by fitting the switching probability $P(H)$ as a function of t_{sw} with $P(H) = 1 - [1 - P^I_g] \exp(-t_{sw}\Gamma^g_{sw})$ (as shown by the dashed line in figure 4.8b).

For a driving amplitude equal to or higher than $I_{b2}(g)$, the L state does not exist when the qubit is in $|g>$. In this case, the state (g, L) is eliminated from

the set of equations (4.5) by assuming that $\Gamma_{\downarrow}^{L}$ is associated with the transition $(e, L) \rightarrow (g, H)$.

If the qubit is in $|e>$, two switching processes are possible, either due to qubit relaxation (rate $\Gamma_{\downarrow}^{L}$), or to switching while the qubit is excited (rate Γ_{sw}^{e}). Depending on the process, the state of the qubit after switching is either $|g>$ or $|e>$. Therefore, it is possible to discriminate between the two processes by measuring the qubit state after a switching event. The sum $\Gamma_{sw} = \Gamma_{\downarrow}^{L} + \Gamma_{sw}^{e}$ and P_e^I are first extracted from the dependence of the switching probability $P(H)$ on the length of the switching plateau in a single readout, given by $P(H) = 1 - x[1 - P_e^I(H)] \exp(-t_{sw}\Gamma_{sw})$, where x is the occupation probability of $|e>$ at the origin of the switching plateau (due to the initial preparation errors 5% and

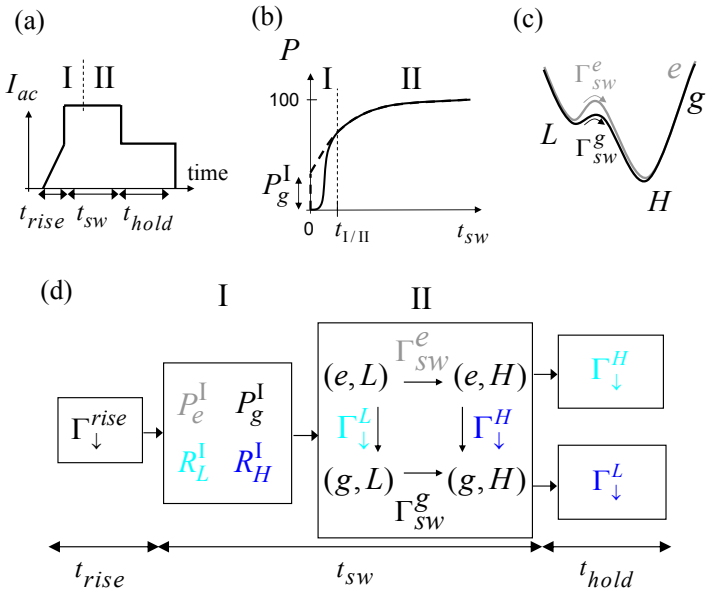


Figure 4.8: (a) Oscillator driving sequence for the qubit readout. (b) Switching probability as a function of the duration of the switching plateau (solid line). (c) Effective potential barrier between L and H when the qubit is in the state $|g>$ or $|e>$. (d) Schematic of the model used to describe the evolution of the qubit and the oscillator during each part of the readout pulse, including two qubit relaxation rates $\Gamma_{\downarrow}^{L}, \Gamma_{\downarrow}^{H}$ depending on the state of the oscillator and two oscillator switching rates $\Gamma_{sw}^{e}, \Gamma_{sw}^{g}$ depending on the state of the qubit. P_g^I, P_e^I and R_H^I, R_L^I correspond to the oscillator switching probability and the qubit relaxation probability in regime I.

the qubit relaxation during the rising part of the readout pulse 5%, $x = 0.90$).

To discriminate between $\Gamma_{\downarrow}^{L}$ and Γ_{sw}^{e}) we probe the qubit state after a switching event using a sequence of two readouts A and B (shown in figure 4.9a). At the end of the switching plateau of readout A, $P(e,H)$ is given by

$$\begin{aligned} P(e,H)(t_{sw}) = & \, x P_e^I R_H^I e^{-t_{sw}\Gamma_{\downarrow}^{H}} \\ & + [1 - x P_e^I] \frac{\Gamma_{sw}^{e}}{\Gamma_{\downarrow}^{H} - \Gamma_{sw}} \left[e^{-t_{sw}\Gamma_{sw}} - e^{-t_{sw}\Gamma_{\downarrow}^{H}} \right] \end{aligned} \tag{4.6}$$

If relaxation is the only process which can lead to oscillator switching then $P(e,H) = 0$. In equation (4.6), the first term proportional to $P_e^I R_H^I$ corresponds to switching events during regime I, whereas the second term proportional to Γ_{sw}^{e} corresponds to switching events during regime II. The occupation probability of $|e>$ after a switching event in readout A, given by the conditional probability $P(e|H) = P(e,H)/P(H)$, is measured with readout B. The conditional switching probability $P_B(H_A)$ in readout B after a switching event in readout A is

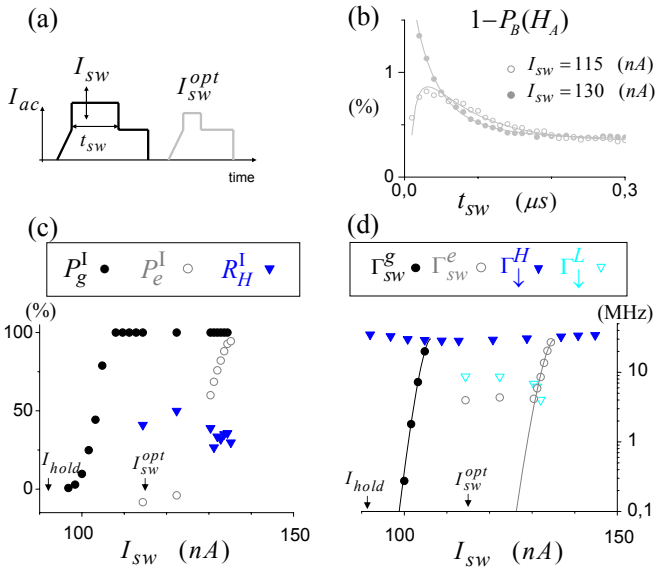


Figure 4.9: (a) Sequence of two successive readouts used to analyze the qubit state after the first measurement. (b) Conditional switching probability $P_B(H_A)$ in readout B after a switching event in readout A. (c),(d) Oscillator switching probabilities P_g^I, P_e^I and qubit relaxation probability R_H^I in regime I, and oscillator switching rates $\Gamma_{sw}^{e}, \Gamma_{sw}^{g}$ and qubit relaxation rates $\Gamma_{\downarrow}^{L}, \Gamma_{\downarrow}^{H}$ in regime II as a function of the switching plateau driving amplitude I_{sw}.

given by $1 - P_B(H_A) = \alpha P(e|H) + \beta$, where $\alpha = 0.9 \exp(-t_{hold}\Gamma_{\downarrow}^{H})$ includes the contrast of readout B and the qubit relaxation during the holding plateau of readout A, and $\beta = 3.5\ 10^{-3}$ is the finite measurement error in readout B when the qubit is in $|g>$. As the qubit relaxation is very strong when the oscillator is in the H state, the remaining signal is very small $1 - P_B(H_A) \approx 10^{-2}$. A key point for our analysis is the very high contrast of the readout allowing a resolution of $1 - P_B(H_A)$ as small as 10^{-3}. Γ_{sw}^{e} and R_H^I are extracted from a fit of $P(e, H)$ to equation (4.6) shown in figure 4.9b. The decay rates Γ_{sw} and $\Gamma_{\downarrow}^{H}$ are fixed (extracted previously), and R_H^I and Γ_{sw}^{e} are fitting parameters. The obtained values of R_H^I, Γ_{sw}^{e} and $\Gamma_{\downarrow}^{L}$ are shown in figures 4.9c,d. For comparison, P_g^I, P_e^I, Γ_{sw}^{g} and $\Gamma_{\downarrow}^{H}$ obtained previously are shown as well.

The ratio $\Gamma_{sw}^{e}/\Gamma_{sw}^{g}$ determines the intrinsic readout fidelity. The solid black lines in figure 4.9d are fits of Γ_{sw}^{e} and Γ_{sw}^{g} using the oscillator escape rate equation as given in [5], from which we extract $I_{b2}(g) = 108$ nA and $I_{b2}(e) = 136$ nA. Extrapolating Γ_{sw}^{e}, the intrinsic readout fidelity would be larger than 99.9 %. However, in practice we observe a saturation of Γ_{sw}^{e} at approximately 4 MHz.

The independent determination of $\Gamma_{\downarrow}^{L}$ and Γ_{sw}^{e} is an important result of our analysis. At the driving amplitude I_{sw}^{opt} used for the measurement, $\Gamma_{\downarrow}^{L}$ is higher than Γ_{sw}^{e}. Therefore, for measurement times beyond the oscillator transient period, we conclude that qubit relaxation is the main process limiting the readout fidelity.

4.5 Summary

In this chapter, we have analyzed the quantum nondemolition character of the AC-switching readout. Based on a sequence of two successive readouts, we find that the QND fidelity is 88 %. The strong correlation between the measurement indicates that the measurement is strongly projective as expected from the high contrast of the readout.

We introduced a simple model to describe the evolution of the qubit and the oscillator during the measurement and analyzed the qubit relaxation induced by the operation of the detector. We find that the qubit relaxation strongly depends on the state and the operation point of the detector. Corrected for qubit relaxation, the fidelity of the readout is at least 95 %.

Bibliography

[1] A. Wallraff, D.I. Schuster, A. Blais, L. Frunzio, J. Majer, M.H. Devoret, S.M. Girvin, R.J. Schoelkopf, *Approaching Unit Visibility for Control of a Superconducting Qubit with Dispersive Readout* Physical Review Letters, **95**, 060501 (2005)

[2] A. Lupaşcu, C.J.M. Verwijs, R.N. Schouten, C.J.P.M. Harmans, J.E. Mooij, *Nondestructive Readout for a Superconducting Flux Qubit*, Physical Review Letters **93**, 177006 (2004)

[3] I. Siddiqi, R. Vijay, F. Pierre, C.M. Wilson, M. Metcalfe, C. Rigetti, L. Frunzio, M.H. Devoret *RF-Driven Josephson Bifurcation Amplifier for Quantum Measurement*, Physical Review Letters **93**, 207002 (2004)

[4] A. Lupaşcu, E.F.C. Driessen, L. Roschier, C.J.P.M. Harmans, J.E. Mooij, *High-Contrast Dispersive Readout of a Superconducting Flux Qubit Using a Nonlinear Resonator*, Physical Review Letters, **96**, 127003 (2006)

[5] M.I. Dykman, M.A. Krivoglaz, *Fluctuations in nonlinear systems near bifurcations corresponding to the appearance of new stable states*, Physica **104A**,480 (1980)

[6] I. Serban, *Nonlinearities in the quantum measurement process of superconducting qubits*, PhD thesis Ludwig-Maximilians University, Munich, Germany, 2008

[7] I. Serban, M.I. Dykman, and F.K. Wilhelm, *Relaxation of a qubit measured by a driven Duffing oscillator*, Physical Review A **81**, 022305 (2010)

Chapter 5

QND measurement with the DC-switching readout

T. Picot, R. Schouten, C.J.P.M. Harmans, J.E. Mooij

The DC-switching SQUID readout is a very simple and sensitive detection scheme for the flux qubit. However, its disadvantage is the relatively strong back-action on the qubit. Here we show that its back-action can be considerably reduced by limiting the switching voltage with a shunt resistor. Using a fast cryogenic amplifier, a single readout can be completed within 25 ns. Coherent Rabi oscillations are recorded with measurement repetition rates up to 1 MHz without loss of contrast. Based on a sequence of two successive readouts we show that the measurement has a clear quantum nondemolition character, with a QND fidelity of 75 %.

The main results of this chapter were published in Physical Review Letters **105**, 040506 (2010)

5.1 Why and How to reduce the back-action of the DC-switch readout

The DC-switching SQUID readout is a very simple detection scheme for the flux qubit. Its principle of operation, sensitivity and back-action have been briefly introduced and discussed in section 3.3. This readout scheme has two main advantages. First, the detector is operated at DC, while dispersive readouts require an AC operation at microwave frequencies. Secondly, the difference of voltages between the two states S and D of the SQUID is very large, typically two orders of magnitude higher than the difference of voltage between the two states L and H of the nonlinear oscillator in the AC-switching readout (see section 3.4). This large difference of voltage allows in principle an extremely fast readout. Ideally, using a cryogenic amplifier, a single measurement could be completed in a time as short as 1 ns, several orders of magnitude faster than AC dispersive readouts.

As mentioned in chapter 3, the back-action of the DC-switching readout is commonly very strong which considerably reduces its efficiency. As we showed in chapter 4, the back-action of AC dispersive detectors is much lower. However, the operation is rather involved. Therefore, the implementation in case of a large number of qubits will be very complex. If the back-action of the DC-switching readout could be reduced, it would provide a very interesting alternative for the detection of large numbers of qubits.

In the following, we present a very simple approach to reduce the back-action of the SQUID in its dissipative state [1] and investigate for the first time the nondestructive nature of this type of detectors. By shunting the DC-SQUID with a resistance R lower than the SQUID normal resistance R_n, the voltage in the dissipative state can be reduced to a value of $V \approx RI_b$ much below the superconducting gap. In this case, all the dissipation is confined in the external shunt resistor. The generation of heat and quasi-particles in the junctions of the SQUID is thus greatly suppressed.

The different regimes of the dynamics of the resistively shunted SQUID are shown in figure 5.1 as a function of the value of the switching voltage (or equivalently the characteristic Josephson frequency $f_J = RI_c/\Phi_0$), and the SQUID plasma frequency f_0 [2]. In this chapter we study three different samples denoted as (1), (2), and (3). The values of the SQUID maximal critical current $I_{c,max}$, its normal resistance R_n, the shunt resistance R and the switching voltage V_{sw} in each sample are given in table 5.1.

The different aspects of the back-action of the DC-switching readout were discussed in detail in section 3.3.3. One important issue is that due to the AC-Josephson effect, when a DC-voltage is present across the SQUID the current in the SQUID oscillates at a high frequency and causes large oscillations of the qubit flux bias. This can lead to spurious qubit transitions and quantum leakage to higher energy levels. The amplitude of the qubit flux bias corresponds to a frequency shift of about $2MI_pJ/h$, where the SQUID circulating current J is on the order of $I_{c,max}\sin(\phi)/2$. The critical current of sample (1) is chosen

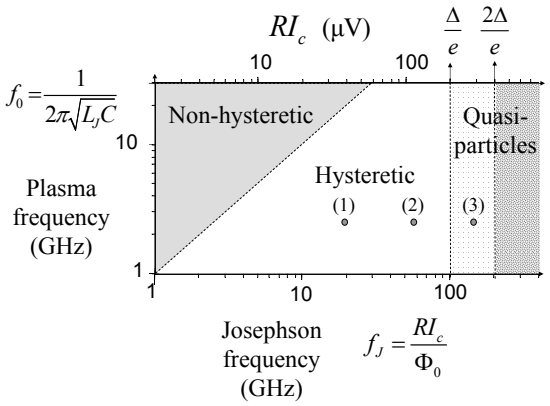


Figure 5.1: Different regimes of operation of the DC-SQUID. The three dots (1) (2) and (3) correspond to the three samples studied in this chapter (see table 5.1)

	sample (1)	sample (2)	sample (3)
$I_{c,max}$	160nA	750 nA	1.5 μA
R_n	2 kΩ	430 Ω	210 Ω
R	125 Ω	125 Ω	2 kΩ
V_{sw}	20 μV	100 μV	400μV
ϕ	0.18	0.33	0.38
$g = 2MI_pJ/h$	1 GHz	10 GHz	20 GHz

Table 5.1: Parameters of the SQUID in the three samples (values of the maximum critical current $I_{c,max} = 2I_{c0}$, the normal resistance R_n, the shunt resistor R, the voltage in the dissipative state V_{sw}, the frustration of the SQUID loop $\phi = \frac{\Phi}{\Phi_0}$ during qubit readout and the amplitude of the qubit-SQUID interaction g).

such that the amplitude of the qubit frequency shift during the operation of the SQUID is smaller than 1 GHz. In samples (2) and (3), the SQUID critical current and the qubit-SQUID interaction are larger.

5.2 Characterization of the readout circuit

In this section we present the DC-switching readout circuit and characterize the basic properties of the detector (I-V characteristic, detector response time and effective temperature of the SQUID).

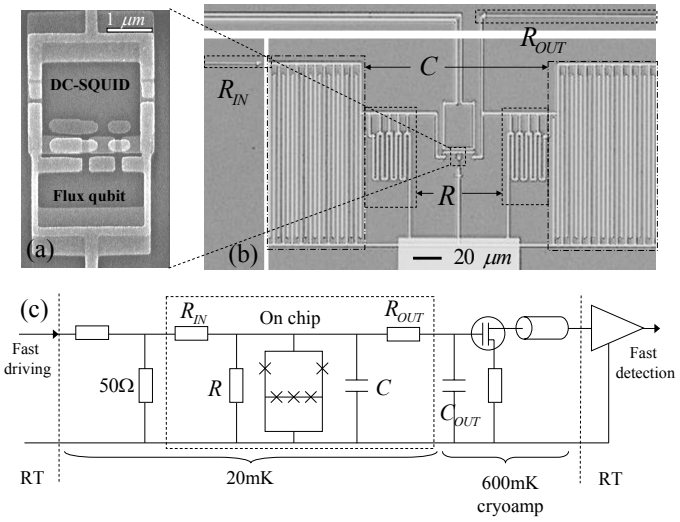


Figure 5.2: (a) Scanning electron microscopy picture of the flux qubit and the DC-SQUID. (b) Optical picture of the readout circuit. (c) Schematic of the readout circuit.

The readout circuit is shown in figure 5.2. A key new element is the resistor R shunting the SQUID. A value of R much lower than the SQUID normal resistance R_n greatly reduces the amount of heating and suppresses the generation of quasi-particles during the readout. To ensure that the resistor acts as a lumped resistance with a constant value from DC to high frequency ($\sim$ 100 GHz), its size is chosen smaller than 100μm and it is placed in direct proximity of the SQUID. The interdigitated capacitor C = 1pF shunting the SQUID has a value large enough to ensure the hysteretic character of all three SQUIDs [2].

5.2.1 I-V characteristics of the SQUIDs

The I-V characteristics of samples (1), (2) and (3) are shown in figure 5.3. The black and grey curves correspond to the value of the voltage V across the SQUID when the current I is ramped with a positive or negative slope respectively. All the SQUIDs have a hysteretic region for currents lower than their critical currents I_c, with two branches corresponding either to a zero voltage superconducting state S or a finite voltage dissipative state D. In samples (1) and (2), the values of the voltage in state D are about 20 μV and 100 μV respectively, while for sample (3), the voltage in state D is about 300 μV. In samples (1) and (2), the voltage in the dissipative state increases almost linearly

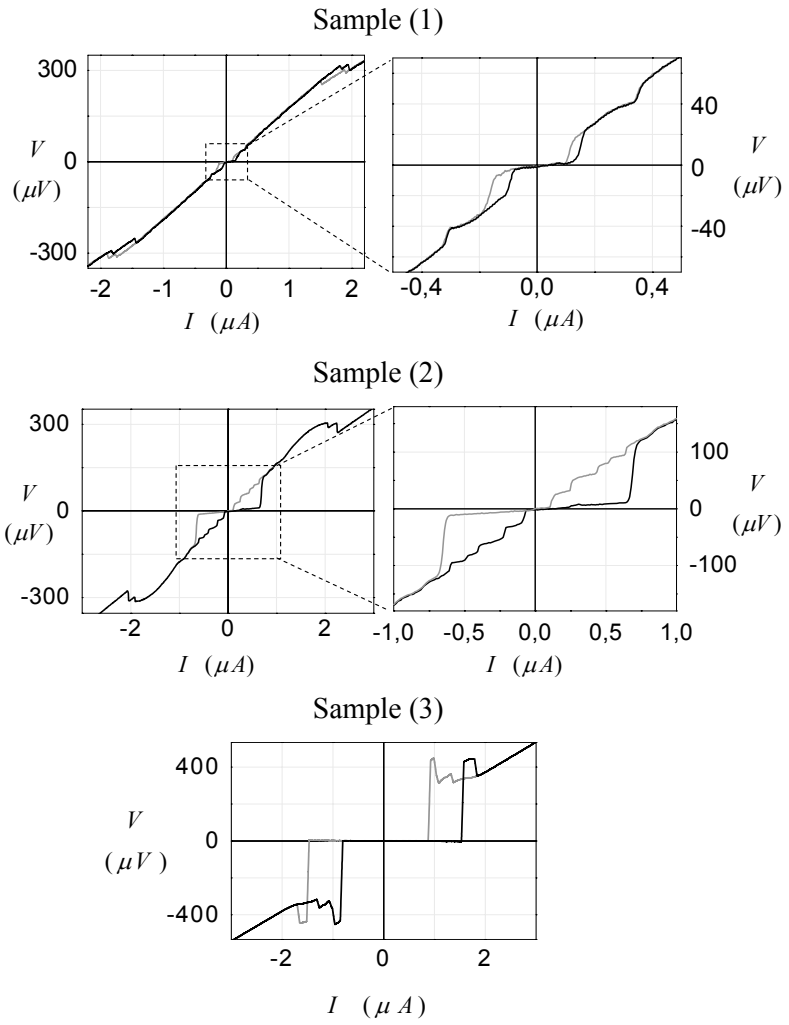


Figure 5.3: I-V characteristic of samples (1), (2), and (3) for a frustration $\phi = \frac{\Phi}{\Phi_0} = 0$ in the SQUID loop. Right panels are enlarged views of the left panels.

as a function of the current, with a slope given by the shunt resistance. Finite voltage steps in the I-V characteristic of sample (2) are possibly due to some high frequency resonances in the electromagnetic SQUID environment. In all samples, a characteristic pattern with a negative slope is visible at a voltage of about 300 μV, associated with the opening of the quasi-particle dissipative channel and the transition of part of the wires connecting the samples from superconducting to normal.

5.2.2 Operation of the SQUID for qubit readout

For the qubit readout the SQUID, initially in the superconducting state S, is biased with a current I_b close to its critical current I_c with a short current pulse. The SQUID might switch to the dissipative state D with a probability P. The resulting state of the SQUID is maintained using a lower bias current $I_b \approx I_c/2$, for a time allowing to discriminate efficiently the two SQUID states. Figures 5.4a and 5.4c show the readout pulse sent to the SQUID and the resulting output voltage (in the case of sample (1)), when the SQUID is in the state S (cyan) or when it is in the state D (magenta). P depends on the flux through the SQUID loop and therefore on the state of the qubit. The detector switching probabilities in the two cases when the qubit is in the ground state or in the excited state are denoted as $P(g)$ and $P(e)$. For a general qubit state with an excited state occupation probability $p(e)$ and a readout contrast $C_m \equiv P(e) - P(g)$ the switching probability is

$$P = P(g) + C_m p(e). \tag{5.1}$$

5.2.3 Response time of the detector

A second key new element of the readout circuit is the ultralow noise cryogenic HEMT amplifier (shown in figure 5.4b) allowing to discriminate very efficiently the two states of the SQUID. The cryogenic amplifier is characterized by a high input impedance, 0.3 GHz bandwidth and a noise level $\backsim 0.25$ nV/$\sqrt{\text{Hz}}$. In order to reduce the capacitance to ground of the line connecting the input of the amplifier with the SQUID, the amplifier is mounted on a Cu strip attached to the refrigerator still at $\sim$ 600 mK and connected to the sample by two 7 cm length superconducting wires. The resulting parallel capacitance between the ground and the input of the amplifier $C_{OUT} \simeq 20$ pF in combination with the serial resistance R_{OUT} (shown in figure 5.2c) defines the rise time τ of the output voltage. For samples (1) and (2), $R_{OUT} = 3$ kΩ and $\tau \sim 50$ ns, while for sample (3) $R_{OUT} = 200$ Ω and $\tau \sim 5$ ns. In sample (3), which has the shortest rise time, a single readout can be completed within 15 ns. In the case of samples (1) and (2), the two states of the SQUID can be well discriminated even for a total duration of the readout pulse shorter than τ. Although a low value of R_{OUT} is attractive for fast readout, it also filters less efficiently any noise coming from the output line. It might thus cause larger fluctuations of the SQUID bias current and reduce the qubit relaxation time.

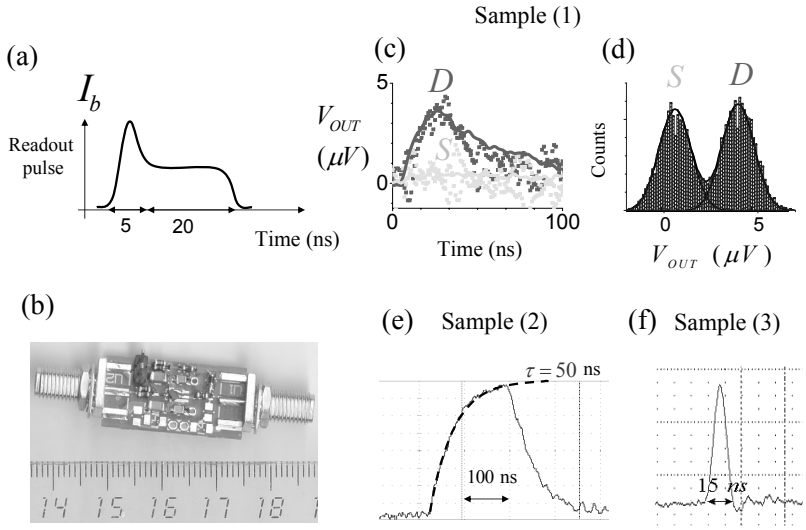


Figure 5.4: (a) Current pulse sent to the SQUID. (b) Cryogenic amplifier. (c) Output voltage of sample (1). Dots correspond to real time signal, while the solid lines are the average of 16 traces corresponding to state S or D. (d) Histogram of the output voltage. (e),(f) Output voltage of samples (2) and (3)

5.2.4 Qubit relaxation induced by the resistor

The resistor R shunting the SQUID induces relaxation in the qubit. This is an important consequence of our approach. In this section, however, we estimate the contribution of this relaxation channel and show that for short readout pulses, the relaxation during the readout is not significantly enhanced.

In the high frequency limit $hf > kT$ and $2\pi L_J f << R$, the noise generated in the resistor causes fluctuations of the SQUID bias current δI_b with a spectral density

$$S_{\delta I_b}(f) = \frac{2hf}{R}\theta(f), \tag{5.2}$$

where $\theta(f) = 0$ for $f < 0$ and $\theta(f) = 1$ for $f > 0$. This in turn causes fluctuations of the SQUID circulating current $\delta J = \frac{dJ(I_b)}{dI_b}\delta I_b$ and so fluctuations of the qubit flux bias. In the qubit energy basis, the qubit Hamiltonian and the energy fluctuations due to the resistor are given by

$$\hat{H} = \frac{E}{2}\hat{\sigma}_Z + \left[\frac{\epsilon}{E}\hat{\sigma}_Z - \frac{\Delta}{E}\hat{\sigma}_X\right]\frac{\delta\epsilon}{2}, \tag{5.3}$$

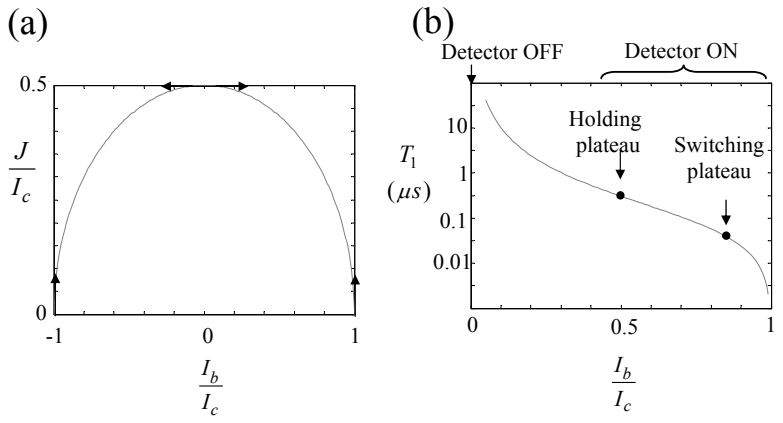


Figure 5.5: (a) Relation between the SQUID bias current I_b and the SQUID circulating current J (in the case of a symmetric SQUID with a frustration $\phi = 0$ in the loop). (b) Calculated qubit relaxation induced by the resistor with the parameters of sample (1) as a function of the SQUID bias current when the SQUID is in state S (using equation (5.4)).

with $E = \sqrt{\epsilon^2 + \Delta^2}$ and $\delta\epsilon = 2MI_p\delta J$. Qubit relaxation is caused by the perpendicular component of the energy fluctuations $\delta E_\perp = (\Delta/E)\delta\epsilon$ at the qubit frequency $F_{qb} = \frac{E}{h}$. Based on Fermi's golden rule, we find that the qubit relaxation rate due to the resistor is

$$\Gamma_\downarrow(I_b) = \frac{1}{4}\frac{S_{\delta E_\perp}(F_{qb})}{\hbar^2} = 2\frac{\Delta^2}{ER}\left[\frac{MI_p}{\hbar}\frac{dJ(I_b)}{dI_b}\right]^2. \tag{5.4}$$

Very importantly, during the coherent manipulation of the qubit, this relaxation channel is closed by operating the SQUID at a bias current such that $\frac{dJ(I_b)}{dIb} = 0$, where external fluctuations of I_b do not couple to the SQUID circulating current J [1, 3]. For a symmetric SQUID, this condition is realized at $I_b = 0$ (see figure 5.5a).

Figure 5.5b shows the qubit relaxation time $T_1 = 1/\Gamma_\downarrow$ as a function of the SQUID bias current, for the parameters of sample (1). During the holding plateau $I_b/I_c = 0.5$ and $1/\Gamma_\downarrow = 300$ ns while during the switching plateau $I_b/I_c \sim 0.9$ and $1/\Gamma_\downarrow \sim 30$ ns. Given the short durations of the holding plateau (25 ns) and the switching plateau ($\sim$ 2 ns), qubit relaxation induced by the operation of the detector in state S is small ($\sim$ 20 %). Qubit relaxation induced by the detector in state D is more difficult to estimate as it involves highly non-linear effects.

5.2.5 Qubit properties

In sample (1), the qubit has a persistent current $I_p = 400$ nA and a tunnel coupling $\Delta = 3.5$ GHz (obtained from the spectroscopy measurements shown

in figure 5.6b). The mutual inductance between the SQUID and the qubit is $M = 30$ pH. It is obtained from the relative difference of the SQUID critical current when the qubit is in the state $| + I_p >$ or $| - I_p >$. For the readout, the SQUID is operated at a critical current $I_c = 140$ nA (where $V \approx RI_c = 17$ μV). The maximum qubit frequency shift during the readout in sample (1), determined from spectroscopy measurements (not shown), is $g = 2MI_pJ/h = 1$ GHz.

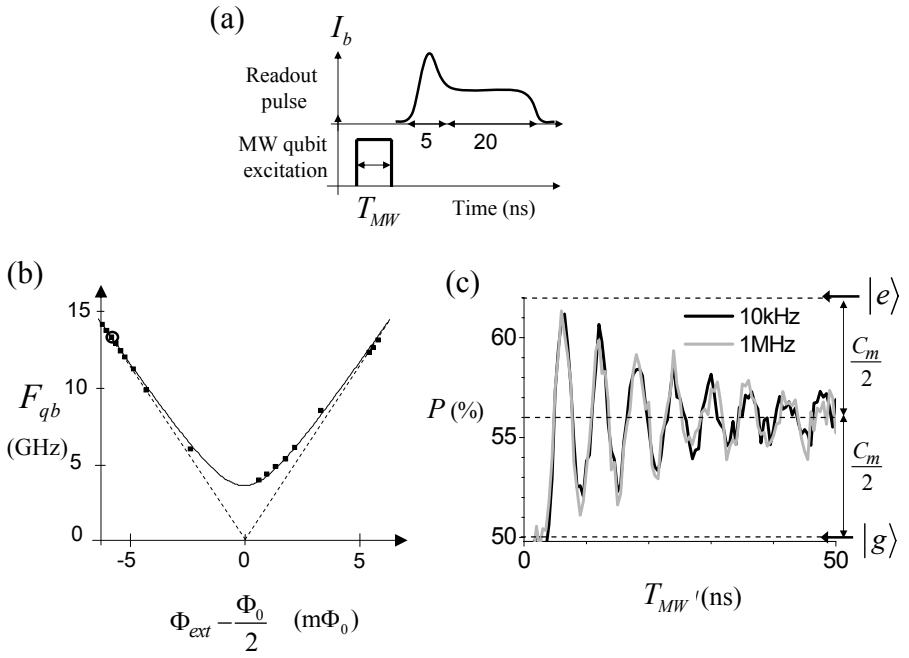


Figure 5.6: (a) Qubit excitation and readout sequence. (b) Qubit energy spectrum in sample (1) as a function of the flux bias. (c) Rabi oscillations in sample (1) for a measurement repetition rate of 10 kHz or 1 MHz with at a qubit frequency of E/h=13 GHz. The three dashed lines represent P(g), P(e) and P_m.

We first investigate the back-action of the resistively shunted SQUID on the coherence of the flux qubit in sample (1) by performing coherent Rabi oscillations at different measurement repetition rates. As can be seen in figure 5.6c, virtually no reduction of coherence is visible up to a measurement repetition rate of 1 MHz, nearly two orders of magnitude higher than previously achieved with unshunted or weakly shunted DC-switching detectors [4]. Although the Rabi coherence time of this qubit sample is relatively short, the fact that such a high measurement repetition rate is possible without any loss of readout contrast and

qubit coherence shows that the back-action is very low.

The contrast of the readout $C_m = P(e) - P(g)$ in sample (1) is obtained from the Rabi oscillations in figure 5.6c. As the qubit energy $E = h \times 13\text{GHz}$ is much higher than the thermal energy $kT \approx h\times 1\text{GHz}$, the qubit is initially in the ground state, corresponding to a detector switching probability $P(g)$. We assume that the oscillation of P as a function of the duration of the Rabi pulse T_{MW} is symmetric around $P_m = (P_g + P_e)/2$, such that in the limit of a long and incoherent pulse $P = P_m$. Based on the values of $P(g)$ and P_m extracted from Fig. 5.6c, we deduce the readout contrast $C_m = 12\%$.

5.2.6 Effective temperature of the SQUID

As mentioned in chapter 3, the sensitivity of the DC-switching readout depends on the effective temperature T_{eff} of the SQUID. For a readout pulse with a switching plateau of duration T_{sw}, the switching probability is $P = 1 - \exp(-T_{sw}\Gamma_{sw})$, where Γ_{sw} is the switching rate of the SQUID at that current level. In the thermal regime, Γ_{sw} is given by [5]

$$\Gamma_{sw}^{th} = f_0 \exp\left\{-\frac{U_0}{kT_{eff}}\left[1 - \frac{I_b}{I_c}\right]^{3/2}\right\}, \tag{5.5}$$

where $U_0 = \frac{4\sqrt{2}}{3}\frac{\Phi_0 I_c}{2\pi}$ and f_0 is the plasma frequency of the SQUID.

To extract the effective temperature of the SQUID, we first measure the switching probability as a function of the duration of the switching plateau T_{sw} for different values of the SQUID bias current I_b (as shown in figure 5.7a). For each value of I_b, Γ_{sw} is obtained using an exponential decay fit. Secondly, we plot $[-\ln(\Gamma_{sw}/f_0)]^{2/3}$ as a function of I_b/I_c, as shown in figure 5.7b. The slope of the curve correspond to $-[U_0/kT_{eff}]^{2/3}$. In the case of sample (1), we find $U_0/kT_{eff} = 30$. Given the critical current of the SQUID at which the SQUID is operated $I_c = 140$ nA we conclude that $T_{eff} = 210 \pm 20$ mK.

The fact that the effective temperature of the SQUID is much higher than the physical temperature of the cryostat $T_{cryo} = 20$ mK might be due to insufficient filtering of the noise coming from the input and output lines of the SQUID. In the experiment presented in this chapter, the cryogenic amplifier is connected to the SQUID using two superconducting wires with a length of about 7 cm. As explained in section 5.2.3, this allows a very short rise time of the output line and a good thermal isolation between the sample and the amplifier. However, it does not provides any filtering of the noise generated by the amplifier. Further optimization of the measurement setup could reduce T_{eff} significantly.

Based on the calculations of chapter 3, the readout contrast should be

$$\Delta P = \left[\frac{E_J}{kT_{eff}}\right]^{2/3} \frac{\pi \tan \pi\phi}{\Phi_0} x_{th} \Delta\Phi, \tag{5.6}$$

with $\Delta\Phi = 2MI_p$. In the case of sample (1), from the properties of the qubit and the detector extracted previously ($M = 30$ pH, $I_p = 400$ nA, $I_c = 140$

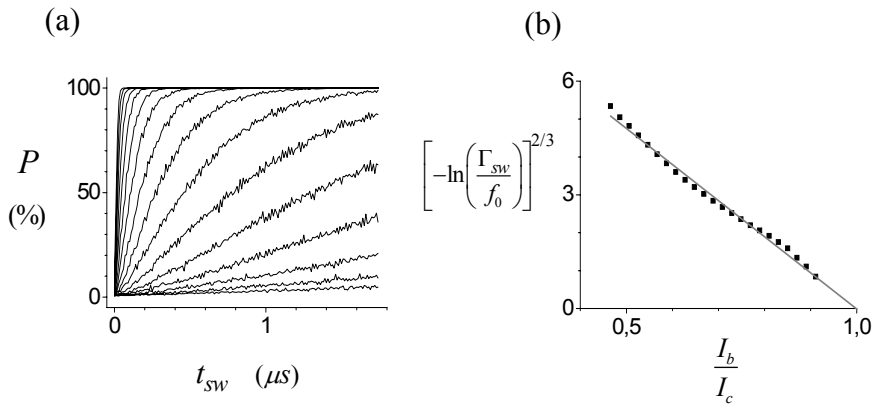


Figure 5.7: (a) Switching probability of the SQUID in sample (1) as a function of the duration of the switching plateau T_{sw} for different values of the bias current I_b. For each value of I_b, the switching rate Γ_{sw} is obtained by fitting $P(T_{sw})$ with an exponential decay. (b) $[-\ln(\Gamma_{sw}/f_0)]^{2/3}$ as a function of I_b/I_c. The solid line is a linear fit.

nA, $\phi = \Phi/\Phi_0 = 0.18$, $T_{eff} = 210$ mK and $x_{th} = 1.1$), we find $\Delta P = 19\%$. This estimation is in reasonable agreement with the observed readout contrast $C_m = 12$ %.

5.3 QND measurement with the DC-switching readout

In this section, we analyze the QND character of the DC-switching readout in sample (1), where the qubit-SQUID interaction and the voltage in the dissipative state of the SQUID are small, using a sequence of two successive readouts A and B. The concept of QND measurement and measurement projectiveness are discussed in chapter 2 (section 2.2).

5.3.1 Qubit relaxation between two successive readouts

First, we measure the switching probabilities P_A and P_B as a function of the delay between the two readouts when the qubit is initially prepared in the excited state using a Rabi pulse $\theta_A = \pi$. As shown in figure 5.8, P_A is constant while P_B decays exponentially. To quantify the effect of readout A on the qubit, we also measure P_B^{free} in the same conditions as previously, except that the readout pulse A is not applied. The exponential decay of P_B^{free}, which is only due to the free relaxation of the qubit (T_1=160 ns) can be directly compared with the decay of P_B. As can be seen in figure 5.8b the decay time of P_B

is equal to the free relaxation time (solid lines are exponential decay fitting curves). From the ratio $P_B/P_B^{free} = 0.8$ we conclude that the qubit relaxation is increased by an amount of 20 % during the measurement due to the operation of the detector.

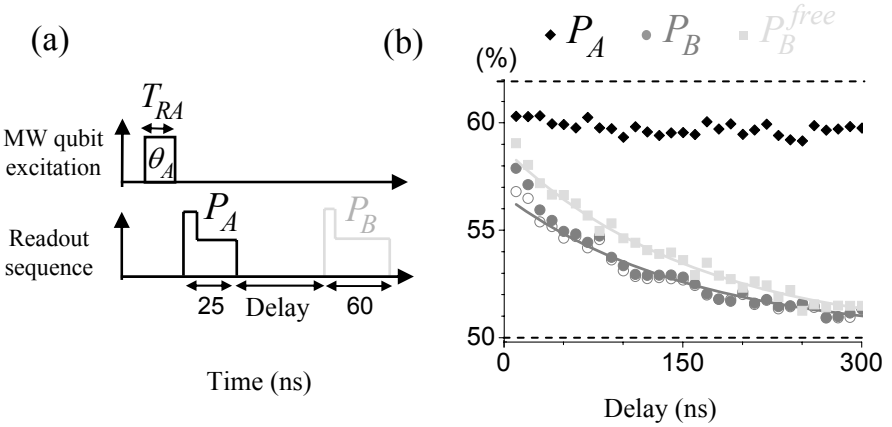


Figure 5.8: (a) Qubit excitation and readout sequence. The qubit operation frequency is set at E/h=13 GHz. (b) Switching probabilities P_A and P_B in the first and the second readout respectively. P_B^{free} is the free qubit relaxation decay measured with readout B without applying the readout pulse A. Open dots represent P_B after applying a small correction taking into account the extra switching events caused by readout A (see text).

In addition to the enhancement of the qubit relaxation during the readout, we observe that the result of the first readout influences the result of the second readout for delay between the measurements shorter than 20 ns. For a delay of 10 ns, the switching probability $P_B(D_A)$ in readout B if the detector was in state D during readout A is increased by about 10 % compared to $P_B(S_A)$ if the detector was in state S. As this effect is not related to the qubit, it can be easily corrected for by measuring the difference $P_B(D_A) - P_B(S_A)$ with the qubit in one specific state, e.g. the ground state. In figure 5.8b the open dots represent P_B after applying this small correction.

5.3.2 Qubit rotation between two successive readouts

Secondly, we measure P_A and P_B as a function of the duration T_{RA} of the Rabi rotation pulse preceding readout A, with a second Rabi pulse between readout A and B, and a fixed delay time of 100 ns between the two measurements (see figure 5.9a). $P_B(\pi)$ and $P_B(0)$ are obtained with or without a π pulse before readout B. Rabi oscillations are visible in P_A, $P_B(0)$ and $P_B(\pi)$ in figure 5.9b. The reduced oscillation amplitude of $P_B(0)$ compared with P_A is in good agreement with the free qubit relaxation during a time of 100 ns and the extra

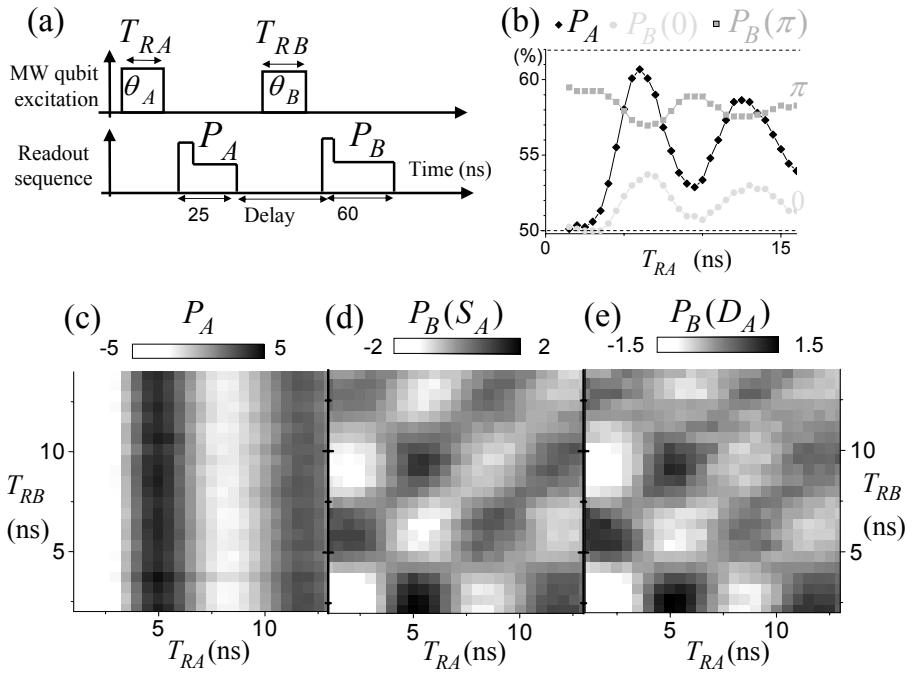


Figure 5.9: (a) Qubit operation and readout sequence including two Rabi oscillations of angles θ_A and θ_B, and two readout pulses A and B. (b) Switching probabilities P_A, P_B in readout A and B as a function of T_{RA}. $P_B(\pi)$ and $P_B(0)$ are the results readout B with or without a π rotation between the two measurements. (c,d,e) Results of the two readouts as a function of T_{RA} and T_{RB}. P_A is the switching probability in readout A, while $P_B(S_A)$ and $P_B(D_A)$ are the conditional switching probabilities for readout B in the cases that the outcome of readout A was S or D.

relaxation due to readout A mentioned above. The fact that the sign of the oscillation of $P_B(\pi)$ is reversed compared to $P_B(0)$ is a clear proof that the qubit state is partially preserved and can be manipulated coherently after a measurement. Furthermore, the averaged value of $P_B(\pi)$ is higher than $P_B(0)$. This is to be expected as the effect of the π pulse is to reverse the qubit state and the qubit relaxation between the measurements is significant.

Figures 5.9c-e show P_A and the two conditional switching probabilities $P_B(S_A)$ and $P_B(D_A)$ for readout B in the cases that the result of readout A is S or D respectively, as a function of T_{RA} and T_{RB}. To improve the visibility of the oscillations of $P_B(S_A)$ and $P_B(D_A)$ a constant offset is subtracted for each duration of the second Rabi pulse T_{RB}. As the discrimination efficiency between $|g>$ and $|e>$ in a single readout is low, the qubit state is only very weakly projected after a measurement. Given the readout contrast $C_m = 12$ %, the correlation between readout A and B due to the qubit state projection is too small to be resolved. The two readouts are thus nearly independent. As can be seen in figures 5.9d,e the qubit state is almost as well preserved if the detector is in state S or in state D. This result shows that the back-action of DC-switching type of detector in the dissipative state can be reduced to a very low level.

5.3.3 QND Fidelity

As explained in section 2.2.2 we define the QND fidelity based on the conditional probabilities that the qubit state after the measurement is the same as before the measurement, irrespective of the measurement outcome, when the qubit is initially in $|g>$ or $|e>$, denoted as $p(g|g)$ and $p(e|e)$ respectively

$$F_{QND} = \frac{p(g|g) + p(e|e)}{2}. \tag{5.7}$$

This definition is only relevant if the readout contrast is high enough with respect to the available statistics. Using relation (5.1) for the readout B, equation (5.7) can be rewritten as

$$F_{QND} = \frac{1}{2}\left[1 + \frac{\Delta P_B}{C_m}\right], \tag{5.8}$$

where $\Delta P_B = P_B(e) - P_B(g)$ is the difference of switching probability in readout B depending on the initial qubit state before readout A. From the measurement of figure 5.8b for a delay between the measurement of 10 ns we find $\Delta P_B \geq 6$ %, without correcting for the initial qubit preparation errors but subtracting for the systematic extra switching probability due to the readout A as explained previously. Assuming the contrast $C_m = 12$ % for readout A as well as for readout B we conclude that $F_{QND} \geq 75$ %, with $p(g|g) \simeq 100$ % and $p(e|e) \geq 50$ %.

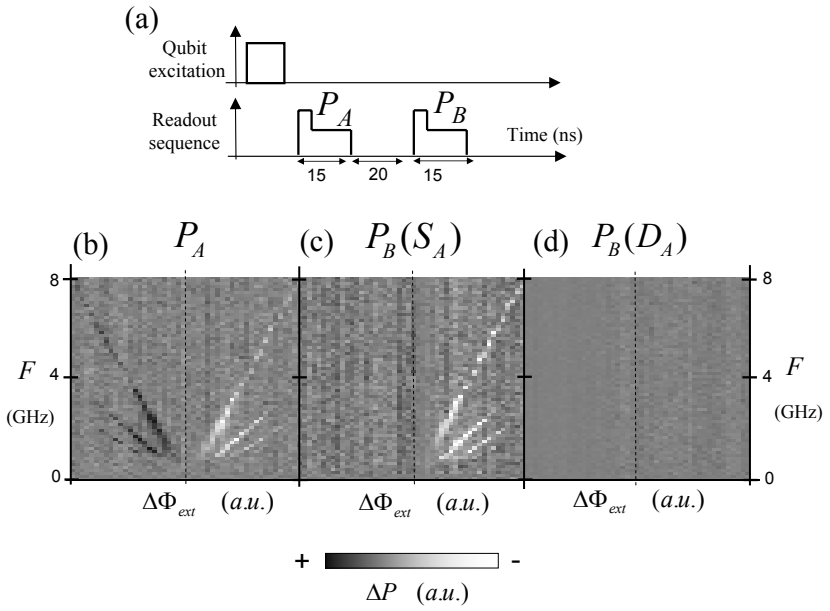


Figure 5.10: Qubit spectroscopy measurements with two consecutive readouts in sample (3). (a) Qubit excitation and readout sequence. (b) Switching probability P_A in readout A as a function of the microwave excitation frequency and the qubit flux bias. (c,d) Conditional switching probabilities $P_B(S_A)$ and $P_B(D_A)$ in readout B in the cases that the outcome of readout A was S or D.

5.4 Back-action for larger qubit-SQUID interaction strengths

In samples (2) and (3), the critical current of the SQUID is larger than in sample (1), while the qubit persistent current and the qubit-SQUID mutual inductance are similar. The qubit-SQUID interaction strength g during the measurement is thus larger (see table 5.1). Additionally, the voltage in the dissipative state is higher. Therefore one can expect that the back-action of the SQUID is stronger.

We first analyze the back-action of the SQUID in sample (2) by performing spectroscopy measurements with single readout at different measurement repetition rates. Similarly as with sample (1), no reduction of contrast is visible up to a measurement repetition rate of 1 MHz (data not shown).

Secondly, we analyze the back-action of the SQUID in samples (2) and (3) by applying a spectroscopy pulse and performing two consecutive measurements.

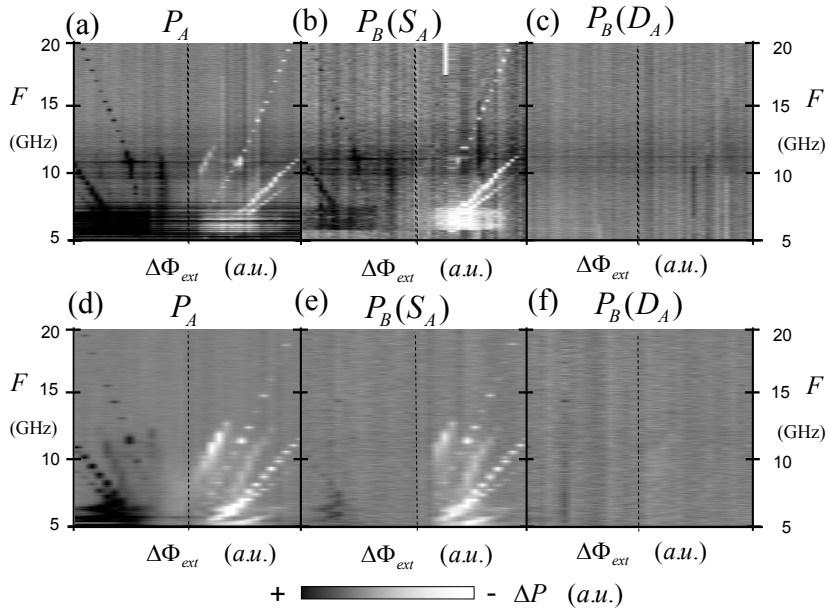


Figure 5.11: Qubit spectroscopy measurements with two consecutive readouts in sample (2). (a,d) Switching probability P_A in readout A. (b,c,e,f) Conditional switching probabilities $P_B(S_A)$ and $P_B(D_A)$ in readout B in the cases the outcome of readout A was S or D. In (a,b,c), the SQUID is operated at a flux bias $\phi_1 = 0.11$, whereas in (d,e,f), the SQUID flux bias is $\phi_2 = 0.33$.

In both samples the qubit relaxation time is about $T_1 \sim 150$ ns, while the delay between the measurement is 20 ns. The switching probabilities P_A, $P_B(S_A)$ and $P_B(D_A)$, in the case of sample (3), are shown in figures 5.10b-d as a function of the qubit flux bias and the microwave excitation frequency. In readout A, the spectrum of the qubit is clearly visible on both sides of the degeneracy. However, if there was a switching event in readout A, the qubit signal in readout B is completely lost (see figure 5.10d). Provided no switching event occurred during readout A, the qubit signal is still visible in readout B, but only on the right side of the degeneracy (see figure 5.10c).

Figures 5.11a-f show the switching probabilities P_A, $P_B(S_A)$ and $P_B(D_A)$, in the case of sample (2), for a similar qubit excitation and readout sequence. In figures 5.11a-c, the SQUID is operated at a frustration $\phi_1 = 0.11$ whereas in figures 5.11d-f the frustration is $\phi_2 = 0.33$. The SQUID sensitivity and the qubit-SQUID interaction are about a factor 3 higher at the frustration ϕ_2 than at the frustration ϕ_1. Similarly to sample (3), the qubit spectrum is clearly visible in readout A but disappears completely in readout B if there was a

switching event during readout A. Provided no switching event occurred during readout A, the qubit signal is still visible in readout B. At the frustration ϕ_1, the qubit spectrum is visible on both sides of the degeneracy (figure 5.11b), whereas at the frustration ϕ_2 the spectrum is only visible on the right side of the degeneracy (figure 5.11e).

Additional measurements of the dependence of the switching probability as a function of the SQUID bias current in sample (2) (not shown here) indicate that the sensitivity of the SQUID in the second measurement is not significantly affected after a switching event (although the switching probability is increased by 10%). Therefore the fact that the qubit signal in sample (2) is lost in readout B after a switching event in readout A suggests that the qubit relaxation is strongly enhanced when the detector is in the D state. Additionally, the qubit relaxation seems also to be increased on one side of the degeneracy when the SQUID is in the S state. The fact that the qubit signal is lost on the side where the switching probability is maximum when the qubit is in the excited state (figures 5.10c and 5.11b) suggests a relaxation mechanism involving the switching character of the readout (see figure 5.12). In this case, one would expect that the qubit relaxation strongly depends on the amplitude of the qubit-SQUID interaction strength. This is consistent with the results of figure 5.11b, where the qubit-SQUID interaction is smaller and the qubit signal is visible on both sides of the degeneracy.

5.5 Discussion and perspectives for high QND fidelity with large readout contrast

In section 5.3, we showed that when the qubit-SQUID interaction is small (< 1 GHz) and the voltage across the SQUID in the dissipative state is low (20 μV), the QND fidelity of the DC-switching readout can be as high as 75 %. However, one important consequence of the small amplitude of the qubit-SQUID interaction is that the readout contrast is low ($C_m = 12$ %). In the perspective of quantum computing, a higher readout contrast allowing to perform single shot measurements would be more attractive. In this section we discuss how the readout contrast could be increased while maintaining a good QND fidelity.

In the experiments presented in this chapter, the effective temperature of the SQUID was about $T_{eff} \sim 210$ mK, much higher than the physical temperature of the cryostat $T \sim 20$ mK). As effective temperatures as low as 35 mK have been reported with similar types of devices [6], it should be possible to reduce T_{eff} significantly. Based on equation (5.6), if T_{eff} could be reduced to 40 mK, the readout contrast would increase by a factor 3 without changing any parameters of the circuit.

In sample (1), the critical current of the SQUID was small (see table 5.1). Using larger values of the critical current results in much larger readout contrast [7]. In sample (2) for example, the readout contrast (deduced from spectroscopy) was 40%. However, the qubit-SQUID interaction is then very large,

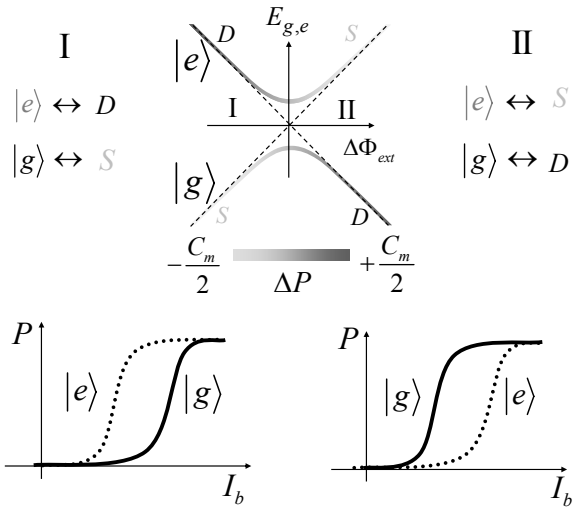


Figure 5.12: Relation between the state of the detector and the state of the qubit as a function of the qubit flux bias Φ_{ext}. Two regimes I and II can be distinguished (see text).

so one can expect that the back-action of the SQUID in the dissipative state is much stronger. Indeed, as we showed in section 5.4, for large qubit-SQUID interactions the qubit relaxation seems to be strongly enhanced when the detector is in its dissipative state. Yet, one important advantage of the flux qubit compared with other superconducting qubits is that the relation between the state of the qubit and the state of the detector can be chosen by setting the qubit flux bias either to a positive value (regime I) or a negative value (regime II). This is illustrated in figure 5.12. In regime I, the switching probability of the SQUID when the qubit is in the excited state is higher than when the qubit is in the ground state ($P(e) > P(g)$), whereas in regime II, the situation is reversed ($P(e) < P(g)$). In regime II, if the readout contrast is high, the SQUID only switches to the dissipative state when the qubit is in the ground state. In this case the enhancement of qubit relaxation when the SQUID is in state D would not affect the QND fidelity. Only the relaxation when the SQUID is its superconducting state S would be important. As shown in figures 5.10b and 5.11b,e, the qubit relaxation when the SQUID is in state S is not significantly increased during the measurement when the qubit is operated in regime II. For example, with a readout contrast of 40 %, the QND fidelity can be as high as 85 % even if the qubit excited state relaxes completely when the SQUID is in state D (as long as the it is preserved when the SQUID is in the state S). Using a large qubit-SQUID interaction ($\sim 10\ GHz$) and operating the qubit in regime

II should allow a high readout contrast with high QND fidelity.

5.6 Summary

In this chapter, we showed that the back-action of the DC-switching readout can be considerably reduced by shunting the SQUID with a low resistance and using a fast cryogenic amplifier. Based on a sequence of two successive readouts we demonstrated that the measurement has a clear quantum nondemolition character, with a QND fidelity of 75 %.

We should emphasize that this chapter presents the results of the first attempt to reduce the back-action of the DC-switching readout. It seems likely that the readout contrast can still be largely improved by reducing the SQUID effective temperature and using larger qubit-SQUID interaction strength while maintaining a good QND fidelity.

Such a simple, fast and low back-action detector is very attractive to study entanglement in a system with multiple-qubits and multiple-detectors and opens new perspectives to investigate fundamental aspects of quantum measurement.

Bibliography

[1] M. Neeley, M. Ansmann, Radoslaw C. Bialczak, M. Hofheinz, N. Katz, E. Lucero, A. OConnell, H. Wang, A. N. Cleland, and J. M. Martinis, *Transformed dissipation in superconducting quantum circuits*, Physical Review B **77**, 180508(R) (2008)

[2] D.E. McCumber, *Effect of ac Impedance on dc Voltage-Current Characteristic of Superconductor Weak-Link Junctions*, Jouranl of Applied Physics **39**, 3113 (1968)

[3] P. Bertet, I. Chiorescu, G. Burkard, K. Semba, C.J.P.M. Harmans, D.P. DiVincenzo, and J.E. Mooij, *Dephasing of a Superconducting Qubit Induced by Photon Noise*, Physical Review Letters **95**, 257002 (2005)

[4] P. Bertet, I. Chiorescu, K. Semba, C.J.P.M. Harmans, J.E. Mooij *Detection of a persistent-current qubit by resonant activation*, Physical Review B, **70**, 100501, (2004)

[5] J.M. Martinis, M. Devoret, J. Clarke, *Experimental tests for the quantum behavior of a macroscopic degree of freedom: The phase difference across a Josephson junction*, Physical Review B **35**, 4682 (1987)

[6] G. Ithier, *Manipulation, lecture et analyse de la décohérence d'un bit quantique supraconducteur*, PhD thesis (2005), (available at http://tel.ccsd.cnrs.fr)

[7] F. Yoshihara, K. Harrabi, A.O. Niskanen, Y. Nakamura, J.S. Tsai *Decoherence of Flux Qubits due to 1/f Flux Noise*, Physical Review Letters **97**, 167001 (2006)

Chapter 6

Perspectives for the quantum measurement of flux qubits

In this thesis, we have analyzed in detail the back-action of two types of readout schemes for superconducting flux qubits: the AC-switching readout, where the detector is operated at microwaves frequencies, and the DC-switching readout, where the detector is operated at DC (or nearly DC). In both cases, we have demonstrated that the back-action of the detector can be controllably reduced to such a level that a quantum nondemolition measurement is possible.

Low back-action detectors are very attractive to study fundamental aspects of quantum mechanics and quantum measurement such as partial collapse [1], uncollapse [2, 3], quantum feedback [4], measurement of weak values [5, 6] or simultaneous measurement of noncommutating variables [7]. However, in general all these 'types' of experiments require a nearly quantum limited detector with a level of back-action that is close to the minimum imposed by quantum mechanics given the amount of information extracted by the detector (see chapter 2). The demonstration of quantum nondemolition measurements of a qubit (presented in chapters 4 and 5 of this thesis) represents a first step in this direction, as it requires a very low level of back-action in terms of qubit relaxation during the measurement. To realize a quantum limited measurement of a qubit both relaxation and decoherence during the measurement should be minimal, which is a much more challenging requirement. Note that although readouts with high contrast and highly projective character are very attractive in the perspective of quantum computing (as is the case of the AC-switching readout studied in this thesis), from a fundamental point of view, weakly projective measurements are more interesting than highly projective measurements. In the following, three possible directions are discussed for realizing a quantum limited measurement which would allow to study some of the fundamental aspects of the quantum measurement mentioned above.

The first possibility is to use an AC-dispersive detector, such as the AC-continuous readout presented in chapter 3. These detectors have an intrinsically small back-action close to the minimum imposed by the Heisenberg uncertainty principle. In that sense they are very good candidates to realize quantum limited measurements. However, the efficiency is currently limited by the noise temperature of the cryogenic microwave amplifier following the detector, which is about two orders of magnitude higher than the quantum limit. Recent developments of nearly quantum limited amplifiers in the microwave frequency range based on superconducting circuits is therefore very promising [8, 9]. Although optimal coupling of a superconducting qubit and its AC-dispersive detector with a state of the art quantum limited amplifier might be a challenging task from an engineering point of view, most of the necessary ingredients are now available [10]. Therefore, it is likely that such type of experiment will be realized in the coming years.

The first demonstration of a quantum nondemolition measurement with a DC detector such as the DC-switching SQUID (presented in chapter 5 of this thesis) is coming unexpectedly at a stage where AC-dispersive detectors tend to become a new standard for qubit readout. This DC detector might provide new alternatives to realize a quantum limited measurement of superconducting qubits with a very simple detector. In particular, it could allow to extend the results obtained with phase qubits where the measurement is partially quantum limited but also partially destructive [1, 3]. Note however that the back-action of the DC-switching readout in terms of decoherence is likely to be very strong, especially when the SQUID is in its dissipative state (as discussed in detail in chapter 3). In the experiment presented in this thesis, the coherence time of the qubit was too short to analyze quantitatively the degree of decoherence induced by the operation of the detector. Further experimental investigation of this aspect of the back-action of the DC-switching readout would be of great value. Additionally, it might also be interesting to study non-hysteretic SQUIDs as they have been shown to reach the quantum limit, provided the effect of the high frequency Josephson oscillation averages out [11]. Although reducing the decoherence of the qubit when the SQUID is in its dissipative state might turn out to be impossible, given the simplicity of this readout scheme it would be very interesting and not so difficult to explore this direction further.

A third direction for realizing a quantum limited measurement of a qubit is to use a system of at least two coupled qubits with two individual detectors. In this case, one qubit can be used as a "probing qubit" to perform an indirect measurement on the "probed qubit". In such a readout scheme, the only interaction between the detector (formed by the probing qubit and its individual readout) and the probed qubit is an entangling gate (such as CNOT) between the two qubits. Following the entangling operation, a single shot measurement of the probing qubit reveals fully or partially the state of the probed qubit, depending on the degree of entanglement between the two qubits. To a first approximation, the quantum fidelity of the measurement should be given by the product of the fidelity of the entangling gate and the contrast of the readout of the probing qubit. To prove that such a measurement is indeed close to the

quantum limit and to quantify its quantum efficiency, it is necessary to test the coherence of the probed qubit after the measurement by manipulating it coherently and detect its final state with a second measurement using the second detector coupled to the probed qubit (which does not need to have a high readout contrast neither a high quantum efficiency). In practice, the critical part of such an experiment is that the two successive readouts should be performed within the coherence time of the probed qubit. In particular, the operation of the detector for the readout of the probing qubit should not introduce spurious dephasing of the probed qubit. This experiment could be implemented in the near future either with the AC-switching readout or the DC-switching readout, as both types of detector should have a negligibly small back-action on the state of the probed qubit to which it is indirectly coupled.

The results presented in this thesis are also very relevant in the perspective of quantum information processing and quantum computing. Given the rapid progress in the field of superconducting qubits (as illustrated for example with the recent realization of the first quantum algorithm with two qubits [12]), one can expect that the realization of systems with a larger number of qubits such as the first quantum byte will be one of next "holy grail" experiments in the field of superconducting qubits. In such an experiment, scalability of the detection scheme and the qubit-qubit (or qubit-cavity bus) coupling mechanism is essential. Given the simplicity of operation of the DC-switching readout compared with the AC-switching readout, the results presented in this thesis show that the DC-switching readout would be more attractive for the readout of a large number of superconducting flux qubits. Although it is technically possible to detect a large number of resonators simultaneously using microwave multiplexing techniques (as recently demonstrated in the context of radio-astronomy [13, 14]), it would require much more efforts, including the development of an advanced and dedicated microwave measurement setup. In the case of the superconducting flux qubits, the operation of a large number of AC-dispersive detectors is not necessary and would only reduce the flexibility and increase the complexity of the whole approach compared with the DC-switching readout.

Bibliography

[1] N. Katz, M. Ansmann, R. C. Bialczak, E. Lucero, R. McDermott, M. Neeley, M. Steffen, E. M. Weig, A. N. Cleland, J.M. Martinis and A. Korotkov, *Coherent State Evolution in a Superconducting Qubit from Partial-Collapse Measurement* Science **312**, 1498 (2006)

[2] A.N. Korotkov and A.N. Jordan, *Undoing a Weak Quantum Measurement of a Solid-State Qubit* Physical Review Letters **97**, 166805 (2006)

[3] N. Katz, M. Neeley, M. Ansmann, R.C. Bialczak, M. Hofheinz, E. Lucero, A. O'Connell, H. Wang, A.N. Cleland, J.M. Martinis and A.N. Korotkov *Reversal of the Weak Measurement of a Quantum State in a Superconducting Phase Qubit*, Physical Review Letters **101**, 200401 (2008).

[4] R. Ruskov and A.N. Korotkov *Quantum feedback control of a solid-state qubit* Physical Review B **66**, 041401(R), (2002)

[5] Y. Aharonov, D.Z. Albert, and L. Vaidman, *How the result of a measurement of a component of the spin of a spin-1/2 particle can turn out to be 100*, Physical Review Letters **60**, 13511354 (1988)

[6] N.S. Williams and A.N. Jordan, *Weak Values and the Leggett-Garg Inequality in Solid-State Qubits*, Physical Review Letters **100**, 026804 (2008)

[7] H. Wei, Y. Nazarov *Statistics of measurement of noncommuting quantum variables: Monitoring and purification of a qubit*, Physical Review B **78**, 045308 (2008)

[8] M.A. Castellanos-Beltran, K.D. Irwin, G.C. Hilton, L.R. Vale, K.W. Lehnert, *Amplification and squeezing of quantum noise with a tunable Josephson metamaterial*, Nature Physics **4**, 929 (2008)

[9] N. Bergeal, F. Schackert, M. Metcalfe, R. Vijay, V.E. Manucharyan, L. Frunzio, D.E. Prober, R.J. Schoelkopf, S.M. Girvin, M.H. Devoret *Phase-preserving amplification near the quantum limit with a Josephson ring modulator*, Nature **465** 64 (2010)

[10] A. Palacios-Laloy, F. Mallet, F. Nguyen, P. Bertet, D. Vion, D. Esteve, A.N. Korotokov, *Experimental violation of Bell's inequality in time with a weak measurement*, Nature physcis, **6**, 442 (2010)

[11] V.V. Danilov, K.K. Likharev, A.B.Zorin, *Quantum noise in SQUIDs*, IEEE transaction on magnetics **19**, 572 (1983)

[12] L. DiCarlo, J.M. Chow, J.M. Gambetta, L.S. Bishop, B.R. Johnson, D.I. Schuster, J. Majer, A. Blais, L. Frunzio, S.M. Girvin, R.J. Schoelkopf, *Demonstration of two-qubit algorithms with a superconducting quantum processor* Nature **460**, 240 (2009)

[13] L.J. Swenson, J. Minet, G.J Grabovskij, O. Buisson, F. Lecocq, C. Hoffmann, P. Camus, J.-C. Villégier, S. Doyle, P. Mauskopf, M. Roesch, M. Calvo, C. Giordano, S.J.C. Yates, A.M. Baryshev, J.J.A. Baselmans, A. Benoit, A. Monfardini, *A Fast, Ultra-Sensitive and Scalable Detection Platform Based on Superconducting Resonators for Fundamental Condensed-Matter and Astronomical Measurement*, AIP Conference Proceedings **1185**, 84-87 (2009), 13^{th} International Worshop on low temperature detectors LTD13.

[14] P.R. Maloney, N.G. Czakon, P.K. Day, R. Duan, J. Gao, J. Glenn, S. Golwala, M. Hollister, H.G. LeDuc, B. Mazin, O. Noroozian, H.T. Nguyen, J. Sayers, J. Schlaerth, J.E. Vaillancourt, A. Vayonakis, P. Wilson and J. Zmuidzinas *The MKID Camera*, AIP Conference Proceedings **1185**, 176-179 (2009), 13^{th} International Worshop on low temperature detectors LTD13.

Summary

In this thesis, we study the quantum measurement of superconducting flux qubits using a DC-SQUID operated in different modes.

Chapter 1 gives a brief introduction to the field of quantum computing with superconducting circuits and presents the basic properties of the flux qubit and the DC-SQUID.

Chapter 2 presents different aspects of the theory of quantum measurement. In the first section, we present a general framework to describe a linear continuous detector treated as a quantum system. In the second section, we introduce a definition for the sensitivity of a switching detector in a form similar to the case of a continuous detector. This allows a direct comparison of the sensitivity of continuous detectors with switching detectors. In the last section, we present the concepts of quantum nondemolition measurement and quantum limited measurement of a qubit and discuss the correlations between the results of two successive measurements in different regimes.

Chapter 3 introduces the basic principles of three different detection schemes for the readout of the superconducting flux qubits based on a DC-SQUID: the AC-continuous readout, the DC-switching readout and the AC-switching readout. The intrinsic sensitivity and the back-action of each readout are analyzed using the common framework introduced in chapter 2. The purpose of this analysis is to provide general guidelines for the design of future experiments, to compare the efficiency of the SQUID in each readout mode and to help understanding the main factors limiting the sensitivity. The intrinsic sensitivity of the SQUID is found to be on the same order of magnitude in all the modes of operation considered. However, in practice, due to several factors specific for each readout, the effective sensitivity of the SQUID is lower. One conclusion of this analysis is that for identical (and typical) values of the parameters characterizing the SQUID, the effective sensitivity of the AC-switching readout should be significantly higher than of the DC-switching readout and the AC-continuous readout.

Chapter 4 presents experiments to investigate and quantify the quantum nondemolition character of the AC-switching readout. Using a sequence of two consecutive measurements it is shown that a measurement can be performed with a QND fidelity of 88 %. The high correlation between the two measurement outcomes reveals the strongly projective character of the measurement. A simple model including the qubit relaxation and the detector switching process

is introduced to analyze the role of relaxation during the measurement. It is found that the relaxation strongly depends on the state of the detector and its operating point. Corrected for qubit relaxation during the measurement, the fidelity of the readout is at least 95 %.

Chapter 5 shows the results of the first attempt to reduce the back-action of the DC-switching readout, lowering the amplitude of the switching voltage by shunting the SQUID with a resistor and using a fast cryogenic amplifier. A single readout can be completed in a time as short as 25 ns. Coherent Rabi oscillations are recorded with measurement repetition rates up to 1 MHz without loss of contrast. Based on a sequence of two successive readouts we show that the measurement has a clear quantum nondemolition character, with a QND fidelity of 75 %. As the readout contrast is small (12 %) the measurement is only weakly projective.

Chapter 6 discusses perspectives for quantum measurement of superconducting flux qubits with a more particular emphasis on the possibility to realize a quantum limited measurement of a qubit in order to investigate experimentally some fundamental aspects of the theory quantum measurement.

Thomas Picot
Delft , August 2010

Samenvatting

In dit proefschrift bestuderen wij de quantummeting van supergeleidende flux qubits met behulp van een DC-SQUID magnetometer die op verschillende manieren wordt gebruikt.

Hoofdstuk 1 geeft een korte inleiding in het gebied van quantum computing met supergeleidende schakelingen en presenteert de basiseigenschappen van het flux qubit en de DC-SQUID.

Hoofdstuk 2 presenteert verschillende aspecten van de theorie van quantummeting. In de eerste sectie presenteren wij een algemeen kader om een lineaire, continue detector te beschrijven als een quantumsysteem. In de tweede sectie introduceren wij een definitie voor de gevoeligheid van een schakelende detector, analoog aan die voor een continue detector. Hiermee wordt een direct vergelijk mogelijk van de gevoeligheid van continue detectors met die van schakelende detectors. In de laatste sectie presenteren wij de concepten quantum-nondemolitiemeting en quantum-gelimiteerde meting van een qubit en wij bespreken de correlaties tussen de uitkomsten van twee achtereenvolgende metingen in verschillende regimes.

Hoofdstuk 3 introduceert de basisprincipes van drie verschillende detectiemethoden voor het uitlezen van supergeleidende flux qubits, die gebaseerd zijn op de DC-SQUID: de wisselstroom-continue uitlezing, de gelijkstroom-schakelende uitlezing en de wisselstroom-schakelende uitlezing. De intrinsieke gevoeligheid en de terugwerking van elke uitlezing worden geanalyseerd met behulp van het algemene kader van hoofdstuk 2. Het doel van deze analyse is om algemene ontwerpregels te verkrijgen voor toekomstige experimenten, om de doelmatigheid van de SQUID in de uitleesmethoden te vergelijken en om te helpen bij het begrijpen van de belangrijkste factoren die de gevoeligheid beperken. De intrinsieke gevoeligheid van de SQUID blijkt van dezelfde orde te zijn bij alle bestudeerde detectiemethoden. In de praktijk is de effectieve gevoeligheid van de SQUID lager door factoren die specifiek zijn voor elke uitlezing. Een gevolgtrekking van deze analyse is dat, voor gelijke (en kenmerkende) waarden van de parameters die de SQUID karakteriseren, de effectieve gevoeligheid van de wisselstroom-schakelende uitlezing significant hoger zou moeten zijn dan die van de gelijkstroom-schakelende en de wisselstroom-continue uitlezing.

Hoofdstuk 4 beschrijft experimenten om het quantum-nondemolitie (QND) karakter van de wisselstroom-schakelende uitlezing te onderzoeken en te kwantificeren. Met behulp van twee achtereenvolgende metingen wordt aangetoond

dat een meting met een QND-betrouwbaarheid van 88 % mogelijk is. Uit de hoge correlatie tussen de uitkomsten van de twee metingen blijkt het sterk projecterende karakter van de meting. Een eenvoudig model waarin relaxatie van het qubit en het schakelproces van de detector zijn opgenomen wordt gebruikt om de rol van relaxatie gedurende de meting te analyseren. Gevonden wordt dat de relaxatie sterk afhangt van de toestand en het werkpunt van de detector. Met correctie voor qubit relaxatie tijdens de meting is de betrouwbaarheid van de uitlezing tenminste 95 %.

Hoofdstuk 5 toont resultaten van de eerste poging om de terugwerking van de gelijkstroom-uitlezing te verminderen door de amplitude van de schakelspanning te verlagen met behulp van een shuntweerstand over de SQUID en een snelle cryogene versterker. Een enkele uitlezing kan voltooid worden binnen 25 ns. Coherente Rabi-oscillaties worden vastgelegd met herhalingsfrequenties tot 1 MHz zonder contrastverlies. Op basis van twee achtereenvolgende uitlezingen tonen we aan dat de meting een uitgesproken quantum-nondemolitie-karakter heeft met een QND-betrouwbaarheid van 75 %. De uitlezing is slechts zwak projecterend door het lage contrast van de uitlezing.

Hoofdstuk 6 bespreekt de perspectieven voor een quantum-meting van supergeleidende flux qubits met bijzondere nadruk op de mogelijkheid om een quantum-gelimiteerde meting tot stand te brengen waarmee enkele fundamentele aspecten van de theorie van quantummeting experimenteel onderzocht kunnen worden.

Thomas Picot
Delft , August 2010

Curriculum Vitae

Nov. 24, 1979	Born in Clichy, France
1997	Baccalauréat Scientifique with high honors at Lycée Jules Ferry in Versailles, France
1997-1999	Classes Préparatoires aux Grandes Ecoles at Lycée Janson de Sailly in Paris, France
1999-2003	General engineering diploma of ESPCI with honors (Ecole Supérieure de Physique et de Chimie Industrielle de la ville de Paris), France
2003-2005	Master of science in theoretical physics with honors, at Ecole Normale Supérieure de Lyon, France
2005-2010	Ph. D. research at Delft University of Technology under supervision of Prof. dr. ir. J.E. Mooij Subject: On the quantum measurement of superconducting flux qubits

List of publications

1. *Quantum nondemolition measurement of a superconducting qubit in the weakly projective regime*
   T. Picot, R. Schouten, C.J.P.M. Harmans, and J.E. Mooij
   Physcial Review Letters, **105**, 040506 (2010)

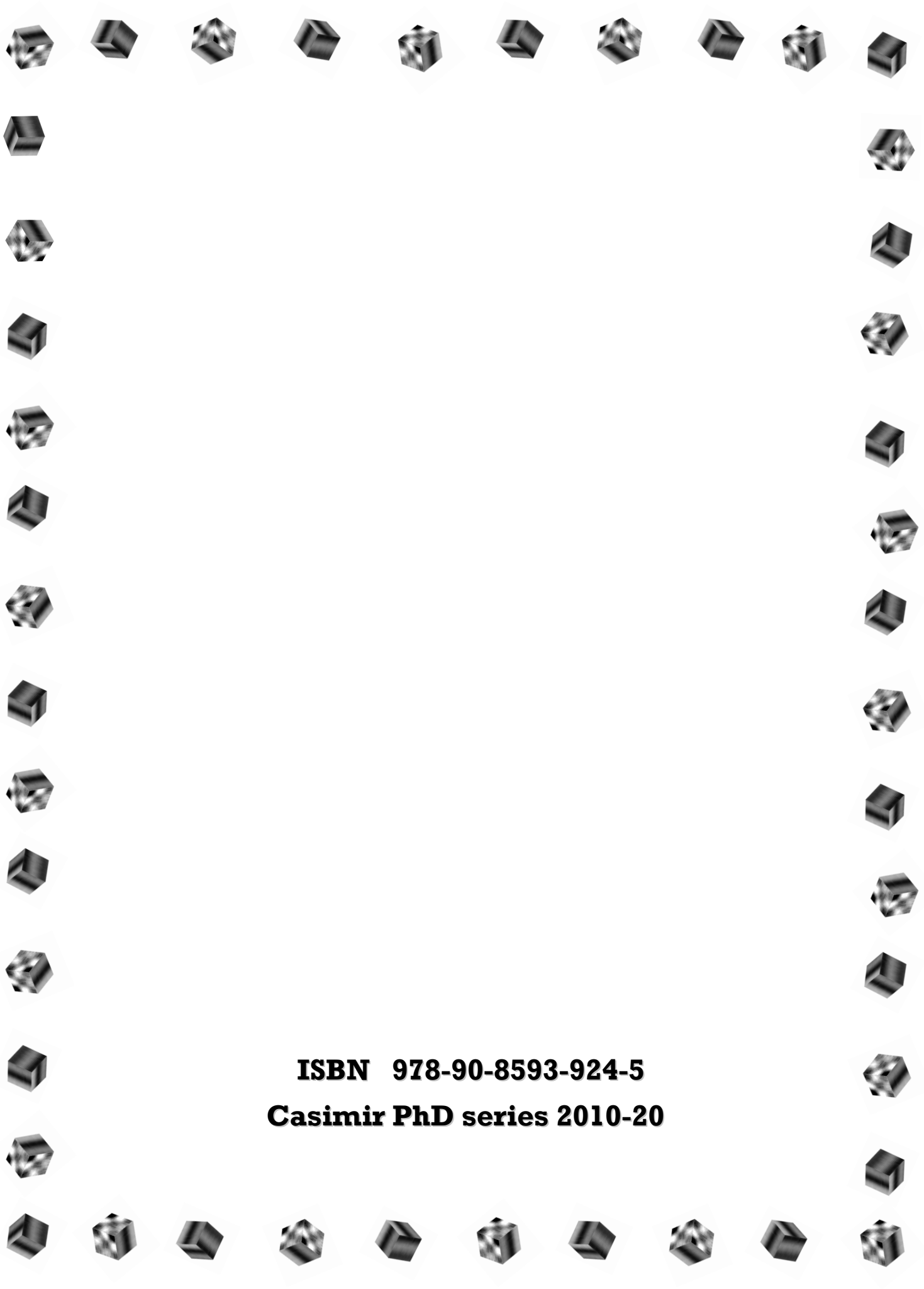
2. *Role of relaxation in the quantum measurement of a superconducting qubit using a nonlinear oscillator*
   T. Picot, A. Lupaşcu, S. Saito, C.J.P.M. Harmans, and J.E. Mooij
   Physical Review B, **78**, 132508 (2008)

3. *Quantum non-demolition measurement of a superconducting qubit*
   A. Lupaşcu, S. Saito, T. Picot, P.C. de Groot, C.J.P.M. Harmans and J.E. Mooij
   AIP Conference proceedings, **1074**, 26 (2008)

4. *Interqubit coupling mediated by a high-excitation-energy quantum object*
   S. Ashhab, A.O. Niskanen, K. Harrabi, Y. Nakamura, T. Picot, P.C. de Groot, C.J.P.M. Harmans, J.E. Mooij, and F. Nori
   Physical Review B, **77**, 014510 (2008)

5. *Quantum non-demolition measurement of a superconducting two-level system*,
   A. Lupaşcu, S. Saito, T. Picot, P.C. de Groot, C.J.P.M. Harmans and J.E. Mooij
   Nature Physics, **3**, 119 (2007)

6. *Predicting activities without computing descriptors: graph machines for QSAR*,
   A. Goulon, T. Picot, A. Duprat, and G. Dreyfus
   SAR and QSAR in Environmental Research **18**, 141 (2007)



ISBN 978-90-8593-924-5

Casimir PhD series 2010-20